| | |
|---|---|
| **Titre:** Title: | Characterization of Flow-Induced Structures in Carbon Nanotube Suspensions |
| **Auteur:** Author: | Fatemeh Khalkhal |
| **Date:** | 2011 |
| **Type:** | Mémoire ou thèse / Dissertation or Thesis |
| **Référence:** Citation: | Khalkhal, F. (2011). Characterization of Flow-Induced Structures in Carbon Nanotube Suspensions [Thèse de doctorat, École Polytechnique de Montréal]. PolyPublie. https://publications.polymtl.ca/677/ |

UNIVERSITÉ DE MONTRÉAL

# CHARACTERIZATION OF FLOW-INDUCED STRUCTURES IN CARBON NANOTUBE SUSPENSIONS

FATEMEH KHALKHAL

DÉPARTEMENT DE GÉNIE CHIMIQUE

ÉCOLE POLYTECHNIQUE DE MONTRÉAL

THÈSE PRÉSENTÉE EN VUE DE L'OBTENTION

DU DIPLÔME DE PHILOSOPHIAE DOCTOR

(GÉNIE CHIMIQUE)

SEPTEMBRE 2011

UNIVERSITÉ DE MONTRÉAL

ÉCOLE POLYTECHNIQUE DE MONTRÉAL

Cette thèse intitulée:

# CHARACTERIZATION OF FLOW-INDUCED STRUCTURES IN CARBON NANOTUBE SUSPENSIONS

présentée par : KHALKHAL Fatemeh

en vue de l'obtention du diplôme de : Philosophiae Doctor

a été dûment accepté par le jury d'examen constitué de:

M. AJJI Abdellah, Ph. D., président

M. CARREAU Pierre J., Ph. D., membre et directeur de recherche

M. FRADETTE Louis, Ph. D., membre

M. RODRIGUE Denis, Ph. D., membre

# DEDICATION

*To my husband, Farhad, for his kindness and encouragements.*

# ACKNOWLEDGEMENT

I enjoyed working with CREPEC group in the last few years. In particular, I appreciate my supervisor, Dr. Carreau, for criticizing my work leading to the improvement of the quality of my published articles. My special thanks to Melina Hamdine for well maintaining the rheology lab and making the equipments accessible to us. I would like to appreciate very kind assistance of Marie Matet and Melina Hamdine for helping me to translate some parts of this thesis to French.

I acknowledge helpful discussions with Dr. Michel Moan and Dr. Frederic Bossard during their short visits to Montreal. I am thankful to Dr. Suong Hoa and Dr. Daniel Theriault for providing access to the facilities at Concordia composite laboratory and three roll mill at the composite laboratory in the mechanical engineering department of Ecole Polytechnique, respectively.

At the end, I like to appreciate my husband, Farhad, and my family for their encouragements and support.

This research was funded in part by NSERC and CRIAQ.

# RÉSUMÉ

Les nanotubes de carbone sont des nanoparticules fibreuses présentes dans de nombreuses applications. Grâce à leur importante surface spécifique apparente, leur densité de courant électrique élevée, leur stabilité thermique et leurs excellentes propriétés mécaniques, les nanotubes de carbone sont utilisés pour améliorer les propriétés physiques des matrices polymériques.

Les propriétés macroscopiques des suspensions proviennent de leurs propriétés à l'échelle du micron et du submicron. La structure des suspensions peut être facilement influencée par de nombreux paramètres tels que les forces de cisaillement externes, la concentration de la suspension, la température, les caractéristiques des particules, etc. L'étude de la structure de la suspension représente un défi majeur et devient un sujet d'intérêt grandissant pour de nombreux chercheurs.

Dans cette étude, la structure d'une suspension modèle de nanotubes de carbone dispersée dans une résine époxy est étudiée en utilisant un ensemble de méthodes rhéologiques, les théories fractales et de mise à l'échelle ainsi qu'un modèle structural thixotropique. L'effet de l'histoire d'écoulement sur les propriétés viscoélastiques linéaires des suspensions et l'évolution de la structure lors de l'arrêt du cisaillement ont été investigués pour une large gamme de vitesse de pré-cisaillement, de concentrations et de températures. Les résultats de ces analyses sont les suivants.

L'effet de l'histoire d'écoulement s'est avéré plus prononcé pour les suspensions diluées ou semi-diluées. Les faibles vitesses de pré-cisaillement entraînent un plus grand nombre d'enchevêtrements entre les particules. Cela résulte de la réduction du seuil de percolation rhéologique. Pour les suspensions diluées ou semi-diluées, après l'arrêt du cisaillement, les

différentes structures métastables formées ont pu être distinguées par leurs différents modules de conservation qui sont inversement reliés à la vitesse de pré-cisaillement. Pour les suspensions concentrées, les structures métastables formées ont donné des modules de conservation équivalents quelque soit le pré-cisaillement appliqué. Il a été montré que la vitesse de formation de ces structures métastables augmentait avec l'augmentation de la concentration. De plus, pour les concentrations faibles et intermédiaires, la vitesse de formation des structures métastables décroît lorsque l'on augmente la vitesse de pré-cisaillement appliqué, alors que pour les concentrations élevées, le pré-cisaillement n'a pas d'influence sur la formation des structures.

Il a été trouvé que le module élastique des structures métastables formées est relié aux vitesses du pré-cisaillement appliquées selon une loi de puissance; les paramètres de celle-ci dépendent fortement de la concentration. Cette corrélation est applicable aux résultats à cisaillements constants pour les suspensions formant une courbe maîtresse sur une large échelle de concentrations, au-dessus et en-dessous du point de gélification. Cela illustre également l'importance du module de conservation des structures métastables comme un paramètre représentant l'évolution de la structure. À la lumière des théories fractales et de mise à l'échelle, il apparaît dans cette recherche que les suspensions de nanotubes étudiées sont classées comme des suspensions à floculation lente pour lesquelles l'élasticité des structures provient à la fois des liaisons inter- et intra-flocs. De plus, le potentiel d'interaction des suspensions est une combinaison des composants centraux et non-centraux. La faible sensibilité de la dimension fractale des suspensions à l'histoire d'écoulement est en accord avec le module de conservation constant des structures métastables, qui est faiblement influencé par la vitesse de pré-cisaillement proche et au-dessus du point de gélification.

Etant donné que les forces de cisaillement perturbent l'état de dispersion et d'enchevêtrement des particules, cela peut causer la formation de structures sous écoulement ou la distorsion des structures dépendant de la concentration et de la vitesse du pré-cisaillement appliquée. En comparant le module de conservation des suspensions sans pré-cisaillement et celui des structures métastables après pré-cisaillement à différentes vitesses, une vitesse de pré-cisaillement critique a été déterminée pour les concentrations faibles et intermédiaires au-dessus desquelles des enchevêtrements de nanotubes se sont rompus; cela réduit leur élasticité et provoque la formation incomplète de la structure au repos. L'évolution de la structure est en accord – qualitativement – avec les prédictions d'un modèle structural thixotropique.

A la différence de nombreuses suspensions de fibres et de nano-composites, le mouvement Brownien est un mécanisme influençant la formation de la structure de la suspension de nanotubes de carbone modèle en l'absence d'écoulement. Cette conclusion a pu être formulée grâce à une analyse quantitative de la vitesse de formation de la structure selon différentes températures conjointement à la réponse de la suspension en démarrage dans des directions opposées.

# ABSTRACT

Carbon nanotubes (CNTs) are fibre-like nano-particles with many different applications. Due to their high specific surface area, high electric current density, thermal stability and excellent mechanical properties, they are used to reinforce physical properties of polymer matrices.

The macroscopic properties of suspensions are inherited from their properties at micron and sub-micron scales. The suspensions structure can be easily influenced by many parameters such as the extent of external shear forces, the suspension concentration, temperature, the particles specifications, etc. This makes the study of the suspension structure a very challenging task and has been the subject of interest to many researchers.

In this thesis, the structure of a model carbon nanotube suspension dispersed in an epoxy is studied by employing a set of rheological methods, scaling and fractal theories and a structural thixotropic model. The effect of flow history on linear viscoelastic properties of suspensions and the evolution of structure upon cessation of shear flow has been studied over a wide range of pre-shearing rates, concentration and temperature. The results of these analyses are as follows.

The effect of flow history is more pronounced on the suspensions structure in dilute and semi-dilute concentration regimes. By pre-shearing at low rates, more inter-particle entanglements were induced, which resulted in reduction of rheological percolation thresholds. After cessation of shear flow, for dilute and semi-dilute suspensions, the formed metastable structures were distinguishable by different storage moduli, which were inversely related to the rate of pre-shearing. However, for the concentrated suspensions, the formed metastable structures had an approximately equal storage modulus regardless of the rate of the applied pre-shearing. It was shown that the rate of formation of these metastable structures was

enhanced by increasing concentration. Furthermore, the rate of structure build-up decreased by increasing the applied pre-shear rate in low and intermediate concentrations, while it remained almost intact with respect to the pre-shearing rate at high concentrations.

It was found that the elastic modulus of the formed metastable structures scaled with the applied pre-shear rate in a power-law form, the parameters of which strongly depended on the concentration. As a result, scaling the steady shear results of the suspensions using this correlation formed a master curve over a wide range of concentrations below and above the gel point; this illustrated the importance of the storage modulus of metastable structures as a parameter, which represented the parameters involved in the evolution of structure. The conducted research in the light of scaling and fractal theories revealed the fact that the model CNT suspensions under investigation was classified as slowly flocculating suspensions in which the elasticity of structures originated from both the inter- and intra-floc links. Moreover, the interaction potential of the suspensions was a combination of central and non-central components. The less sensitivity of the fractal dimension of the suspensions to the flow history was in agreement with the invariant storage modulus of the metastable structures, which was barely influenced by the rate of pre-shearing near and above the gel point.

Since application of shear forces disturbed the state of dispersion and particle entanglements, it may cause formation of some flow-induced structures or distortion of structures depending on the concentration regime and the rate of the applied pre-shearing. By comparing the storage modulus of the suspensions without pre-shearing and the one for the metastable structures after pre-shearing at various rates, a critical pre-shear rate was found at low and intermediate concentrations above which some nanotube entanglements broke down; this reduced their elasticity and resulted in the incomplete structure build-up at rest during transient flow

reversal measurements. The structural evolution that has been explained so far was shown to be in qualitative agreement with the predictions of a structural thixotropic model.

Unlike many fiber suspensions and nano-composites, the Brownian motion was an influential mechanism in structure build-up of the carbon nanotube model suspensions in the absence of flow. This was concluded by a quantitative analysis of the rate of the structural build-up under the variation of temperature in conjunction with the extent of structure reconstruction at rest in a set of transient stress growth measurements in opposite directions.

# CONDENSÉ EN FRANÇAIS

Une recherche approfondie a été dédiée à l'étude de l'état de floculation, de défloculation et de l'orientation des nanotubes de carbone en suspension selon différentes conditions d'écoulement comme dans [Lin-Gibson *et al.* (2004); Hobbie and Fry (2006)]. Ces études ont été en grande partie effectuées par la technique de dispersion de la lumière applicable aux suspensions diluées et semi-diluées. Toutefois, il est important de noter que la structure n'évolue plus lorsque le cisaillement est stoppé. Plus récemment, Mobuchon *et al.* (2009) et Negi et Osuji (2010) ont montré que l'histoire de l'écoulement influence fortement l'évolution de la structure des suspensions non-aqueuses d'argile aussi bien que celle des suspensions aqueuses de laponite. Néanmoins, ces études étaient limitées à une seule concentration ou à une gamme de concentration limitée alors que les propriétés rhéologiques peuvent changer radicalement d'une concentration à une autre. De plus, les mécanismes qui entrent en jeu dans l'évolution de la structure doivent être étudiés pour comprendre leur influence sur l'état de dispersion des suspensions.

Dans cette thèse, la structure d'une suspension de nanotubes de carbone modèle dispersée dans de l'époxy est caractérisée par un ensemble de tests rhéologiques, des théories fractales et de mise à l'échelle et un modèle structural thixotropique. Le but est de déterminer plus particulièrement les mécanismes impliqués dans la formation de la structure et de déterminer aussi de quelle manière la variation des paramètres, dont la concentration, la température et le taux de pré-cisaillement, vont influencer l'état de dispersion des suspensions.

Les nanotubes de carbone multifeuillets avec un facteur de forme de 45 en moyenne sont dispersés dans de l'époxy Epon 828 de densité 1.16 g/mL et de viscosité 12.33 Pa.s (à 25 °C),

en utilisant un laminoir à trois rouleaux. Des suspensions de différentes concentrations ont été préparées.

Au début, il a été montré, qualitativement, que l'histoire de l'écoulement influence fortement les propriétés viscoélastiques linéaires des suspensions. L'application de faibles forces de cisaillement implique des enchevêtrements entre les particules plus nombreux, tandis que le fort taux de pré-cisaillement provoque une destruction de la structure et le désenchevêtrement de nanotubes. Cette conclusion provient du fait que le début de la création d'un réseau de nanotubes de carbone interconnectés se déplace vers les faibles concentrations lorsque le taux de pré-cisaillement décroît. Le seuil de percolation rhéologique a été déterminé à environ 2.5 % en poids après un taux de cisaillement de 100 $s^{-1}$, tandis que l'application d'un pré-cisaillement à 0.01 $s^{-1}$ aboutit à un seuil de percolation de 1 % en poids.

La mesure du module de conservation des suspensions à une basse fréquence constante et à une contrainte dans la région linéaire a montré que l'évolution de la structure continue après l'arrêt du cisaillement. Les modules mesurés évoluent de manière exponentielle dans le temps pour chaque concentration. Différentes structures métastables se forment après un certain temps à la suite de l'arrêt du cisaillement. Les structures métastables créées se distinguent par les différents modules de conservation pour les systèmes dilués et semi-dilués, ceux-ci sont inversement reliés aux taux de pré-cisaillement. Cependant, pour les suspensions plus concentrées, les structures métastables formées ont approximativement le même module de conservation après le pré-cisaillement à différents taux. Ces observations révèlent que la structure des suspensions est plus sensible à l'histoire de l'écoulement pour des concentrations faibles et intermédiaires. En effet, pour de telles concentrations, les interactions entre les particules ne sont pas assez fortes; alors la structure fragile des suspensions est plus

susceptible d'être affectée par les forces de cisaillement externe. Toutefois, pour les fortes concentrations, les particules interagissent selon des forces hydrodynamiques et des forces de friction suffisamment fortes; alors la structure enchevêtrée formée est plus résistante au champ de cisaillement externe et le pré-cisaillement a une faible influence sur leur structure et sur leurs propriétés macroscopiques.

Des analyses supplémentaires sur l'effet de l'histoire de l'écoulement sur les structures métastables formées montrent que le module élastique de ces structures est lié au taux de pré-cisaillement selon une loi puissance telle que $G'_\infty = \kappa \dot{\gamma}_i^{-\varepsilon}$, ses paramètres étant fortement dépendants de la concentration. En appliquant ce modèle aux résultats à cisaillement constant des suspensions, une courbe maîtresse est sur une large échelle de concentrations, au-dessus et en-dessous du point de gélification; cela illustre l'importance du module de conservation des structures métastables comme un élément caractéristique, lequel représente un paramètre important de l'évolution de la structure.

En comparant les modules de conservation des suspensions avant le pré-cisaillement (excepté pour l'échantillon chargé dans l'instrument), $G'_{ref}$, avec ceux obtenus pour les structures métastables, $G'_\infty$, il a été montré qu'il existe un taux de cisaillement critique pour les concentrations intermédiaires et faibles en-dessus duquel les enchevêtrements des nanotubes sont rompus impliquant une élasticité plus faible de la suspension. Le taux de cisaillement critique a été quantifié en traçant ces deux modules en fonction du taux de pré-cisaillement appliqué; le taux de pré-cisaillement correspondant au point d'intersection est appelé taux de cisaillement critique, $\dot{\gamma}_c$, et est compris entre 1.7 $s^{-1}$ à 0.5 % en masse et 10 $s^{-1}$ à 3 % en masse avec une erreur expérimentale de ±15%. Pour les concentrations plus élevées, aucun taux de

cisaillement critique n'est observé dû à la présence d'enchevêtrements forts de nanotubes. En effectuant un pré-cisaillement à un taux de cisaillement plus faible que le taux critique ( $\dot{\gamma}_i < \dot{\gamma}_c$ ), il y a formation d'un plus grand nombre d'enchevêtrements entre les nanotubes; cela amène une plus grande élasticité des structures métastables formées ( $G'_\infty > G'_{ref}$ ). À l'inverse, l'application d'un taux de cisaillement plus élevé ( $\dot{\gamma}_i \geq \dot{\gamma}_c$ ) entraîne une rupture partielle de la structure et en conséquence l'élasticité des structures métastables diminue ( $G'_\infty \leq G'_{ref}$ ).

L'étendue de la formation et de la rupture de la structure au voisinage des taux de cisaillement critiques a été quantifiée par un ensemble d'expériences en écoulement transitoire inverse. Il apparaît que la formation de la structure est complète lorsque le taux de cisaillement appliqué est inférieur au taux critique. Cela a été caractérisé en approchant la valeur du pic de la contrainte inverse à une valeur similaire du pic de la contrainte dans le sens des aiguilles d'une montre après un temps de repos suffisant. Dès l'application de taux de cisaillement plus élevés, la structure se développe partiellement dû au désenchevêtrement de certains nanotubes. Pour les plus hautes concentrations, les pics de contrainte dans des directions opposées se chevauchent après un temps de repos suffisant quelque soit le taux de cisaillement appliqué.

La vitesse de formation des structures et la formation des structures métastables après l'arrêt du pré-cisaillement ont été caractérisées en déterminant le temps caractéristique du système en fonction de la concentration, du taux de pré-cisaillement et de la température. Le temps caractéristique décroît avec la concentration révélant une reconstruction de la structure plus rapide. Cependant, cette variation en ce qui concerne le taux de pré-cisaillement est fortement dépendante de la concentration. Pour les suspensions diluées, il augmente significativement

avec le taux de pré-cisaillement, révélant une reconstruction de la structure plus lente tandis qu'il reste presque identique pour les suspensions plus concentrées.

L'autre paramètre influençant la vitesse de formation des structures est la température. Toutefois, l'étude de l'effet de la température est plus compliquée puisque les interactions entre particules et les propriétés rhéologiques de la matrice polymérique sont toutes les deux sensibles aux variations de température. Donc, pour l'interprétation des résultats, il est essentiel de distinguer ces deux phénomènes. En normalisant la viscosité en cisaillement ainsi que les modules de conservation et de perte des suspensions aux valeurs correspondantes au polymère pur pour chaque température, l'effet des interactions entre particules est mis en évidence. Les valeurs normalisées augmentent avec la température, ce qui reflète l'augmentation des interactions entre particules. En observant la même tendance pour le module de conservation normalisé des suspensions métastables avec le module complexe de l'époxy pur pour chaque température, on aboutit à la même conclusion.

La variation de la température affecte le temps caractéristique de la formation des structures métastables. On observe que la vitesse de formation des structures métastables croît avec la température indépendamment de la concentration ou du taux de pré-cisaillement. Cela correspond à l'observation de la vitesse de formation des structures plus élevée lorsque la concentration augmente pour une température constante. A partir de ces deux observations, on peut conclure que les interactions entre particules ont un rôle crucial dans la formation des structures métastables. D'un autre coté, le temps de diffusion diminue avec la température; cela démontre le rôle important que jouent les forces Browniennes dans la formation des structures de suspensions de nanotubes de carbone en l'absence d'écoulement. Cela correspond au fait que le temps caractéristique des suspensions métastables diluées, pour de

forts taux de pré-cisaillement, diminue avec la température dans une gamme plus grande comparé aux faibles taux de pré-cisaillement. Cela veut dire qu'en l'absence de fortes interactions entre particules (déformation des structures possible pour les plus hauts taux de pré-cisaillement), la vitesse de reconstruction des structures augmente avec la température puisque fortement influencée par les forces Browniennes. En conclusion, dans une large gamme de concentrations, de taux de pré-cisaillement et de températures, le mouvement Brownien et les interactions entre particules sont deux mécanismes importants dans le développement des structures métastables.

L'importance des forces Browniennes et des interactions entre particules dans le développement des structures a été étudiée à travers un ensemble d'expériences en écoulement transitoire inverse au voisinage des taux de cisaillement critiques. Il a été observé que la formation des structures avait lieu en grande partie durant les 300 premières secondes de repos après l'arrêt de l'écoulement transitoire dans la direction dans le sens des aiguilles d'une montre; ce temps est comparable au temps de diffusion, $1/D_r$ égal à 314 s pour les systèmes dilués et même plus court ($D_r' \sim D_r / \phi^2$) pour les suspensions semi-diluées. Cependant, la formation complète d'une structure prend plus de temps (~ 1 h) révélant le fait que les forces Browniennes ne peuvent pas être le seul mécanisme rentrant en jeu au repos. D'un autre coté, comme discuté plus tôt, l'insuffisance d'interactions entre particules dû à l'application de forts taux de pré-cisaillement ($\dot{\gamma} \geq \dot{\gamma}_c$) et à la déformation de la structure, aboutit, lors des mesures en écoulement transitoire inverse, à une structure partielle. Donc, les forces Browniennes conjointement avec les interactions entre particules sont nécessaires à la reconstruction de la structure d'une suspension de nanotubes pré-cisaillée en l'absence d'écoulement.

En utilisant le modèle structural thixotropique d'Yziquel *et al.* (1999), le comportement transitoire des suspensions de nanotubes est comparé aux prédictions obtenues du modèle. Le modèle prédit qualitativement les résultats de l'expérience ainsi que le développement d'une structure partielle pour des taux de cisaillement supérieurs aux taux de cisaillement critique. Cependant, le pic inverse et le temps de repos requis pour une formation complète de la structure sont surestimés.

Une plus ample interprétation du comportement de la structure des suspensions grâce à la théorie de mise à l'échelle apporte des informations précieuses sur la nature du réseau de nanotubes. Il a été démontré que les suspensions de nanotubes forment un réseau auto-assemblé au voisinage et au-dessus du point de gélification qui est supposément formé de paquets serrés de flocons fractals. La nature fractale du réseau a été mise en évidence en observant le comportement du plateau du module de conservation à basses fréquences des suspensions et la contrainte pour la limite maximale de linéarité, $\gamma_c$, avec la concentration suivant la loi de puissance. En utilisant les exposants de la corrélation de la loi de puissance adaptée, la dimension fractale des suspensions est estimée à environ 2.15 pour les suspensions à floculations lentes. Cela explique pourquoi le temps d'utilisation des suspensions est limité à quelques mois. Au vu de la théorie de mise à l'échelle, les liaisons inter- et intra-flocons sont à l'origine de l'élasticité des réseaux.

À partir de ce point de vue, les variations complexes des propriétés rhéologiques des structures métastables sous écoulement ont été étudiées. Il a été montré que les exposants des paramètres $G'_\infty$ et $\gamma_c$ de la loi de puissance, en ce qui concerne la concentration, augmentent significativement avec le taux de pré-cisaillement appliqué. Cependant, les dimensions fractales résultantes ont légèrement changé de 2.13 à 2.31 après un pré-cisaillement

respectivement de 0.1 $s^{-1}$ et de 100 $s^{-1}$. En fait, la faible différence entre les dimensions fractales des structures métastables est comprise dans l'erreur expérimentale, alors la superstructure du réseau des suspensions montre seulement une faible variation avec l'histoire de l'écoulement; cela est relié à la structure compacte initiale des suspensions avant le pré-cisaillement ($d_f \sim 2.15$). La faible sensibilité de la dimension fractale des suspensions à l'histoire de l'écoulement est en accord avec le module de conservation constant des structures métastables, qui est très peu influencé par le taux de pré-cisaillement au voisinage et au-dessus du point de gélification. De plus, l'exposant *m* de la loi de puissance relié à la variation du rayon de giration ($\xi$) des agrégats avec le taux de cisaillement appliqué ($\xi \sim \dot{\gamma}^{-m}$) a été trouvé dans la gamme de 0.36-0.38 et dans la limite des valeurs théoriques pour les agrégats rigides et mous. Cela illustre bien que les agrégats sont partiellement mous et partiellement rigides et que leur potentiel d'interaction est une combinaison des composants centraux et non-centraux.

Lors de la dernière étape, l'effet de la température sur le comportement de mise à l'échelle des suspensions a été caractérisé. Les modules de conservation réduits des suspensions augmentent avec la température alors que $\gamma_c$ diminue révélant la formation d'une structure plus fragile. Cela est en contradiction avec les travaux d'Abbasi *et al.* (2009) qui ont montré que $\gamma_c$ augmentait avec la température, qu'il y avait formation d'un réseau plus fort et que les nanotubes de carbone étaient mieux dispersés dans le nano-composite. Dans ce sens, la diminution de $\gamma_c$ avec la température pourrait être l'indication qu'il y a plus agrégats lorsque la température augmente. Pourtant, aucune séparation de phase n'a lieu puisque la superposition temps-température est valide sur l'étendue des températures étudiées. Les exposants du module de conservation de la loi de puissance et $\gamma_c$, et alors les dimensions

fractales estimées, présentent des erreurs importantes et la difficulté est donc de savoir si la superstructure des suspensions est influencée par la température; cela peut être dû à la plage limitée de température de seulement 30 °C.

# TABLE OF CONTENTS

# LIST OF TABLES

# LIST OF FIGURES

# LIST OF SYMBOLS AND ABBREVIATIONS

## Latin symbols

| | |
|---|---|
| $a$ | particle diameter, consistency index |
| $A_H$ | Hamaker constant |
| $a_T$ | shift factor |
| $b$ | flow behaviour index |
| $c_2$ | constant |
| $d$ | fibre diameter, mean value of outer diameter, Euclidean dimension |
| $De$ | Deborah number |
| $d_f$ | fractal dimension |
| $D_r$ | rotational diffusion coefficient |
| $E_a$ | activation energy |
| $E_c$ | the work required to break up the elastic structure |
| $E_Y$ | Young modulus |
| f($\xi$) | empirical function in structural model |
| $G(\gamma, t)$ | relaxation modulus |
| $G'$ | storage modulus, macroscopic elastic constant of a system with size $L$ |
| $G'_0$ | low angular frequency storage modulus |
| $G'(t)$ | storage modulus |
| $G'(\xi)$ | structured modulus in structural model |
| $G'_i$ | initial storage modulus right after pre-shearing |
| $G'_{ref}$ | storage modulus of suspensions before pre-sharing |
| $G_\infty$ | storage modulus of destroyed structure in structural model |

| | |
|---|---|
| $G'_{\infty}$ | equilibrium storage modulus |
| $(G'_{\infty})_{\min}$ | minimum value of equilibrium storage modulus |
| $(G'_{\infty})_{\max}$ | maximum value of equilibrium storage modulus |
| $(G'_{\infty})_{\exp}$ | equilibrium storage modulus from experiment |
| $(G'_{\infty})_{\text{model}}$ | equilibrium storage modulus from model |
| $G''$ | loss modulus |
| $G^*_s$ | complex modulus of neat polymer |
| $h$ | Planck constant |
| $ID$ | inner diameter |
| $k_1$, $k_2$ | kinetic constants of structural model |
| $k_B$ | Boltzmann constant |
| $K_{chain}$ | elastic constant of a linear chain |
| $K_0$ | bending constant between two neighbouring springs |
| $K_{eff}$ | effective elastic constant of a floc |
| $K_l$ | inter-floc elastic constant |
| $K_L$ | storage modulus of suspension |
| $K_\xi$ | elastic constant of a floc, intra-floc elastic constant |
| $L$ | fibre length |
| $N$ | number of experimental data, number of springs in a floc |
| $m$ | power-law exponent |
| $m_{rigid}$ | power-law exponent for rigid aggregates |
| $m_{soft}$ | power-law exponent for soft aggregates |
| $n$ | power-law exponent |

| | |
|---|---|
| $n_1$ | relative refractive index of a particle |
| $N_1$ | first normal stress difference |
| $N_2$ | second normal stress difference |
| $n_3$ | relative refractive index of neat polymer |
| $OD$ | outer diameter |
| $Pe$ | Peclet number |
| $r$ | distance between particles |
| $R$ | gas constant |
| $R^2$ | a measure of the extent to which the total variation of the dependent variable *is* explained by the regression |
| $S^{eff}$ | effective stiffness |
| $t$ | time |
| $T$ | temperature |
| $T_0$ | reference temperature |
| $t_{diffusion}$ | characteristic diffusion time |
| $x$ | fractal dimension of backbone |

## Greek symbols

| | |
|---|---|
| $\alpha$ | fitting parameter, coefficient of proportionality |
| $\beta$ | power-law coefficient |
| $\gamma$ | strain, power-law exponent |
| $\gamma_1$ | the power-law exponent relating the storage modulus to the concentration |
| $\gamma_c$ | maximum limit for linearity |
| $\dot{\gamma}$ | shear rate |

| | |
|---|---|
| $\dot{\gamma}_i$ | rate of pre-shearing |
| $\dot{\gamma}_c$ | critical shear rate |
| $\varepsilon$ | power-law exponent |
| $\varepsilon_1$ | permittivity of particles |
| $\varepsilon_3$ | permittivity of neat polymer |
| $\eta$ | shear viscosity |
| $\eta(\dot{\gamma})$ | shear viscosity |
| $\eta_0$ | characteristic viscosity |
| $\eta_s$ | viscosity of suspending medium |
| $\eta^*$ | complex viscosity |
| $\eta_r$ | reduced shear viscosity of suspension |
| $\eta_\infty$ | high shear viscosity |
| $\eta(\xi)$ | structured viscosity |
| $[\eta]$ | intrinsic viscosities |
| $\kappa$ | constant |
| $\lambda_0$ | characteristic time related to particle interactions |
| $\nu_e$ | absorption frequency |
| $\nabla \nu$ | velocity gradient |
| $(\nabla \nu)^{\mathrm{T}}$ | transpose of velocity gradient |
| $\xi$ | effective floc size, radius of gyration of fractal flocs, structural parameter |
| $\xi_{CCW}$ | steady-state value of the structural parameter at the end of CCW |
| $\xi_0$ | characteristic length scale |
| $\rho$ | mass density |
| $\sigma$ | shear stress |

| | |
|---|---|
| $\sigma^+$ | transient shear stress in a stress growth experiment |
| $\sigma^+_{max}$(CCW) | transient shear stress in a counter-clockwise stress growth experiment |
| $\sigma^+_{max}$(CW) | transient shear stress in a clockwise stress growth experiment |
| $\sigma_N$ | normalized standard deviation |
| $\tau$ | characteristic time, shear stress |
| $\tau_y$ | apparent yield stress |
| $\phi$ | particle concentration |
| $\phi_{\text{int}}$ | internal concentration |
| $\phi_{pt}$ | concentration at percolation threshold |
| $\phi_v$ | volume concentration |
| $\phi'_v$ | transition concentration from dilute to semi-dilute regime |
| $\phi''_v$ | transition concentration from semi-dilute to concentrated regime |
| $\Phi$ | interaction potential |
| $\omega$ | angular frequency |

## Abbreviations

| | |
|---|---|
| CCW | counter clockwise |
| CNF | carbon nano-fibre |
| CNT | carbon nanotube |
| CTAB | cetyl trimethyl ammonium bromide |
| CW | clockwise |
| DWCNT | double wall carbon nanotube |
| iPP | isotactic polypropylene |

| | |
|---|---|
| LVE | linear viscoelastic |
| MWCNT | multiwall carbon nanotube |
| ODA | octadecylamine |
| PB | polybutene |
| PBSA | poly[butylene succinate-co-adipate] |
| PBT | polybutylene terephthalate |
| PDI | poly-dispersity index |
| PEO | polyethylene oxide |
| PIB | poly-iso-butylene |
| PMMA | poly-methyl-methacrylate |
| PP | polypropylene |
| PS | polystyrene |
| SANS | small angle neutron scattering |
| SAOS | small amplitude oscillatory shear |
| SDBS | sodium dodecyl benzene sulfonate |
| SDS | sodium dodecyl sulfate |
| SWCNT | singlewall carbon nanotube |
| 3RM | three-roll mill |
| TEM | transmission electron microscopy |

# LIST OF APPENDICES

# CHAPITRE 1 INTRODUCTION AND OBJECTIVES

## 1.1 Introduction

Carbon nanotubes show many potential applications and have been widely used to improve the physical properties of polymers such as their electrical conductivity [Zhang *et al.* (2006); Kota *et al.* (2007)], mechanical properties [Allaoui *et al.* (2002); Gojny *et al.* (2004)], thermal properties [Lau *et al.* (2005); Nanda *et al.* (2008)] and inflammability [Schartel *et al.* (2005); Cipiriano *et al.* (2007)]. The stability and dispersion quality of nanotube suspensions are crucial for different applications. The state of dispersion of the suspensions depends on the internal and external forces. Repulsive inter-particle interactions help to keep the particles dispersed while attractive interactions can result in aggregation.

Depending on the preparation conditions, particles disperse differently in the suspending medium and form numerous structures. A qualitative definition of structure is the interrelation or arrangement of particles in the dispersing medium. Application of shear forces at various amplitudes during processing can strongly influence the structure, the quality of dispersion of particles in the suspension and their macroscopic properties. A great deal of research has been devoted to analyze the effect of various processing parameters on the dispersion quality and macroscopic properties of colloidal suspensions.

If the particles associate by attractive forces or due to flow conditions, they aggregate. There are two types of aggregation: flocculation and coagulation [Larson (1999)]. Flocculation is a reversible aggregation and is usually the result of a physical change in the system. It can be reversed by the application of mechanical processes such as shaking or stirring. The

breakdown of aggregates (flocculates) and re-dispersion of particles in the suspension is called dis-aggregation or de-flocculation. Coagulation is a fast irreversible aggregation.

Application of external fields such as shear field may cause aggregation or dis-aggregation. If the particles are stiff enough and interact by large friction forces, shear forces induce aggregation even in the absence of attractive inter-particle interactions [Switzer III and Klingenberg (2003)]. The stiffness of particles not only depends on their physical properties such as the Young modulus and particle dimensions, but also on the viscosity of the suspending medium and the flow conditions; thus, same particles may act as flexible or rigid ones depending on the rate of the applied shear or the properties of the matrix. By applying high shear forces, the aggregates can break down and the particles re-disperse in the suspensions more homogenously.

The state of flocculation/de-flocculation of suspensions under the influence of flow strongly depends on the rate of the applied shear and the concentration. Depending on their concentration, the suspensions may belong to dilute, semi-dilute or concentrated regime. In dilute systems, the particles are theoretically isolated and free to rotate without being disturbed by the presence of other particles. Thus, the inter-particle interactions are very weak and the fragile structure of suspensions can be easily influenced by shear forces. In semi-dilute regime, the particles interact through excluded volume interactions and form a relatively stronger structure; though, their structure can be influenced by high shear forces. The particles overlap in concentrated regime and interact by mechanical contacts and hydrodynamic interactions; hence, external shear forces can barely influence their structure.

In the particular case of nanotube suspensions, Brownian motion competes with short range attractive van der Waals forces between nanotubes in the absence of external forces to keep

them suspended. During flow, long range hydrodynamic forces compete with Brownian motion; the dominating force determines the final microstructure of the suspension.

The fact that the suspensions structure can be easily influenced by many parameters such as external shear forces, suspension concentration, particles stiffness, etc., makes the study of structure very challenging.

Light scattering techniques can provide morphological information about suspensions structure at certain length scales. However, in most cases, a combination of scattering techniques should be accessible to have a thorough understanding about the microstructure over a wide range of length scales from few nanometres to tens of microns [Pignon *et al.* (1997)]. Moreover, these techniques are limited to very dilute systems. A more applicable tool for characterizing the microstructure is through the study of the rheological behaviour of the suspensions which can detect structural changes at submicron scales over a wide range of concentrations.

## 1.2 Objectives

An extensive research has been devoted to investigate the state of flocculation, de-flocculation and orientation of CNT suspensions subjected to different flow conditions such as those in [Lin-Gibson *et al.* (2004); Hobbie and Fry (2006)]. These studies have been mainly performed by light scattering techniques applicable to dilute and semi-dilute concentrations. However, it should be noted that the evolution of structure does not stall upon cessation of shear flow. Recently, Mobuchon *et al.* (2009) and Negi and Osuji (2010) have shown that flow history strongly influenced the evolution of structure of the non-aqueous layered silicate suspensions as well as the aqueous laponite suspensions respectively. Nevertheless, these studies have

been restricted to a single or a limited range of concentrations while the rheological properties can dramatically change from one concentration regime to another. Furthermore, the mechanisms involved in the structure evolution need to be investigated as how they influence the state of dispersion of suspensions.

In this thesis, the structure of a model carbon nanotube suspension dispersed in an epoxy is characterized by employing a set of rheological methods, scaling and fractal theories and a structural thixotropic model. In particular, it is aimed to determine the mechanisms involved in the formation of the structure and the extent by which the variation of the parameters namely concentration, temperature and pre-shear rate affect the state of dispersion of the suspensions.

Multiwall carbon nanotubes with relatively short lengths and the average aspect ratio of about 45 are dispersed in an epoxy Epon 828 using a three-roll mill mixer and suspensions with a wide range of concentrations are prepared. Initially the size and size distribution of nanotubes are determined by transmission electron microscopy (TEM) and image analysis. These results are used to elaborate the limits of our system including the concentration regimes of the suspensions, the effective stiffness of nanotubes and the rotary diffusion coefficient. A variety of rheological measurements including non-destructive small amplitude oscillatory shear (SAOS) measurements as well as the steady shear and transient flow measurements have been performed to pursue the objectives of this thesis. The results of the rheological measurements have been interpreted in the light of the scaling theories [Shih *et al.* (1990); Wu and Morbidelli (2001)], fractal theories [Potanin (1991); Potanin (1993)] and a structural kinetic

model [Yziquel *et al.* (1999)]. The main contributions of this research are highlighted as the following:

1) The suspensions microstructure and its evolution were analyzed under the simultaneous influence of pre-shearing, concentration and temperature in a quantitative manner.

2) It has been shown that pre-shearing at low rates induced more entanglements between carbon nanotubes and resulted in the formation of a percolated network at lower concentrations. By increasing the rate of pre-shearing, more nanotubes disentangled and the onset for the formation of an interconnected network shifted to higher concentrations.

3) A critical shear rate was obtained that exhibits a limit for the applied pre-shear rate at low and intermediate concentrations to avoid the breakdown of nanotube entanglements.

4) The kinetics of structure build-up under the influence of flow history, concentration and temperature was analyzed.

5) The nature of nanotubes network structure and the origin of its elasticity were determined using the scaling theories.

6) The influence of flow history and temperature on the microstructure and the degree of compactness of suspensions structure was quantitatively characterized using fractal dimension analysis.

7) The mechanisms of structure evolution during flow and in quiescent was studied by comparing the stress growth transient results with a structural kinetic model and the

importance of Brownian forces as a possible mechanism in structural evolution was shown.

# CHAPITRE 2 LITERATURE REVIEW

In this chapter, a brief review on the properties of CNTs and their potential applications are presented. Then, different suspension preparation techniques as well as other dispersion techniques useful for nanotubes are reviewed. A more in-depth critical review on the rheology of these suspensions as well as the influential parameters on the rheological properties of nanotube suspensions (composites) is presented. Given the extent by which we use the scaling theory and a thixotropic model to interpret the measured rheological properties, they have been reviewed in the last sub-sections of this chapter.

## 2.1 Carbon nanotubes

Carbon nanotubes (CNTs) are fibre-like particles made up of graphite sheets with a small diameter in the range of few nanometres and lengths of few microns to few millimetres. They are formed of carbon atoms with $sp^2$ bonds which are stronger than $sp^3$ bonds found between carbon atoms in diamond which makes them very strong and stiff fibres. They may have different structures depending on their length, thickness, number of layers and chirality. The most commonly used types of CNTs are single wall carbon nanotubes (SWCNTs), double wall carbon nanotubes (DWCNTs) and multi-wall carbon nanotubes (MWCNTs). Figure 2-1 represents a schematic of the three types of nanotubes.

Although the structure of carbon nanotubes is similar to graphite, they show different electrical properties depending to their chirality. In theory, metallic nanotubes can carry an electric current density of more than 1,000 times greater than metals such as copper [Hong and Myung (2007)]. The thermal stability of carbon nanotubes is estimated to be up to 2800 °C in vacuum and about 750 °C in air [Thostenson *et al.* (2005)].

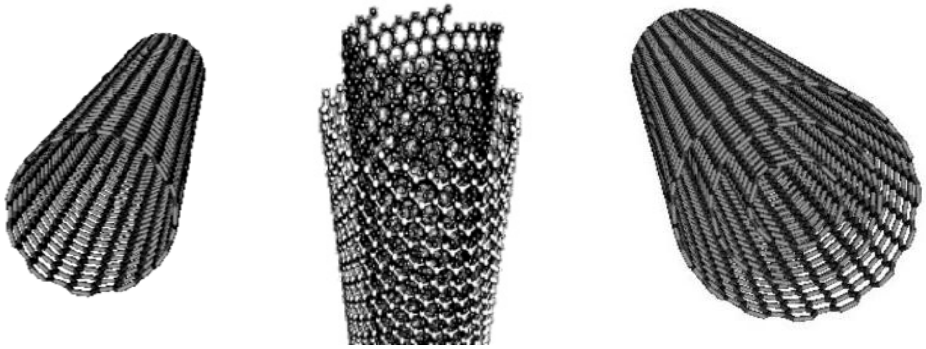

Figure 2-1: A schematic of SWCNT (left[1]), DWCNT (middle[2]) and MWCNT (right[3]).

Some properties of CNTs are summarized and compared with glass fibre as a non-conductive fibre and PAN-based carbon fibre [Wypych (2000)] as a conductive fibre in Table 2-1. The properties of carbon nanotubes are obtained from MSDS of a thin MWCNT (NC7000 Series) produced by NANOCYL ™. From this table, it can be observed that carbon nanotubes have a high specific surface area; this makes them good candidates as fillers since the addition of small quantities of nanotubes can provide a large surface area available to the suspending medium. They are also very strong fibres with tensile strength of more than 10 GPa and stiff with the Young's modulus of about 1 TPa. They break at much larger (~10 %) elongation compared to carbon fibre (~2%) or glass fibre (~ 4.5%). Considering copper as a metal with very low electrical resistivity (~$10^{-6}$ Ω-cm), carbon nanotubes are relatively conductive fillers whereas glass fibre (~$10^{13}$-$10^{16}$ Ω-cm) is almost an isolator similar to most polymers such as epoxy resins (~$10^{12}$-$10^{14}$ Ω-cm).

---

[1] http://www.physorg.com/news11668.html

[2] http://www.nec.co.jp/press/ja/pr-room/cnt-img/cnt-01.jpg

[3] http://itech.dickinson.edu/chemistry/?cat=74

Table 2-1: Physical properties of some fibres in comparison with CNTs.

| | Specific surface area ($m^2/g$) | Young's Modulus (TPa) | Tensile Strength (GPa) | Elongation at break (%) | Thermal conductivity (W/K.m) | Electrical volume resistivity (Ω.cm) |
|---|---|---|---|---|---|---|
| **MWCNT (Nanocyl)** | 250-300 | 1.00 | 10-60 | 10 | ≥ 3000 | $10^{-7}$-$10^{-6}$ |
| **Carbon fibre-PAN** | 0.27-1.0 | 0.23-0.50 | 3.0-5.5 | 0.4-2.0 | 9-100 | $10^{-2}$-$10^{-5}$ |
| **Glass fibre** | …… | 0.07 | 3.1-3.8 | 4.5-4.9 | 1 | $10^{13}$-$10^{16}$ |

The unique properties of carbon nanotubes make them good candidates for polymer reinforcements and fabrication of multi-functional nano-composites. Addition of small quantity of CNTs to polymers can significantly change their physical properties such as electrical conductivity, electromagnetic shielding effectiveness and thermal conductivity.

## 2.2 Dispersion of CNTs

Since, CNTs have a smooth surface and attract each other by weak van der Waals forces, they tend to entangle; this makes their dispersion into polymer matrices very challenging. A schematic of 0.1 wt% pristine MWCNTs dispersed in acetone is presented in Figure 2-2. As it can be observed, it is not possible to identify the single nanotubes in this micrograph.

Dispersion exhibits how uniformly CNTs are distributed in the suspensions and strongly depends on the processing conditions. Huang *et al.* (2006) reported a critical mixing time is required at a certain mixing shear stress and concentration to well disperse nanotubes in a suspension. Insufficient mixing time results in jamming of clusters and instabilities in the form of sedimentation.

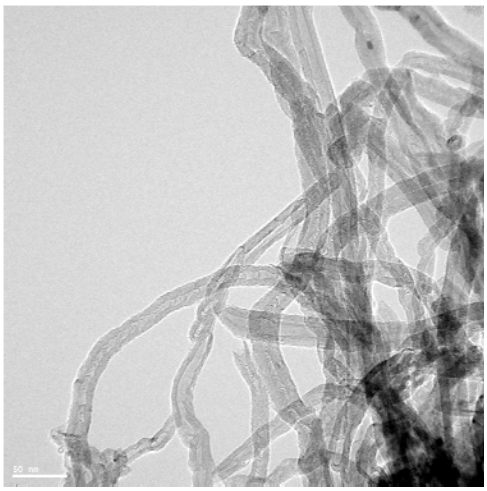

Figure 2-2: A transmission electron micrograph of MWCNTs dispersed in acetone by sonication at 240 W for few minutes. The scale bar shows 50nm.

In addition, they emphasized that the shear stress energy delivered to the nanotubes clusters during processing must exceed the van der Waals forces between the nanotubes in order to break the clusters and well disperse the nanotubes in the suspensions. If large aggregates are present in the structure of final nano-composites, they act as stress accumulators and diminish the mechanical properties. On the other hand, the presence of an interconnected network is necessary to make electrically conductive nano-composites. Thus, an efficient technique needs to be used to disperse nanotubes homogenously in the matrix while preserving the network structure for electrical conductivity.

In some cases, the addition of a surfactant, such as sodium dodecyl sulfate (SDS), sodium dodecyl benzene sulfonate (SDBS) or cetyl trimethyl ammonium bromide (CTAB) can improve the quality of dispersion and stability of CNT suspensions, by reducing the surface tension of the dispersing medium and improving the separation of nanotubes. In this thesis, SDS was used to well disperse CNTs in water in order to perform image analysis on their TEM micrographs and characterize their dimensions. The surfactant should be soluble in the

dispersing medium. This introduces a new challenge since it is difficult to find a surfactant for many polymer matrices. Moreover, the addition of surfactant can affect the rheological properties and diminish the electrical conductivity of the final nano-composites if it helps to improve the dispersion of the nanotubes and opens up their entanglements thoroughly.

Depending on the viscosity of the dispersing medium, different techniques can be used to disperse nanotubes. For high viscosity polymer matrices, twin-screw extrusion [Bose *et al.* (2007)], melt mixing in an internal mixer [Abbasi *et al.* (2009)] or micro-compounder [Abdel-Goad and Potschke (2005)] can be used. Usually a master-batch of high concentrated composite is diluted with the neat polymer at high temperatures. For relatively low viscosity matrices, mechanical stirring or sonication [Kim *et al.* (2006)] are used. Addition of a solvent can sometimes improve the dispersion quality since the solvent helps to reduce the viscosity of medium and facilitates the diffusion of particles [Lau *et al.* (2005)]. However, after mixing, the solvent needs to be removed which makes it a time-consuming and a non-environmentally friendly technique. In addition, some traces of solvent may remain in the suspension since by increasing the concentration of particles it is more difficult to evaporate the solvent. This can definitely influence the rheological properties of the suspensions. In a direct mixing technique, no solvent is involved but the quality of dispersion may not be perfect even when a combination of mechanical stirring and sonication techniques are used.

Another technique has been recently used which makes the dispersion of particles in polymer matrices more efficient. In this method, the particles are manually mixed with the dispersing medium with a spatula and then the mixture is poured between the rolls of a three roll mill where each two rolls rotate in opposite directions. The rotation speed and the gap size between the rolls can be adjusted by the user. By decreasing the gap size between the mills and circulating the sample in the mixer for a number of times, a relatively homogenous suspension

can be obtained. However, it should be noted that this technique is restricted to room temperature and is not suitable for volatile suspensions. A schematic of a three-roll-mill mixer is shown in Figure 2-3.

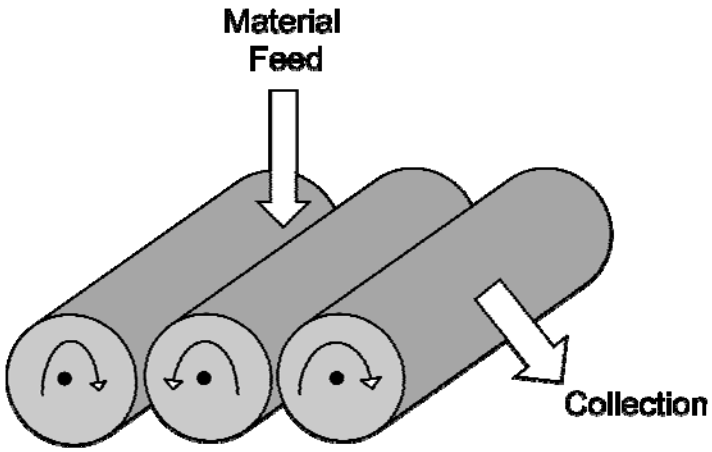


Figure 2-3: Schematic of a three-roll-mill.

A comparative study was performed to evaluate the dispersion quality of a 1 wt% MWCNT in an epoxy prepared by sonication with and without solvent and mixing in a three-roll-mill. The results are shown in Appendix A.

## 2.3 Rheology of CNT suspensions

CNTs are fibre-like nano-sized particles that are highly entangled in the absence of any surfactant or functional groups. Hence, there should be some similarities between their rheological behaviour and rheology of short fibre suspensions on one hand and nano-composites on the other hand. A great deal of research has been devoted to study the rheological properties of CNT suspensions. Different parameters have been shown to influence the rheology of CNT suspensions among which are concentration, surface treatment,

orientation, aspect ratio and flexibility of nanotubes as well as the dispersion quality of CNT suspensions.

Functionalization or surface treatment of carbon nanotubes can be performed by various techniques such as acid treatment, amine treatment or heat treatment [Lee *et al.* (2007)]. In the former technique, the nanotubes are passed through solutions of super acids for a number of times, then rinsed with deionised water and dried in vacuum at high temperature. As a result, the impurities such as amorphous carbons, graphite particles and metal catalysts are removed from the surface of nanotubes. In addition, some functional groups such as hydroxyl group (O-H) and carboxyl group (C=O) are introduced during the functionalization process. If the acid treated nanotubes are heated with octadecylamine (ODA) for few days and then washed in ethanol for a couple of times, (N-H) groups appear on the surface of nanotubes. Heat treatment can be performed by heating the pristine nanotubes at high temperature in air where hydroxyl groups appear on the surface of nanotubes.

Introduction of functional groups to the surface of nanotubes results in better dispersion of nanotubes in the suspensions (or polymer melts) and strong interactions between the polymer molecules and the nanotubes surface. Consequently, higher rheological properties, e.g. storage modulus and complex viscosity can be obtained [Song (2006); Lee *et al.* (2007)]. Furthermore, a strong attachment of nanotubes to polymer molecules via the functional groups allows more efficient stress transfer between CNT and the matrix which consequently improves the mechanical properties of the resulting composites [Kim *et al.* (2008)]. However, functionalization can cause morphological damages to the surface of nanotubes and reduce their length and their aspect ratio which consequently reduces their effectiveness as reinforcing agents. If this is the case, the rheological properties of surface treated CNT

suspensions are influenced by a compromise of the two effects as a result of functionalization [Fan and Advani (2007)].

Similar to fibre suspensions, the orientation state of nanotubes can influence their rheological properties. Du *et al.* (2004) showed that the SWNTs aligned by melt fibre spinning in poly-methyl-methacrylate (PMMA), have lower storage modulus than the isotropically dispersed nanotubes in the nano-composites. For initially aligned nanotubes in the flow direction, Abbasi *et al.* (2010) has recently shown that the complex viscosity significantly decreased and the rheological and electrical percolation thresholds increased remarkably.

The aspect ratio of nanotubes affects their hydrodynamic volume and so their rheological properties [Cipiriano *et al.* (2007); Xu *et al.* (2008); Wu *et al.* (2010)]. By increasing the nanotubes aspect ratio, their rheological properties such as storage modulus increase upon addition of small quantities of nanotubes to the polymer matrices. Xu *et al.* (2008) reported positive normal stress differences at high shear rates in low aspect ratio CNT-isotactic polypropylene (iPP) composites and negative normal stress differences in high aspect ratio CNT composites. The former was in-line with the observation of die swell during the extrusion process and latter with die shrinkage. Moreover, a percolated nanotube network forms at much lower concentrations as the aspect ratio increases [Cipiriano *et al.* (2007)]. Recently, Keshtkar *et al.* (2009) has shown that the onset of transition from dilute to semi-dilute and semi-dilute to concentrated regimes shifts to lower concentrations for different micron-size fibres when their aspect ratios increased. A similar behaviour is expected to be observed in CNT suspensions.

CNTs may act as rigid or flexible fibres depending on CNTs aspect ratio, the applied shear rate and the properties of the suspending medium. The flexibility of nanotubes can be verified

by the effective stiffness $S^{eff}$ from the following correlation proposed by [Switzer and Klingenberg (2003)] for fibres:

$$S^{eff} = \frac{E_Y \pi d^4}{64 \eta_s \dot{\gamma} L^4} \tag{2-1}$$

where, $E_Y$ is the fibre Young modulus, $d$ and $L$ are the fibre diameter and length, $\eta_s$ is the viscosity of the suspending medium and $\dot{\gamma}$ is shear rate. According to Switzer and Klingenberg (2003), $S^{eff}$ describes the relative importance of the fibre stiffness and the hydrodynamic torque in determining the bending of a fibre in shear flow. When $S^{eff} \to 0$ the fibres behave like flexible strings whereas for very large values $S^{eff} \to \infty$, the fibres become rigid and maintain their equilibrium shape during flow. The fibre flexibility can considerably affect the viscous and elastic properties of the suspensions. Keshtkar *et al.* (2009) has recently shown that by increasing the fibre flexibility, it is more difficult to align the fibres in the flow direction by calculating the required energy per unit volume for orienting the fibres. In this work, the CNTs that are dispersed in a low viscosity Newtonian fluid behave more like stiff fibres in the range of shear rates studied.

The dispersion quality of suspensions has a significant influence on their rheology. Conflicting results about the effect of the quality of nanotubes dispersion quality on the rheological properties of polymer melts and suspensions have been reported. Du *et al.* (2004) reported higher storage modulus with a low frequency plateau modulus in SWCNTs dispersed in poly-methyl- methacrylate (PMMA) with better dispersion and a liquid-like behaviour for poorly dispersed nanotube suspensions at similar concentrations. On the other hand, Song and Youn (2005) observed that the MWCNTs-epoxy nano-composites with poorly dispersed nanotubes exhibited higher storage modulus, loss modulus, and complex viscosity than the

ones with well dispersed nanotubes. It should be noted that the presence of very large clusters in suspensions (or polymer melts) can result in the arrest of flow and apparent large viscosities; in this case, the rheological measurements are flawed and unreliable. The origin of contradiction between the results of these two groups cannot be easily investigated since the particles dispersion is a qualitative matter. Besides, the mixing technique may have strongly influenced their rheological properties which make the comparison more difficult. Thus it seems necessary to develop more precise experimental procedures to well characterize the suspensions and make model suspensions, where their rheological properties do not depend on the choice of preparation condition or the type of materials.

Recent experimental studies show that flow induced flocculation in CNT suspensions is very common especially in confined geometries. Lin-Gibson *et al.* (2004) used rheo-optical studies and reported that the structure of carbon nanotube suspensions becomes unstable under weak shear by forming macroscopic domains of nanotube networks for a sufficiently small gap size. Using a wide range of concentration, shear stress and gap size (confinement), Hobbie and Fry (2006) obtained a universal non-equilibrium phase diagram that described a transition from solid-like networks to flowing nematics under an applied shear stress. At higher shear forces, the aggregates break down and the nanotubes orient in the flow direction while they mostly rotate in the flow gradient plane [Hobbie *et al.* (2003)]. The degree of anisotropy of nanotubes was quantified by Fry *et al.* (2005; 2006) who showed that anisotropy increased by increasing the shear stress due to the enhanced flow alignment at a constant concentration; furthermore, the anisotropy increased by increasing the concentration due to the rotational excluded volume interactions at a constant stress.

The previous rheo-optical analysis was used to establish a microstructure-property relationship by various light scattering techniques. However, these techniques are applicable

at relatively low concentrations. In addition, in most cases, the evolution of the microstructure has been investigated under flow, while the structural evolution does not end upon cessation of shear flow.

Kinloch *et al.* (2002) studied the evolution of the microstructure of a functionalized aqueous CNT suspension by means of linear viscoelastic measurements. They observed that the storage and loss moduli of the high concentration suspension approached to their initial values (before pre-shearing) within 1.5 h. However, no structural evolution was observed in a MWCNT suspension dispersed in epoxy after cessation of pre-shearing at high rates at 100 μm scale by Rahatekar *et al.* (2006). The apparent contradiction between both cases could be due to the fact that the evolution of the microstructure after cessation of shear flow is limited to local re-arrangements of particles at a submicron scale that could not be detected by rheo-optical techniques. This highlights the importance of rheological measurements in detecting small variations in the suspensions structure.

The majority of the previous work in literature has been focused to analyze the effect of various parameters on the structure and rheology of CNT suspensions. However, no attempt has been made to find out the mechanisms involved in the formation and evolution of structure, regardless of the system parameters. This is especially important when modeling the behaviour of these suspensions.

The inter-particle interactions increase with increasing concentration of nanotubes in the suspensions, which result in higher elasticities and shear viscosities. However, depending on the quality of dispersion and the concentration regime, the rheological properties may originate from the interactions between individual nanotubes or their clusters. If the CNTs are dispersed in a Newtonian fluid, the elasticity of the resulting suspensions can be attributed to the presence of nanotubes and the type of structure they form in the suspensions. It should be

noted that it is very difficult to relate the rheological properties to single tube interactions or their aggregates; however, one can verify the origin of the suspensions elasticity using the concept of scaling theory which will be briefly reviewed in the next section.

## 2.4 Scaling theory

Colloidal suspensions form a three dimensional network above their gel point; the properties of this network is dominated by the fractal nature of the flocs which are the building blocks of the system. Shih *et al.* (1990) developed a scaling theory for colloidal gels similar to the one for polymeric solutions. The basic concept in this theory is to relate the elastic properties of a gel to its network structure.

Fractal networks are formed of small flocs with diameter of $\xi$ and have a self-similar structure where the flocs fill the suspension volume as repeating units of the gel network. Figure 2-4 shows a schematic of a colloidal gel with a fractal structure.

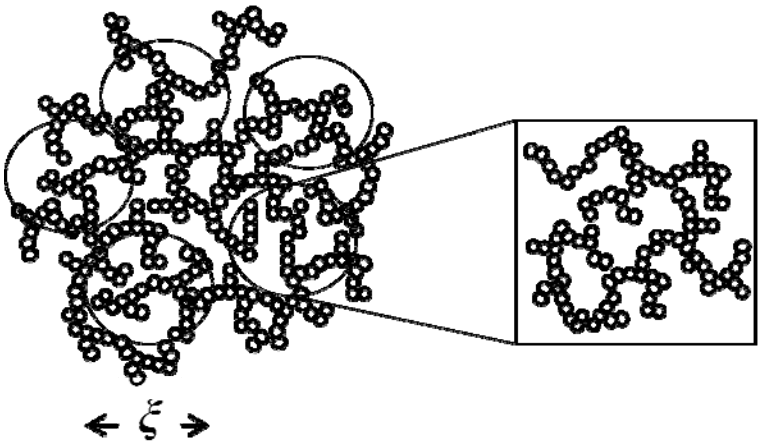


Figure 2-4: Schematic structure of a colloidal gel. The circles show the fractal flocs with the radius of $\xi$. The regions between flocs are considered as links. On the right, a schematic of the backbone structure of a floc is shown, which is a self-similar system with a different fractal dimension of $x$.

According to Shih *et al.* (1990) the average floc size $\xi$ is related to the particle concentration $\phi$; Approximating the concentration inside the flocs ($\phi_{\text{int}}$) as the overall particle concentration $\phi$ yields:

$$\xi \sim \phi^{1/(d_f - d)} \tag{2-2}$$

where $d_f$ and $d$ are the fractal and Euclidean dimensions, respectively. The backbone structure of flocs is assumed to be formed of linear chains with radius of gyration of $\xi$; each linear chain is formed of $N$ springs, where a spring represents a bond between two neighbouring particles. The backbone structure of a floc itself can be a self-similar system with a fractal dimension of $x$, which is smaller than that of the flocs and should exceed 1 to provide connected paths. The elastic constant of a linear chain of springs with the radius of gyration of $\xi$ is:

$$K_{chain} = \frac{K_0}{N\xi^2} \tag{2-3}$$

where $K_0$ is the bending constant between two adjacent springs and is assumed to be independent of particle concentration. The number of springs in a floc constituted of linear chains with the radius of gyration of $\xi$ can be estimated by:

$$N \sim \xi^x \tag{2-4}$$

Since the elastic properties of flocs are inherited from their backbone, one can approximate the elastic constant of the backbone $K_\xi$ with that of a linear chain with the radius of gyration of $\xi$ which yields:

$$K_\xi \sim \frac{K_0}{\xi^{2+x}} \tag{2-5}$$

According to this correlation, by increasing the floc size, the elasticity of flocs diminishes. Finally, for a system of size $L$, the macroscopic elastic constant can be written in terms of that of the individual flocs as:

$$K_L \sim \left[\frac{L}{\xi}\right]^{d-2} K_\xi \tag{2-6}$$

where $K_L$ is the storage modulus of the suspension. The degree of compactness of the network structure of gels can be identified by its fractal dimension $d_f$, which strongly depends on the aggregation mechanism. For fast aggregation, where flocs grow by merging into one another as soon as they collide, $d_f$ = 1.7–1.8 similar to the one for cluster–cluster aggregation and $d_f$ = 2.0–2.2 for slow aggregation or the so-called reaction limited aggregation where flocs penetrate to one another partially after collision [Larson (1999)].

The elastic constant of flocs may be different from that of the links between flocs. Based on that, Shih *et al.* (1990) defined two regimes of strong-link and weak-link. In the former, the macroscopic elastic constant of the system is dominated by the elastic constant of the flocs $K_\xi$ whereas in weak-link regime, it is controlled by the elastic constant of the links between flocs. In addition, in weak-like region $K_L$ (or $G'$) increases more slowly compared to strong-link region and $\gamma_c$, the strain for the limit of linearity, increases with increasing particle concentration while it decreases with increasing concentration in strong-link region. The correlations for strong-like and weak-link regions are summarized as the following:

strong-link region: $\begin{cases} G' \sim \phi^{(d+x)/(d-d_f)} \\ \gamma_c \sim \phi^{-(1+x)/(d-d_f)} \end{cases}$ weak-link region: $\begin{cases} G' \sim \phi^{(d-2)/(d-d_f)} \\ \gamma_c \sim \phi^{1/(d-d_f)} \end{cases}$

The scaling theory developed by Shih *et al.* (1990) was shown to be in good agreement with many different colloidal gels such as boehmite alumina gels, Catapal and Dispal powders

[Shih *et al.* (1990)], casein gels [Chaplain *et al.* (1994)], fat crystal networks [Narine and Marangoni (1999)] and so on. However, in some cases, this scaling theory fails by predicting a negative value for the fractal dimension *x* of clusters. On the other hand, Wu and Morbidelli (2001) defined a macroscopic elasticity which comes from the contributions from inter- and intra-floc links. As a result, $K_\xi$ in Eq. (2-6) should be replaced by $K_{eff}$ given by:

$$\frac{1}{K_{eff}} = \frac{1}{K_\xi} + \frac{1}{K_l} \tag{2-7}$$

where $K_\xi$ and $K_l$ are the intra-floc and inter-floc elastic constants respectively. By approximating $1/(1+K_\xi / K_l)$ with $(K_l / K_\xi)^\alpha$ where $\alpha \in [0,1]$ and substituting this correlation into (2-6) and (2-2), the final correlation for the macroscopic elasticity with particle concentration can be obtained as:

$$G' \sim \phi^{\frac{\beta}{d-d_f}} \tag{2-8}$$

where

$$\beta = (d-2) + (x+2)(1-\alpha) \tag{2-9}$$

Similarly, the critical strain for the maximum limit of linearity was approximated by:

$$\gamma_c \sim \phi^{-n} \sim \phi^{\frac{d-\beta-1}{d-d_f}} \tag{2-10}$$

For $\alpha = 0$, correlations (2-8) and (2-10) reduce to that of Shih *et al.* (1990) for the strong-link region and for $\alpha = 1$, they lead to the ones for weak-link region.

Hobbie and Fry (2007) and Mobuchon *et al.* (2009) approximated the apparent yield stress of a suspension with its low-frequency plateau storage modulus as:

$$\tau_y = G' \gamma_c \tag{2-11}$$

Thus, from Eq. (2-11), the following correlation can be obtained which relates the apparent yield stress to concentration:

$$\tau_y \sim \phi^{\frac{d-1}{d-d_f}} \tag{2-12}$$

The deformation and breakup of colloidal aggregates under shear flow was modeled and simulated by Potanin (1993) who classified the aggregates into rigid and soft. The interaction potential of particles is non-central in rigid aggregates and is expressed by a function of angles between neighbouring bonds. Furthermore, rigid aggregates respond elastically to small deformations. The elastic response is distinguished by an elastic modulus and a yield stress that are related to each other and are correlated to the radius of gyration ($\xi$) and the internal concentration ($\phi_{\text{int}}$) in a power-law form as:

$$G' \sim \tau_y \propto \xi^{-\gamma} \propto \phi_{\text{int}}^{\gamma_1} \tag{2-13}$$

From Eq. (2-2) $\phi_{\text{int}} \sim \xi^{(d_f - d)}$ and therefore the power-law exponent $\gamma_1$ which relates the storage modulus to the concentration is:

$$\gamma_1 = \gamma/(3-d_f) \tag{2-14}$$

where, $d$ equals 3.

On the other hand, in soft aggregates, the interaction potential of particles is purely central and depends on the distance between the centers of the adjacent particles. In addition, the internal structure of the soft aggregates does not elastically respond to small deformations. Potanin (1993) suggested that in general, the interaction potential of spherical particles is a superposition of central and non-central components.

Sonntag and Russel (1986; 1987) showed that the radius of gyration of aggregates decrease with shear rate in a power-law form as:

$$\xi \sim \dot{\gamma}^{-m} \tag{2-15}$$

where $m$ was characterized to be in the range of 0.23-0.29 for purely rigid aggregates ($m_{rigid}$) and about 0.4-0.5 for purely soft aggregates ($m_{soft}$) by Potanin (1993). He showed that the exponents $m_{rigid}$, $\gamma$ and $\gamma_1$ can be related to the exponents characterizing the geometrical properties of the internal aggregates structures and its backbone such as their fractal dimension. By comparing the simulation results with some experimental results, he indicated that the expected value of *m* for different suspensions should remain in the range of [$m_{rigid}$, $m_{soft}$].

## 2.5 Thixotropic models

Thixotropic behaviour as a time-dependent phenomenon has been commonly observed in many flocculating suspensions with technical and industrial applications such as paints, personal and chemical products and precursors. Mewis (1979) and more recently Barnes (1997) have broadly reviewed this subject. In general, thixotropy has been referred to "the reversible changes from a flowable fluid to a solid-like elastic gel". The structure of thixotropic suspensions breaks down by shearing and reconstructs upon cessation of shear forces. This makes their processing and handling very challenging. The time scales involved during structure break down and build-up range from many minutes to many hours respectively [Barnes (1997)]. To better understand the thixotropic behaviour of suspensions

and their structural evolutions during and after processing, a number of models have been proposed by many researchers.

Dullaert and Mewis (2006) have briefly reviewed and classified thixotropic models in three categories: a continuum mechanics approach, a micro-structural and a structural kinetics ones. In the former, a time-dependent yield surface and/or a time-dependent viscosity function are introduced to the existing models such as Bingham equation. However in this category, the model parameters are not associated with the physical mechanisms involved in structural changes. An example of these models is given in Montes *et al.* (1988). On the contrary, the micro-structural thixotropic models take into account the physical mechanisms involved during structure build-up and breakdown of aggregates such as the ones developed in de Rooij *et al.* (1993), Potanin (1993) and Potanin *et al.* (1995). However, these models are limited to very dilute systems due to their high computational cost. Moreover, knowledge of the physical mechanisms involved in structural variations is nontrivial in many practical cases. In structural kinetic models, a parameter is introduced which represents the instantaneous state of the structure. The rate of the variation of this structural parameter is defined in a kinetic equation which needs to be solved with a constitutive equation relating the shear stress to the structural parameter, shear rate and time. An advantage of the structural kinetic models is that they are applicable over a wide range of concentrations. To make a new structural model, one can use a non-linear variant of an ordinary viscoelastic equation such as the Maxwell or the Jeffrey model as a basic constitutive equation and incorporate a viscoelastic contribution of the structural parameter to the stress.

An example of a structural kinetic model is the one presented by Yziquel *et al.* (1999) where the shear stress is described by a modified form of the upper convected Jeffreys model as it follows:

$$\frac{\delta}{\delta t}\left[\frac{\sigma}{G(\xi)}\right]+\frac{\sigma}{\eta(\xi)}=\left(1+\frac{\eta_\infty}{\eta(\xi)}\right)\dot{\gamma}+\eta_\infty\frac{\delta}{\delta t}\left(\frac{\dot{\gamma}}{G(\xi)}\right) \tag{2-16}$$

In this equation, $\delta/\delta t$ is the upper convected derivative and is defined as:

$$\frac{\delta\sigma_i}{\delta t}=\frac{d\sigma_i}{dt}-\nabla v.\sigma_i-\sigma_i.(\nabla v)^{\mathrm{T}} \tag{2-17}$$

where, $\nabla v$ is the velocity gradient and $(\nabla v)^{\mathrm{T}}$ is the transpose of the velocity gradient. $\sigma$ is the shear stress, $t$ is time, $\dot{\gamma}$ is the shear rate and $\eta_\infty$ is the viscosity of the destroyed structure. The structural parameter, $\xi$, describes the evolution of suspension structure through a kinetic equation quantitatively and varies between 1 for completely structured suspensions and 0 for completely destroyed structure. $G(\xi)$ and $\eta(\xi)$ are the structured modulus and viscosity, which are defined in Eq. (2-18) and Eq. (2-19), respectively.

$$G(\xi)=G_0\xi+G_\infty \tag{2-18}$$

where, $G_\infty$ is the elastic modulus of the destroyed structure and $G_\infty + G_0$ (when $\xi = 1$) is the equilibrium value of the elastic modulus of the structure.

$$\eta(\xi)=\frac{\eta_0}{f(\xi)} \tag{2-19}$$

where, $\eta_0$ is a characteristic viscosity and f($\xi$) is an empirical structural function defined so that the elastic behaviour is predicted at very small strains and the steady shear viscosity is described in a power-law form with a limiting high shear viscosity. The definition of f($\xi$) relies on the choice of the kinetic equation. Yziquel *et al.* (1999) proposed three kinetic

equations. In each one of those, the evolution of the structure is a balance between the structure build-up and breakdown. The former is governed by Brownian motion and is proportional to the number of physical bonds in the system, being expressed as (1-$\xi$). The kinetic equations proposed by Yziquel *et al.* (1999) are different in the term describing the rate of structure break down. In the first equation, the breakdown of the structure is controlled by the second invariant of the rate of strain tensor. In the second one, it is assumed that the structure evolution is associated with the stored elastic energy in the system. However, in the third one, the structure breaks down due to the rate of flow-induced energy dissipation. The latter kinetic equation which is also called the energy dependent equation, has been shown to better perform in predicting the behaviour of flocculating suspensions by Yziquel *et al.* (1999).

f($\xi$) can be defined as the following for this type of kinetic equation:

$$f(\xi) = \left(\frac{1}{\xi} - 1\right)^{(1-n)/(1+n)} \tag{2-20}$$

where, $n$ is an empirical power-law coefficient. The so-called energy dependent kinetic equation yields:

$$\frac{\lambda_0}{k_1}\frac{\partial \xi}{\partial t} = (1-\xi) - \frac{{\lambda_0}^2}{\eta_0}\frac{k_2}{k_1}\xi\left|\sigma : \dot{\gamma}\right| \tag{2-21}$$

where, $\lambda_0 = \eta_0/(G_0 + G_\infty)$ is a characteristic time related to the particle interactions. $k_1$ and $k_2$ are two kinetic constants that control the rate of the structure build-up and the structure breakdown, respectively. In Eq. (2-21) the flow-induced structure breakdown due to the energy dissipation is expressed by ($\left|\sigma : \dot{\gamma}\right|$). The model has seven parameters including $\eta_0$, $\eta_\infty$, $G_0$, $G_\infty$, $k_1$, $k_2$ and $n$.

In this thesis, the Yziquel *et al.* (1999) structural model in conjunction with the energy dependent equation (2-21) have been used to evaluate the thixotropic behaviour of carbon nanotube suspensions at various flow conditions.

The model parameters should be obtained from a minimization procedure. It should be noticed that finding the best fit is non-trivial and the model convergence strongly depends on the initial guess for the fitting parameters. However, some parameters can be obtained from the experiments to reduce the number of fitting parameters. Initially, the steady shear results should be compared with the model predictions. According to Eq. (2-16), the steady-shear viscosity can be defined by:

$$\eta(\dot{\gamma}) = \frac{\sigma_{12}}{\dot{\gamma}} = \eta_\infty + \left[ \eta_0 \left( \lambda_0 \sqrt{\frac{k_2}{k_1}} \right)^{n-1} \right]^{\frac{2}{n+1}} \left( \eta(\dot{\gamma})\dot{\gamma} \right)^{\frac{n-1}{n+1}} \tag{2-22}$$

where, $n$ is the power-law exponent. $\eta_0(\sqrt{k_2/k_1}\lambda_0)^{n-1}$ can be referred to $m$ hereafter for simplicity. Eq. (2-22) is an implicit equation in terms of $\eta(\dot{\gamma})$ and should be solved in an iterative procedure. From curve fitting of the steady shear results, $m$, $n$ and $\eta_\infty$ can be obtained. By keeping these three parameters constant, the fitting parameters for transient stress growth results will be reduced to $G_0$, $G_\infty$, $k_1$ and $k_2$. From $m$ and the other four parameters, $\eta_0$ can then be estimated. The elastic modulus of the destroyed structure, $G_\infty$, can be set equal to the storage modulus of the neat polymer or zero in case of an inelastic dispersing medium.

$G_0 + G_\infty$ is the frequency independent storage modulus of the suspensions that can be obtained from experiments. However, in some cases, the low frequency plateau modulus is not accessible. In that case, $G_0$ should be considered as a fitting parameter. The thixotropic behaviour of the suspensions is controlled by $k_1$. It directly influences the rate of the stress

relaxation and structure build-up at rest. On the other hand, $k_2$ determines the rate of flow-induced structure break down and $k_2/k_1$ controls the steady-state stress. $k_1$ and $k_2$ are determined from curve fitting.

# CHAPITRE 3 SUMMARY OF ARTICLES

This thesis is composed of three articles which are presented in the following chapters. Initially, the effect of flow history on linear viscoelastic (LVE) properties as well as the evolution of the structure in MWCNT-epoxy suspensions has been extensively shown in Chapter 4. The details of material characterization and sample preparation before rheological measurements are elaborated. Moreover, the technique used to determine the concentration regimes is presented in this chapter. The kinetics of structure build-up after cessation of pre-shearing is analyzed under the influence of pre-shearing rate, concentration and temperature. Finally the importance of Brownian forces as a possible mechanism for structure build-up in the absence of flow was evaluated.

In Chapter 5, the concept of scaling and fractal theories is employed to examine the variations of microstructure of suspensions under the influence of flow history and temperature. It has been shown the flow-induced storage modulus of the metastable suspensions structure scaled with the applied pre-shearing rate for a wide range of concentrations. Using these theories, fruitful information was obtained about the nature of network structure of the suspensions, the origin of their elasticity and the type of interaction potentials in the suspensions. Since the application of light scattering techniques is limited to very dilute systems, the approach introduced in this chapter is very helpful to characterize the microstructure of the opaque CNT suspensions.

By further analysis on the effect of flow history on the storage modulus of the metastable structures in Chapter 6, it has been shown that at low and intermediate concentrations, there is a critical shear rate which is the limit for pre-shearing rate to avoid the break down in nanotube entanglements. The transient response of the suspensions is later analyzed below

and above the critical shear rates to evaluate the extent of structural reconstruction in quiescent upon cessation of transient flow. The results are then compared with predictions of a structural kinetic model and the mechanisms of structure evolution are verified.

# CHAPITRE 4 EFFECT OF FLOW HISTORY ON LINEAR VISCOELASTIC PROPERTIES AND THE EVOLUTION OF THE STRUCTURE OF MULTIWALLED CARBON NANOTUBE SUSPENSIONS IN AN EPOXY

Fatemeh Khalkhal and Pierre J. Carreau

*Department of Chemical Engineering, Center for Applied Research on Polymers and Composites (CREPEC), Ecole Polytechnique, P.O. Box 6079, Stn Centre-Ville, Montreal QC H3C 3A7, Canada*

Gilles Ausias

*Laboratoire d'Ingénierie des Matériaux de Bretagne (LIMATB), UBS, Université Européenne de Bretagne, rue de St. Maudé, 56325 Lorient, France*

J Rheol 55(1), 153-175 January/February (2011)

 (DOI: 10.1122/1.3523628)

## Synopsis

This paper analyzes the effect of flow history on the linear viscoelastic properties of suspensions of multiwalled carbon nanotubes in an epoxy as well as the evolution of the suspension microstructure under small deformations for different concentrations and temperatures. The effect of the flow history on the microstructure is interpreted in the light of the variation of the rheological percolation threshold, which is shown to increase with the pre-shear rate. After cessation of the shear flow, the storage modulus increased with time revealing the build-up of the structure. By decreasing the pre-shear rate, the resulting storage modulus increased and the relative increase of the storage modulus with respect to the pre-shear rate was more pronounced at lower concentrations. The rate of increase in the storage modulus drastically increased with the concentration and temperature while its variation with respect to the pre-shear rate depended on the concentration. In dilute suspensions, it decreased dramatically by increasing the rate of pre-shear, revealing a slower structure build-up while it remained almost intact in more concentrated suspensions. The increase in kinetics of structure build-up with temperature suggests the importance of Brownian forces in the absence of flow regardless of concentration or applied pre-shear rate.

## 4.1 Introduction

Carbon nanotubes (CNTs) have been the subject of interest since their discovery and have been used to enhance different physical properties of polymer composites such as electrical conductivity [Dufresne *et al.* (2002); Ounaies *et al.* (2003); Sandler *et al.* (2003); Kharchenko *et al.* (2004); Kim *et al.* (2005); Zhang *et al.* (2006); Kota *et al.* (2007); Bangarusampath *et al.* (2008)], mechanical properties [Allaoui *et al.* (2002); Bai and Allaoui (2003); Gojny *et al.*

(2004); Gojny *et al.* (2005)], thermal properties [Lau *et al.* (2005); Ding *et al.* (2006); Miyagawa *et al.* (2006); Park *et al.* (2007); Shen *et al.* (2007); Nanda *et al.* (2008)] and fire retardancy [Schartel *et al.* (2005); Cipiriano *et al.* (2007); Kashiwagi *et al.* (2008)]. To make multi-functional nano-composites and control their processing, it is important to understand their rheology.

The rheology of CNT suspensions have been studied by many researchers [for example see the work of Kinloch *et al.* (2002); Potschke *et al.* (2002); Du *et al.* (2004); Abdel-Goad and Potschke (2005); Huang *et al.* (2006); Fan and Advani (2007); Hobbie and Fry (2007); Lee *et al.* (2007); Ma *et al.* (2008); Tiwari *et al.* (2009)]. As for fibre suspensions, different parameters have been shown to affect the rheology of CNT suspensions among which are the aspect ratio, concentration, surface treatment and network structure of CNTs [Du *et al.* (2004); Song (2006); Fan and Advani (2007); Bose *et al.* (2008); Xu *et al.* (2008); Wu *et al.* (2009)] as well as the orientation state of CNTs [Hobbie *et al.* (2003a; 2003b); Hobbie (2004); Fry *et al.* (2005); Fry *et al.* (2006); Hobbie and Fry (2006); Pujari *et al.* (2009)] and the dispersion quality of CNT suspensions [Song and Youn (2005); Huang *et al.* (2006); Fan and Advani (2007)]. Depending on their aspect ratio and the properties of the suspending medium in the applied shear rate, CNTs can act as rigid or flexible fibres.

Recent theoretical studies of Schmid *et al.* (2000) and of Switzer III (2002) show that fibres can flocculate even in the absence of attractive inter-particle forces provided that they are stiff enough and interact through a sufficiently large coefficient of friction. A similar flow induced aggregation has been observed for CNT suspensions. Lin-Gibson *et al.* (2004) reported the formation of “macroscopic domains of diffuse nanotube networks” under weak shear for a sufficiently small gap size in a suspension of semi-dilute MWCNTs in a polyisobutylene

(PIB). By decreasing the gap size or the applied shear stress, the clusters formed a periodic pattern of nanotube bands in the flow-vorticity plane. These studies were later extended by Hobbie and Fry (2006) over a wider range of concentrations and shear stress at different gap sizes. They reported a universal non-equilibrium phase diagram that described a transition from solid-like networks to flowing nematics under an applied shear stress.

Although the microstructure of CNT suspensions becomes unstable at low shear rates because of flocculation, the application of high shear forces can destroy the aggregates and orient the tubes in the flow direction like rigid rods and other fibre suspensions. The extent to which the shear response of CNTs is similar to that of macroscopic fibres has been shown to depend on the Deborah number (*De*) by Hobbie *et al.* (2003b) in polymers with different viscoelastic properties. The structural anisotropy of a semi-dilute CNT suspension was quantified by Hobbie *et al.* (2003a) under steady shear flow who reported CNT alignment in the flow direction while they mostly rotated within the flow gradient plane. Fry *et al.* (2005; 2006) established a relationship between the anisotropy of sheared CNT suspensions and nanotube concentration, aspect ratio as well as shear rate and the viscosity of the suspending medium. They have quantitatively shown that, at a constant concentration, the degree of anisotropy increased as the shear stress increased due to the enhanced flow alignment; at a constant stress, by increasing the concentration, the anisotropy increased due to the rotational excluded volume interactions.

The extensive work performed to verify the degree of flocculation, de-flocculation and orientation of CNTs, was used to establish a relationship between the microstructure and rheology of these suspensions by various light scattering techniques. However, it should be noted that these techniques are restricted to very low concentrations. Another interesting

common point in all of these studies is that the evolution of the microstructure has been investigated under flow, while the structural evolution does not stall after cessation of shear flow. It is important to know how much time a suspension requires to re-establish its microstructure after being prepared and before curing in the case of an epoxy.

One of the micro-structural studies of suspensions upon cessation of shear forces can be traced back to 1997 [Rueb and Zukoski (1997)] where the evolution of the microstructure of a thermo-reversible silica gel was investigated by means of linear viscoelastic measurements. The authors reported that the storage modulus $G'(t)$ increased with the elapsed time upon cessation of shear flow in the following form:

$$G'(t) = G'_{\infty}[1 - \exp(-\alpha t)] \tag{4-1}$$

where $G'_{\infty}$ is the equilibrium value and $\alpha$ is a fitting parameter. However, such structure build-up was not detected by small angle neutron scattering (SANS) patterns. They reported that the equilibrium storage modulus ($G'_{\infty}$) and its rate of increase ($\alpha$) in Eq. (4-1) scaled with the volume concentration. Similar structure builds-up have been observed by Derec *et al.* (2003) and Coussot *et al.* (2006) in colloidal pastes at small deformations upon cessation of shear flow. Kinloch *et al.* (2002) observed the evolution of an aqueous functionalized nanotube suspension at near rest conditions (at 10 rad/s and stress amplitude of 1 Pa). They observed that the storage and loss moduli of a high concentration suspension recovered to their initial values within 1.5 h. On the other hand, Rahatekar *et al.* (2006) probed the microstructure of a 0.35 wt% CNT suspension in an epoxy by rheo-optical techniques during 1 h rest after shearing at high rates and did not observe any change in the microstructure at 100 μm scale. The apparent contradiction between the observations of Rahatekar *et al.* (2006) and Kinloch *et*

*al.* (2002) could be due to the fact that the evolution of the microstructure after cessation of shear flow is limited to local re-arrangements of particles at a submicron scale that could not be detected by rheo-optical techniques in CNT suspensions or SANS in silica gels [Rueb and Zukoski (1997)]. This highlights the importance of rheological measurements in detecting small variations in the suspensions structure. More recent studies on a non-aqueous layered silicate model suspension by Mobuchon *et al.* (2007; 2009) led to the characterization of the microstructure after various pre-shear histories and they showed that the characteristic length scale ($\xi_0$) of the clusters decreased as the pre-shear rate increased.

While the previous research is a primary step toward the establishment of a relationship between the evolution of the microstructure and the suspension rheology at small deformations, they have been mostly restricted to a single concentration or a limited range of concentration above the gel point. Hence, a more in-depth analysis on the influence of the flow history on the suspensions microstructure and its growth rate at various concentrations is necessary. Indeed, the Brownian forces that are not important during flow at high Peclet numbers ( $Pe > 1$ ), may play a role in the structure build-up of suspensions at rest that have not been evaluated previously.

In this paper, the effect of flow history on linear viscoelastic properties of multiwalled carbon nanotube (MWCNT)-epoxy suspensions as well as the evolution of the suspensions microstructure is analyzed at very small deformations to probe the influence of concentration and temperature and obtain a quantitative relationship between these variables. A wide range of concentration (from dilute to concentrated regime) is considered which makes it possible to derive a relation between the rheological percolation threshold and the applied pre-shear rate.

Furthermore, the rate of structure build-up is analyzed as a function of the applied pre-shear rate, the concentration (below and above the percolation threshold) and temperature.

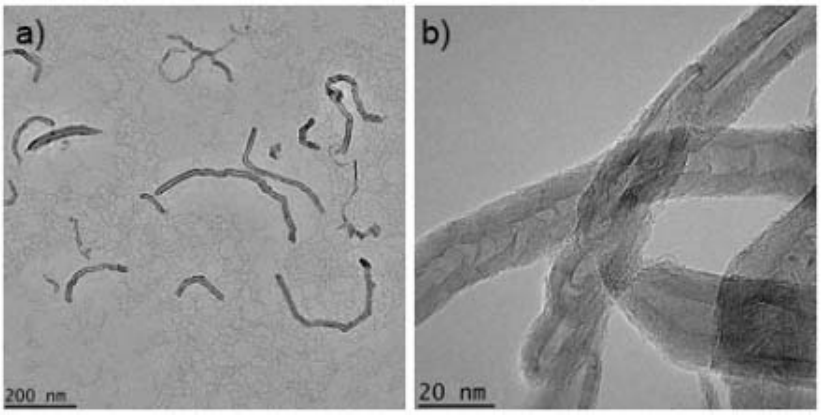


Figure 4-1: (a) TEM micrographs of MWCNTs. (b) Higher magnification of some overlapped MWCNTs.

The article is organized as follows. Initially, the CNTs are characterized using transmission electron microscopy and image analysis in Sec.4.2 to obtain the length and outer diameter distributions for the CNTs. We stress that there is limited information on CNT length and diameter distribution in the literature. These data are used to elaborate the limits of our investigation, including the concentration regimes of the suspensions, the effective stiffness of nanotubes and the rotary diffusion coefficient. To better understand the effect of flow history on the structure, the suspension properties such as the linear viscoelastic properties before pre-shearing need to be verified, which are summarized in Sec.4.3. In Sec.4.3.1, the influence of the flow history on the storage modulus is investigated over a wide range of frequencies at a single concentration followed by the results of the evolution of the suspensions microstructure upon cessation of shear flow at a single frequency and a wide range of concentrations. The latter results are further analyzed in Sec.4.3.2 from a structural point of view followed by the

effect of temperature on the evolution of suspensions microstructure. Finally, the concluding remarks are summarized in Sec.4.4.

## 4.2 Materials and their characterization

An epoxy Epon 828 (HEXION$^{TM}$ Specialty Chemicals Inc.) with a density of 1.16 g/mL and viscosity of 12.33 Pa.s (at 25$^{o}$C) was used as the dispersing medium and suspensions of nanotube-epoxy were prepared by mixing using an EXAKT three roll mill (from EXAKT TECHNOLOGIES. INC. located in Concordia Composite Lab) at room temperature.

Multiwalled carbon nanotubes (MWCNTs) from Cheap Tubes Inc.© were initially characterized by transmission electron microscopy. For this purpose, the entangled nanotubes were dispersed in an aqueous solution of sodium dodecyl sulfate (SDS). After evaporation of the solvent, the nanotubes were characterized by TEM. Figure 4-1 shows micrographs of some nanotubes. We remark that the tubes are bent. An image analysis software (Clemex Vision$^{TM}$) was used to estimate the dimensions of the nanotubes, using raw TEM images. The inner (*ID*) and outer diameter (*OD*) of nanotubes were around 5-10 nm and 7-25 nm, respectively, and their length (*L*) was obtained by taking into account the bending of nanotubes and was in the range of 0.1-2.2 μm. Figure 4-2 shows the distributions of *OD* and *L* of the nanotubes after image analysis. The polydispersity index (PDI) was calculated using the number and weight-average *L* and *OD* of CNTs. The length of more than 300 CNTs was measured and the PDI for *L* was found to be 1.25. However, it was not that simple to measure the *OD* of CNTs, as higher magnification TEM images were required and some scattered light from the edges of individual nanotubes made a precise measurement of *OD* more challenging.

As a result the *OD* was measured for only 30 particles and the PDI was found to be around 1.025. The aspect ratio is hence in the range of 4-314.

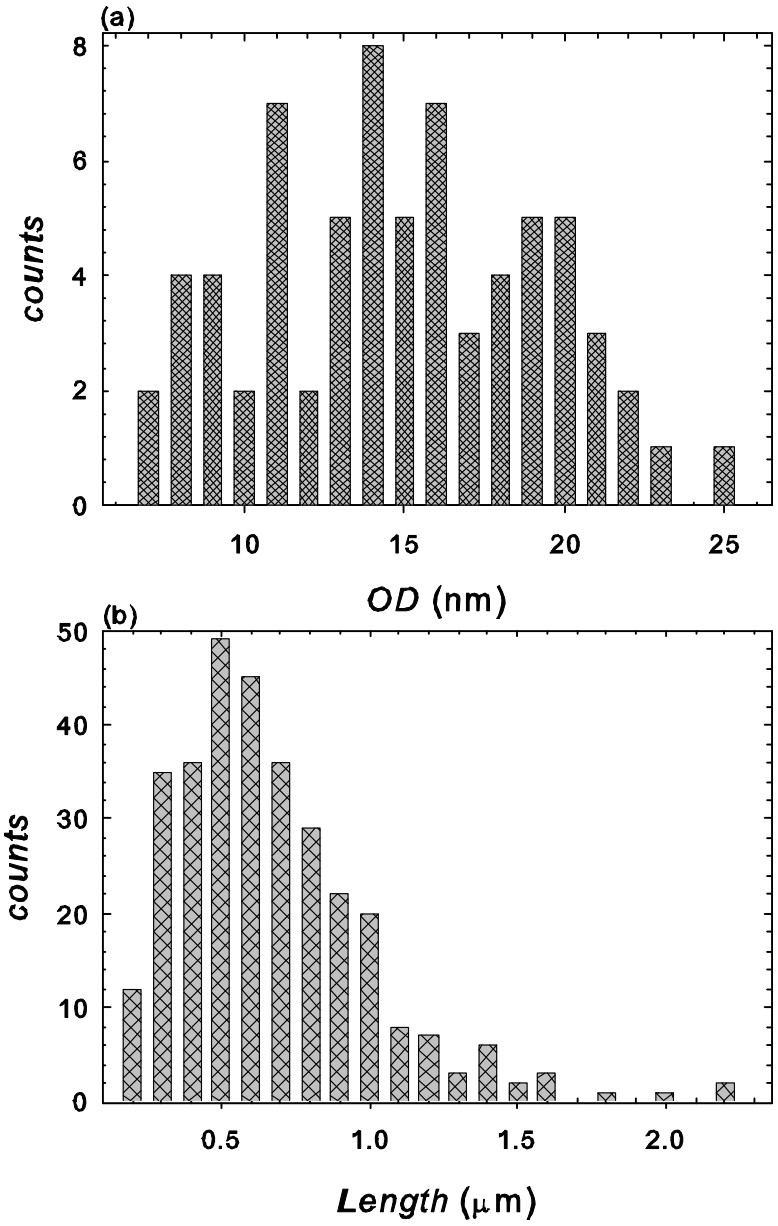


Figure 4-2: (a) Outer diameter (*OD*) and (b) length (*L*) distribution of MWCNTs obtained by image analysis on TEM results using Clemex$^{TM}$ Vision software.

In order to quantify the flexibility of the nanotubes for the range of shear rates studied ( $0.01\,\mathrm{s}^{-1} \le \dot{\gamma} \le 100\,\mathrm{s}^{-1}$), the effective stiffness $S^{eff}$ was calculated using the following expression proposed by Switzer and Klingenberg (2003):

$$S^{eff} = \frac{E_Y \pi d^4}{64 \eta_s \dot{\gamma} L^4} \tag{4-2}$$

where $E_Y$ is the Young modulus of the nanotubes and is considered to be 40 GPa according to Hobbie and Fry (2007), compared to nylon ($E_Y$ ~1.5-2 GPa), PVA ($E_Y$ ~26 GPa) and Vectran ($E_Y$ ~ 76 GPa) [Keshtkar *et al.* (2009)], $d$ (~14.86 nm) and $L$ (~670 nm) are mean values of the outer diameter and length of the nanotubes (average values obtained from Figure 4-2); $\eta_s$ is the viscosity of the suspending medium (~12.33 Pa.s for the neat epoxy at room temperature) and $\dot{\gamma}$ is the shear rate. According to Switzer and Klingenberg (2003), the effective stiffness describes the relative importance of the fibre stiffness and the hydrodynamic torque in determining the bending of a fibre in a shear flow. When it tends to zero, the fibres behave like flexible strings whereas for very large values ($S^{eff} \to \infty$), the fibres become rigid and maintain their equilibrium shape during the flow. The value of $S^{eff}$ is so estimated to be in the range of 0.385 to 3850, compared to the values for nylon fibres with large aspect ratio ($S^{eff}$ ~0.001 ) and Vectran with low aspect ratio ($S^{eff}$ ~ 1000) [Keshtkar *et al.* (2009)]. The effective stiffness of the CNTs is large enough to categorize them among rigid rods.

To prepare the suspensions, the CNTs were mixed as received with the epoxy. No surfactants or additives were added during the preparation of the suspensions. The concentrations were varied from 0.5 wt% to 5 wt%. In order to calculate the volume fractions, it was assumed that the density of CNTs is equal to the density of graphite of about 2.

The samples were mixed initially by hand and then were poured into the three roll mill (3RM). The speed of the mixer was maintained at 150 rpm. The gaps between the mill rolls were equally set at different sizes and were reduced gradually from 100 μm to 5 μm in order to break large CNT aggregates and obtain more homogenous suspensions. Each sample was circulated between the gaps of the rolls once at the 100 μm and 50 μm gap sizes, twice at the 20 μm and 10 μm gap sizes and four times at the 5 μm gap size.

To verify the dispersion quality of the prepared samples, electron microscopic images of cured epoxy-CNT suspensions have been used by some researchers [Song and Youn (2005); Fiedler *et al.* (2006); Abdalla *et al.* (2007); Yuen *et al.* (2007)], which may not be a proper representative of the suspension microstructures as the curing process may change the local arrangement of nanotubes, their aggregates in clusters and the suspension microstructure to some extent. For this reason, we only used optical microscopy to verify the dispersion quality of our suspensions. Optical micrographs of 0.5 wt% and 1 wt% suspensions are shown in Figure 4-3. The darker areas show CNT clusters and the lighter area is the neat epoxy. From the micrographs, a good homogeneity of the dispersions can be observed at the 200 μm scale. As the concentration increases from 0.5 wt% to 1 wt%, small aggregates appear in non-isometric domains probably due to the excluded volume interactions. It was not possible to observe the microstructure of suspensions at larger concentrations by optical microscopy. The reproducibility of the rheological results was then considered as a criterion for the homogeneity of the suspensions.

The relative importance of the Brownian forces to shear forces was assessed using the Peclet (*Pe*) number calculated by the following expression [Larson (1999)]:

$$Pe = \frac{\pi \eta_s L^3 \dot{\gamma}}{3k_B T\left[\ln(L/d) - 0.8\right]} \tag{4-3}$$

where $k_B$ is the Boltzman constant and $T$ is the temperature. In the range of shear rates studied here, ($0.01\,s^{-1} \le \dot{\gamma} \le 100\,s^{-1}$), the $Pe$ values range from 3.13 up to 31000 and so the suspensions can be considered as non-Brownian under flow. $Pe$ can be taken as the ratio of $\dot{\gamma} / D_r$, where $D_r$ is the rotational diffusion coefficient. In this case, $D_r$ is equal to 0.0032 $s^{-1}$ in the dilute regime and the characteristic time of one particle Brownian rotation is so estimated to be $1/D_r \sim 314$ s. The CNTs used in this study are quite short compared to the ones used by Rahatekar *et al.* (2006), which were in the range of $L \sim 25$ μm. As a result, the corresponding rotational diffusion coefficients ($D_r$) for our CNTs are much higher and Brownian forces might be important in the absence of flow.

A Physica MCR501 (Anton Paar) rheometer with a parallel plate geometry (PP50 with the diameter of 49.96 mm) and 1 mm gap was used to perform the rheological measurements. The temperature was controlled by a Peltier (P-PTD 200) system. Steady shear viscosity measurements were performed at different gaps (0.8, 1 and 1.2 mm) to prove the absence of wall slip or wall effects during the experiments. In order to prevent the aging effect, all the experiments were performed two days after the sample preparation. We also observed that two batches of each sample prepared at the same concentration and under the same processing conditions exhibited somewhat different rheological properties. This was also reported by Fan and Advani (2007) for non-functionalized MWCNT suspensions prepared by ultrasonic mixing. So to verify the reproducibility of different experiments, samples from the same batch were used at each concentration. The maximum error for each set of experiments was calculated and is reported separately where the pertinent results are presented.

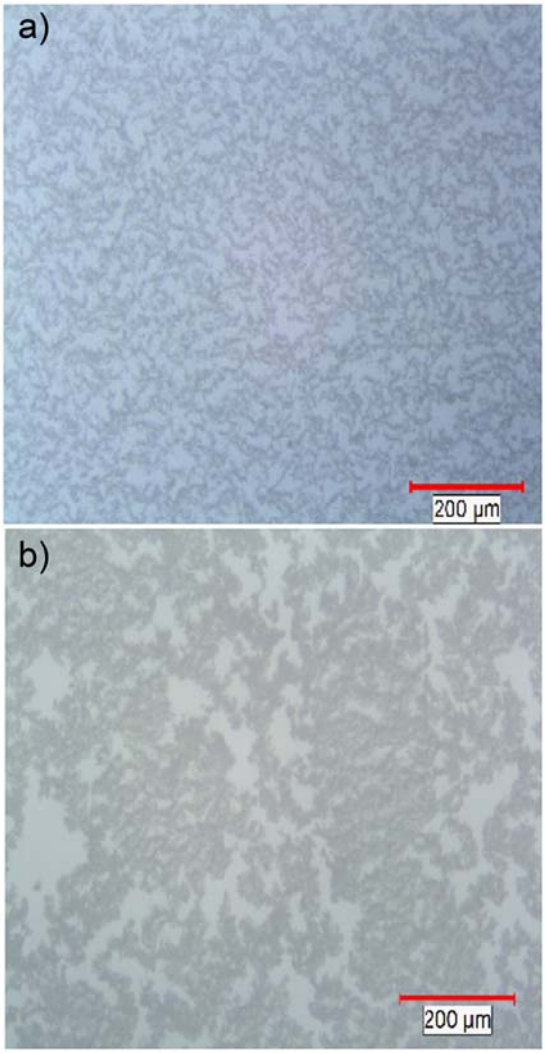


Figure 4-3: Optical micrographs of CNT-epoxy suspensions (a) 0.5 wt% and (b) 1 wt% concentration. The scale bars are 200 µm in both cases.

According to Larson (1999), the volume fractions marking the boundaries between the concentration regimes of suspensions of anisometric particles can be defined as a function of the aspect ratio of particles *L/d*.

- Transition from dilute to semi-dilute regime: $\phi_v^{'} \approx 24(d/L)^2$
- The onset for the concentrated isotropic regime: $\phi_v^{''} \approx \pi d/4L$

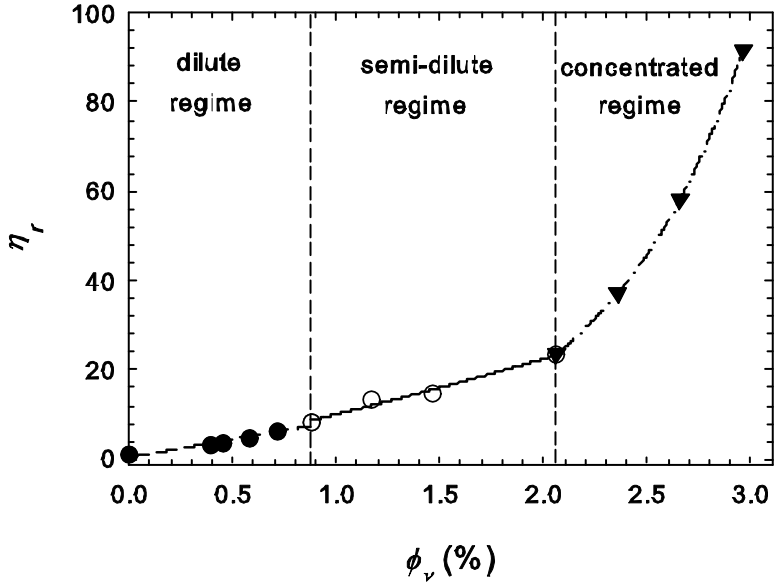


Figure 4-4: Reduced viscosity of suspensions at 0.5 $s^{-1}$ versus volume fraction of MWCNTs.

For the polydisperse CNTs (see the distributions in Figure 4-2), the mean values of the outer diameter (*OD*) and length (*L*) are used to obtain first approximations. So to be in the dilute regime, the suspension concentration should be $\phi_v < 1.18\,\%$ (or less than 2.03 wt%) and the onset for the concentrated isotropic regime is 1.74% (or 2.96 wt%). However, as a result of the polydispersity in CNTs, the above estimated concentration regimes might be ambiguous and need to be confirmed by more reliable rheological techniques. To achieve this, the reduced shear viscosity of the suspensions, $\eta_r$, which is the viscosity of the suspension at 0.5 $s^{-1}$ divided by the viscosity of the neat epoxy (12.33 Pa.s) is plotted against the CNT volume concentration in Figure 4-4. The data at 0.5 $s^{-1}$ were selected as the low shear limit where the viscosity results were reproducible especially at high concentrations. The following concentration regimes can be distinguished, based on $\eta_r$ versus $\phi_v$:

- Dilute regime: $\eta_r \propto \phi_v,\ \phi_v \leq 0.9\% - 1.47\%;\ R^2 = 0.95;$

- Semi-dilute regime: $\eta_r \propto \phi_v^2$, $0.9\% - 1.47\% \le \phi_v \le 2.05\%$; $R^2 = 0.98$;
- Concentrated regime: $\eta_r \propto \phi_v^3$, $\phi_v \ge 2.05\%$; $R^2 = 1.0$.

The lines in Figure 4-4 are the best polynomial fit with the experimental results. The vertical dashed lines show the limits of the different concentration regimes. The limiting concentration of dilute regime from semi-dilute was considered to be in the range of 0.9% (1.54 wt%) to 1.47% (2.5 wt%) by taking into account $R^2$ values from the best linear fits. In such dilute suspensions, the particles are theoretically isolated. In the intermediate range of concentrations ($0.9\% - 1.47\% \le \phi_v \le 2.05\%$) particles have hydrodynamic interactions [Larson (1999)] resulting in a stronger dependence of the reduced viscosity on concentration ($\eta_r \propto \phi_v^2$) but still do not overlap. Ferec *et al.* (2009) developed a model for rigid fibre suspensions in non-dilute regime including particle interaction in simple shear and their model predicts a viscosity proportional to $\phi_v^2$. In the semi-dilute regime the fitted curve, which is a second degree polynomial, appears to be a straight line in Figure 4-4. This is due to the narrow range of concentrations in this region. At higher concentrations ($\phi_v > 2.05\%$ or 3.48 wt%), the increasing interactions result in a stronger dependence of the reduced viscosity on concentration ($\eta_r \propto \phi_v^3$). These results are not too far from our earlier estimations (1.18 vol% for the transition from the dilute to the semi-dilute regime and 1.74 vol% for the onset of the concentrated regime); however, the latter estimates are more reliable and will be taken as the basis for the concentration limits of our suspensions. We comment that the relative viscosity reported in Figure 4-4 increases with concentration at a much higher extent than other systems containing micro particles [Sepehr *et al.* (2004); Mobuchon *et al.* (2005); Rong *et al.* (2005)].

## 4.3 Results and discussion

Initially, the linear viscoelastic properties of the CNT suspensions were determined by non-destructive small amplitude oscillatory shear (SAOS) measurements in the linear region. A typical shear-thinning behaviour was observed after the addition of nanotubes to the neat epoxy with a Newtonian behaviour. A transition from liquid-like behaviour at low concentrations to solid-like behaviour at high concentrations was observed near 2 wt% where the storage $G'$ and loss $G''$ moduli exhibited a low frequency plateau with $G'$ dominating $G''$. The critical concentration of 2 wt% was consequently considered as the rheological percolation threshold where an interconnected network of CNTs forms [Potschke *et al.* (2002); Zhang *et al.* (2006); Fan and Advani (2007); Kota *et al.* (2007)]. The emergence of a network at 2 wt% was later confirmed by the observation of an apparent yield stress at near 2 wt% from the steady shear viscosity measurements.

Our percolation value is lower than the values reported by Kalgaonkar and Jog (2008) in copolyester-MWCNTs (3 wt%) and slightly larger than those reported by Kota *et al.* (2007) in polystyrene-MWCNT composites (1 wt%), Bose *et al.* (2008) for co-continuous polyamide 6 /ABS blends with purified MWCNTs (~ 1-2 wt%) and Zhang *et al.* (2006) for single-walled carbon nanotube-high density polyethylene (1.5 wt%) composites. Potschke *et al.* (2002) and Abbasi *et al.* (2009) reported rheological percolation thresholds for polycarbonate-MWCNTs of about 2 and 1 wt%, respectively. Much smaller values have been reported, around 0.6 wt % for polyethylene terephthalate-MWCNTs [Hu *et al.* (2006)] and about 0.12 wt% for polymethyl methacrylate-MWCNTs [Du *et al.* (2004)]. It should be noticed that the key parameters such as the aspect ratio of the nanotubes and the efficiency of mixing (dispersion

degree) can make significant differences on the rheological properties of these suspensions and this could explain the differences between percolation thresholds reported in the literature.

We comment that the entangled nanotube network observed at low frequencies could be quite fragile and be strongly influenced by the effect of the pre-shearing. In Secs.4.3.1-4.3.3, we investigate the influence of the flow history on the elastic modulus and the percolation threshold of the suspensions. Furthermore, the micro-structural evolution is monitored upon cessation of shear flow at different concentrations and temperatures to probe the effect of inter-particle interactions.

### 4.3.1 Effect of flow history on LVE results

Figure 4-5 reports the effect of pre-shearing on the storage and loss modulus of the 1 wt% suspension at 25 $^{o}$C for frequencies ranging from 0.143 rad/s to 100 rad/s. As small amplitude oscillatory shear (SAOS) measurements take a relatively long time (about 10 min), 5000 s rest was given after each pre-shearing to ensure that changes of the microstructure with time had negligible influence on the results. From this figure, a strong dependence of the storage and loss modulus to the flow history can be observed especially at lower frequencies. Much larger values of the storage and loss moduli are observed for samples pre-sheared at low rates (similar results were obtained for the other concentrations). As the pre-shear rate is increased, the resulting low frequency moduli evolve from those of a solid at the low rates (i.e. 0.1 and 0.01 $s^{-1}$) to those of a liquid at high rates. The crossover of the storage and loss modulus varies from a frequency of 4.9 rad/s (where initially $G'$ dominates $G''$) after pre-shearing at 0.01 $s^{-1}$ to 1.43 rad/s at 0.1 $s^{-1}$ and 0.58 rad/s at 1 $s^{-1}$. For larger pre-shear rates, $G''$ dominates $G'$ at all frequencies.

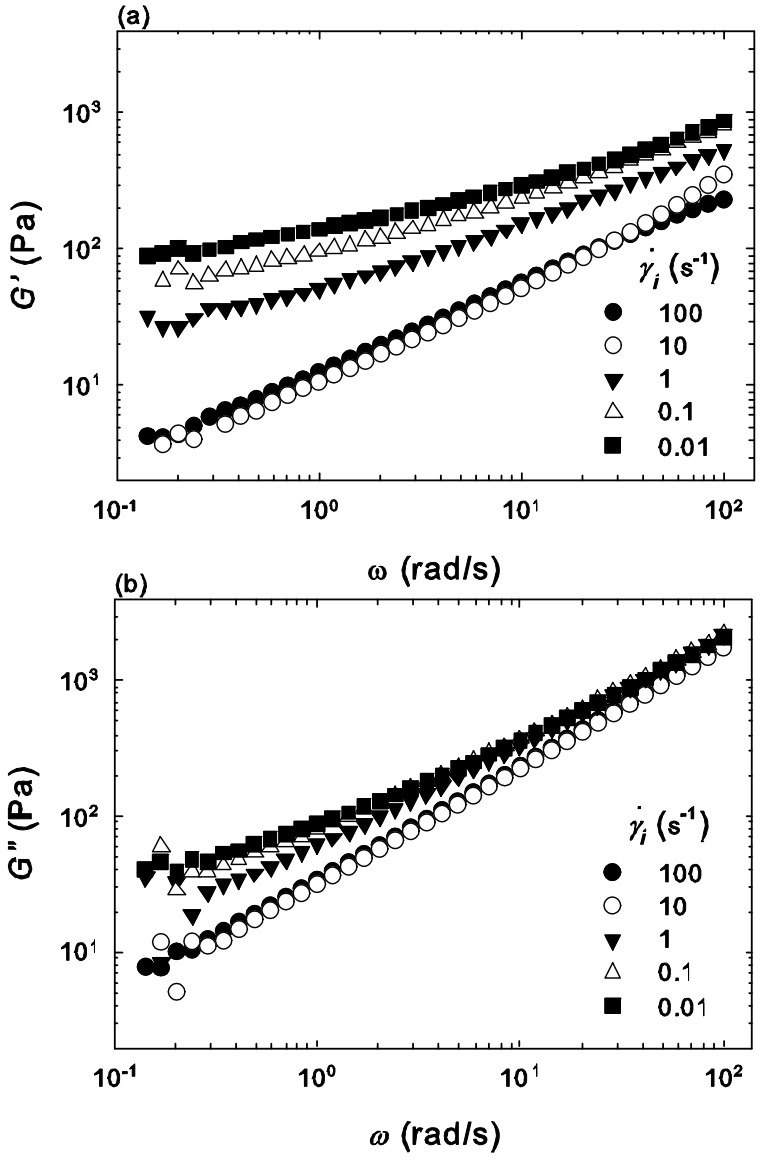


Figure 4-5: Effect of pre-shearing on the storage modulus (a) and loss modulus (b) of a 1 wt% MWCNT-epoxy suspension as functions of frequency at a strain of 0.01 after pre-shearing under different rates followed by 5000 s rest.

Using a wide range of concentration, the rheological percolation threshold could be determined for our suspensions. Different models have been developed to characterize the suspension properties near the gel point. According to Stauffer and Aharony (1985) a scaling

relation for the elastic properties predicts a power-law dependency on the volume fraction as $G' \sim \delta^{\beta}$ where $\delta$ equals $(\phi - \phi_{pt})$ or $(\phi / \phi_{pt} - 1)$ and measures how far the system is from the rheological percolation threshold, $\phi_{pt}$. Although such a scaling law should be valid at concentrations close to the percolation value, it could be extended at concentrations far above the percolation threshold [as an example, see the work of Takigawa *et al.* (1992) and Rueb and Zukoski (1997)]. In some cases, the suspension storage modulus do not even follow a power-law scaling behaviour [Goodwin *et al.* (1986)].The storage modulus of all our suspensions for all pre-shear rates scales with concentration in a power-law form over a wide concentration range below and above the percolation threshold; that could originate from the fractal nature of the microstructure of these suspensions as was imparted by Hobbie and Fry (2006; 2007). We determine the percolation threshold at the crossover of the low frequency ( $\omega = 0.588$ rad/s) of $G'$ and $G''$ when plotted against concentration; for the pre-sheared samples at 100 $s^{-1}$, the crossover of $G'$ and $G''$ versus concentration occurred at 1.63 wt% while a low frequency plateau modulus was not observed until the concentration reached 3 wt%. In this case, the average concentration between 2 and 3 wt% was considered as the percolation threshold.

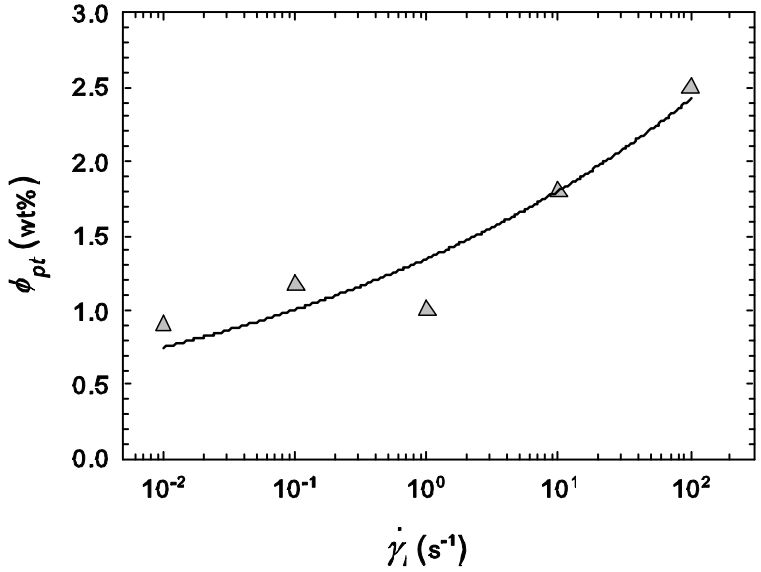


Figure 4-6: Rheological percolation threshold as a function of the pre-shear rate, 5000 s after pre-shearing at room temperature.

If the percolation threshold is determined from the same technique for the suspensions without any pre-shearing, a value of 1.8 wt% will be obtained, which is pretty similar to 2 wt% that was obtained previously. The percolation threshold is plotted in Figure 4-6 as a function of the pre-shear rate for the SAOS measurements carried out after 5000 s rest. Note that a percolation threshold value of 2 wt% obtained from the SAOS measurements before pre-shearing, suggests an effective pre-shear of about 20 $s^{-1}$ during the sample loading into the rheometer when examined in the light of Figure 4-6. As expected lower percolation values are obtained for the suspensions pre-sheared at low rates. An intuitive explanation from a structural point of view is that pre-shearing at low rates increases the density of the physical bonds between nanotubes and forms aggregates as experimentally demonstrated by Hobbie *et al.* (2003b), Lin-Gibson *et al.* (2004) and Hobbie and Fry (2006). On the other hand, since the CNTs used in this study are stiff and possess a curved equilibrium shape, they are prone to

flocculate under weak shear as predicted by Schmid *et al.* (2000) and Switzer and Klingenberg (2003; 2004) for fibre suspensions. By increasing the pre-shear rate, the percolation threshold shifts to higher concentrations due to the breakdown of the aggregates and re-dispersion of particles [Lin-Gibson *et al.* (2004); Hobbie and Fry (2006)]. Consequently, the percolation threshold shifts from 0.9 wt% for a pre-shear of 0.01 $s^{-1}$ to 2.5 wt% for 100 $s^{-1}$. It should be noted that the application of large shear forces can also result in the orientation of nanotubes as observed by Hobbie *et al.* (2003a; 2003b), Hobbie (2004), Fry *et al.* (2005; 2006) and Hobbie and Fry (2006).

### 4.3.2 Effect of flow history on the evolution of the microstructure

The evolution of the microstructure of CNT-epoxy suspensions after cessation of shear flow is determined from SAOS measurements, using the storage modulus. For the very high concentrations it was not possible to reach steady-state conditions for pre-shearing at very low rates. So the lower limit of the pre-shear rate was set to 0.1 $s^{-1}$ and 1 $s^{-1}$ for the 3 and the 5 wt% suspensions, respectively. The upper limit for the shear rate was taken as 100 $s^{-1}$ to avoid viscous dissipation effects. Following steady-shear flows, SAOS measurements were performed during 5000 s right after the cessation of the shear flow at 1 rad/s and strain amplitudes of 0.0072 and 0.0025 for the 2 and 5 wt% suspensions, respectively. The results are shown in Figure 4-7 (a) and (b), respectively. Some data have been eliminated to clarify the curves. For the sake of brevity, the structure build-up curves for the 0.5, 1 and 3 wt% suspensions are not presented, but have been used for further analysis.

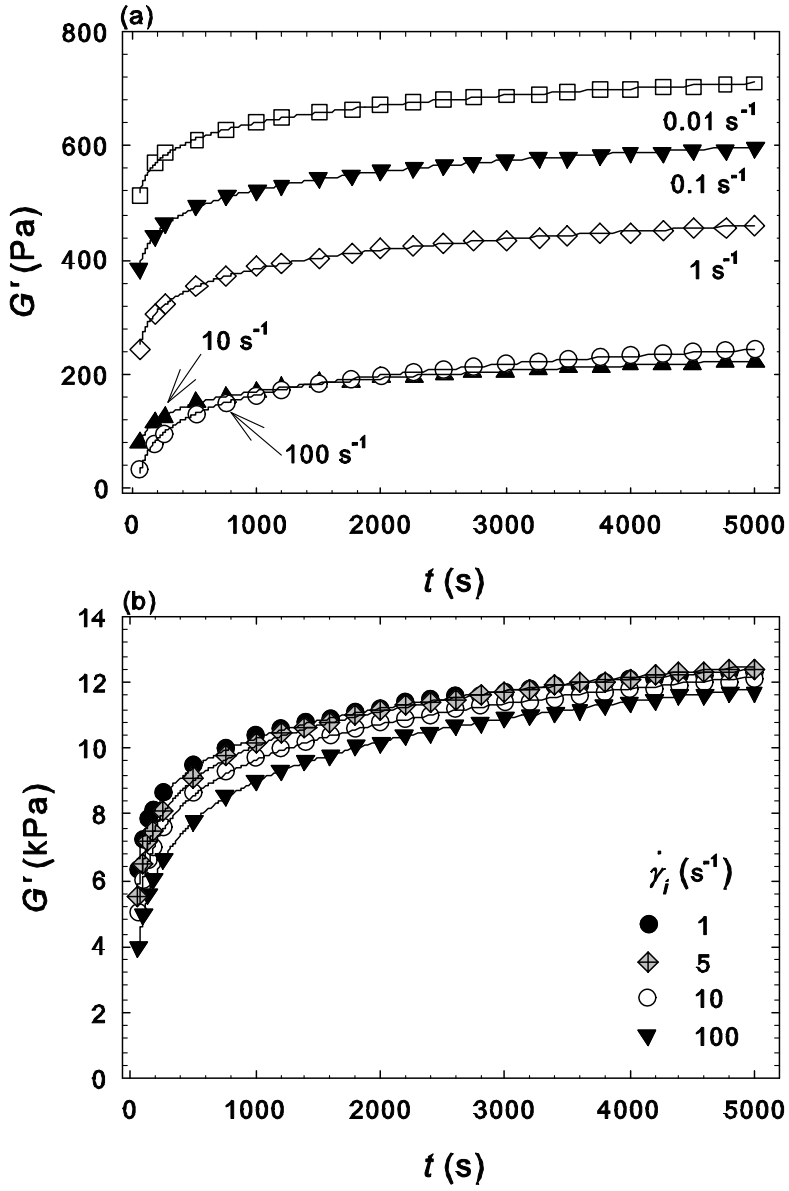


Figure 4-7: Development of the elastic modulus at 1 rad/s for MWCNT-epoxy suspensions versus time after cessation of shear flow for different pre-shearing rates: (a) 2 wt% concentration at strain amplitude of 0.0072 and (b) 5 wt% concentration at strain amplitude of 0.0025.

A similar methodology has been employed by Mobuchon *et al.* (2007; 2009) to analyze the effect of flow history on the structure of a nano-clay model suspension. However, our results are further analyzed to investigate the effect of concentration and temperature on the structure

development of the pre-sheared suspensions as well as the kinetics of structure build-up quantitatively. Since the neat epoxy is Newtonian, the suspensions elasticity originates from the presence of CNTs in the suspensions; thus, $G'$ is a more suitable parameter to characterize the structure of suspensions. Recently, Ma *et al.* (2009) monitored the stress relaxation of functionalized CNT suspensions in an epoxy by a set of step strain experiments. They reported that the relaxation modulus, $G(\gamma,t)$, decayed exponentially after a step change in strain and the stress relaxation of epoxy molecules was delayed by the addition of CNTs. However, they did not analyze the effect of inter-particle interactions nor the kinetics of stress relaxation quantitatively.

Table 4-1: Variations of $\tau$(s) and $\phi_{pt}$ with pre-shear rate for different concentrations.

| Pre-shear rate ($s^{-1}$) | 0.5 wt% | 1 wt% | 2 wt% | 3 wt% | 5 wt% | $\phi_{pt}(wt\%)$ |
|---|---|---|---|---|---|---|
| 0.010 | 833 | 909 | 833 | – | – | 0.90 |
| 0.100 | 909 | 909 | 833 | 833 | – | 1.17 |
| 1.00 | 1110 | 1000 | 909 | 909 | 833 | 1.00 |
| 5.00 | – | – | – | – | 909 | – |
| 10.0 | 2500 | 2000 | 1111 | 1000 | 909 | 1.80 |
| 50.0 | – | – | – | – | 1000 | – |
| 100 | 5000 | 5000 | 1250 | 1111 | 1000 | 2.50 |

Note that the SAOS measurements are not destructive and represent the evolution of the structure in the absence of shear forces. At very small strain amplitudes these conditions are equivalent to rest; we verified that the same $G'$ value was attained after 1000 s of rest and

under SAOS measurements. We believe that 5000 s is long enough to capture most of the structure development although it is obvious that the structure keeps developing continuously and in some cases is far from equilibrium. Besides, 5000 s is much longer than the rotational diffusion time ($1/D_r$) of 314 s estimated for the carbon nanotubes in epoxy.

The reproducibility of the results was verified by repeating each experiment several times and the maximum error in the storage modulus was estimated to be ± 15 %. From Figure 4-7, it can be observed that pre-shearing at low concentrations resulted in the formation of different structures characterized by different storage modulus curves. The lower was the pre-shear rate, the higher was the storage modulus. Moreover, by pre-shearing at 10 $s^{-1}$ and 100 $s^{-1}$, the resulting $G'$ data for the 2 wt% suspension are comparable, indicating the formation of similar microstructures. As the concentration increased to 5 wt%, the suspension microstructure was not much affected by pre-shearing and it could eventually build-up after sufficient time to form a similar structure, characterized by approximately the same $G'$ as seen in Figure 4-7. To further analyze these observations, a simple model based on the one used by Rueb and Zukoski (1997) is employed to explain the growth of the storage modulus upon cessation of shear flow as follows:

$$G'(t) = G'_i + (G'_\infty - G'_i)[1 - \exp(-t/\tau)] \tag{4-4}$$

where, $G'_i$ is the storage modulus right after pre-shearing (at $t = 0$) and $G'_\infty$ is the storage modulus as $t \to \infty$; $\tau$ is the characteristic time of the system and represents the rate of structure build-up (the time required for $G'$ to reach 63% of its final value, $G'_\infty$). $G'_i$, $G'_\infty$ and $\tau$ are fitting parameters in Eq. (4-4). The lines in Figure 4-7 show the best fits of the experimental data with Eq. (4-4). The characteristic time of the system ($\tau$) which is used to

evaluate the kinetics of structure build-up will be shortly discussed in Table 4-1 as a function of concentration and pre-shear rate.

The effect of concentration on the variation of the storage moduli $G_i'$ and $G_\infty'$ with the pre-shear rate can be compared in a single plot shown in Figure 4-8. To avoid crowding of several curves, the results for the 1 and 3 wt% suspensions are not shown as they are analogous to those for 0.5 and 5 wt%, respectively. We observe that the resulting moduli $G_i'$ and $G_\infty'$ increase with concentration for each pre-shear rate, the values of $G_\infty'$ being significantly larger than those of $G_i'$. Also for the low suspension concentrations of 0.5 to 2 wt%, the resulting storage modulus decrease as the applied pre-shear rate increase. This is in agreement with our previous observations in Figure 4-6, regarding the increase of the percolation threshold with the applied pre-shear rate. However, for the high concentrations of 3 and 5 wt%, these storage moduli ($G_i'$ and $G_\infty'$) remain almost invariant with pre-shear rate, which implies the formation of a strong CNT network and high inter-particle interactions that protect the structure from abrupt changes even upon the application of higher shear forces.

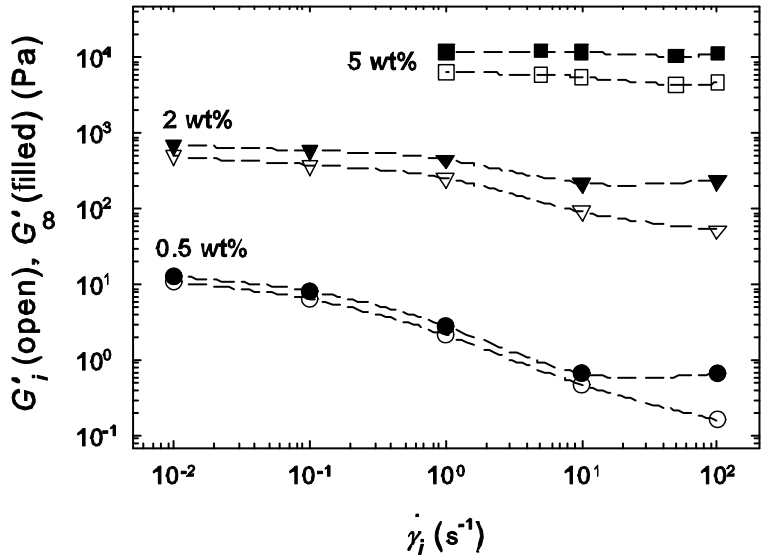


Figure 4-8: $G'_i$ and $G'_\infty$ as functions of the pre-shear rate for the 0.5, 2 and 5 wt% suspensions at room temperature.

The results presented in this section show a strong dependence of the microstructure and its evolution on the flow history. Besides, by increasing the CNT content, the interactions between nanotubes are intensified and a stronger interconnected network is formed. Thus, it is more difficult to induce a new structure at high concentrations and the effect of the flow history is less pronounced. The relative increase in the elastic modulus $\left\{(G'_{\infty\,\max} - G'_{\infty\,\min}) \times 100 / G'_{\infty\,\max}\right\}$ during the period of 5000 s was calculated to be about 95 % for the 0.5 wt%, 90% for the 1 wt%, 69% for the 2 wt%, 34% for the 3 wt% and 15% for the 5 wt% suspensions.

Another consequence of the structure development of suspensions at small deformations is the rate of structure build-up that can be evaluated from the characteristic time ($\tau$) obtained from Eq. (4-4). Table 4-1 shows the variation of $\tau$ as a function of pre-shear rate for the various

concentrations. The deviation of the percolation threshold with pre-shear rate is also shown in this table to simplify the micro-structural analysis. At low pre-shear rates of 0.01 and 0.1 $s^{-1}$, $\tau$ values are similar. However, for larger pre-shear rates, $\tau$ increases significantly with pre-shear representing a slower structure build-up. This behaviour is more dramatic for the low concentration suspensions while the variation of $\tau$ with the shear rate is very weak for the high concentration suspensions. Furthermore, at a constant pre-shear rate, the rate of the structure development increases ($\tau$ decreases) with concentration upon cessation of shear flow.

These observations reveal that the extent of the structure build-up strongly depends on the inter-particle interactions (different concentrations) as well as on the pre-shear rate. This is in contrast to the findings of Mobuchon *et al.* (2007) who reported a single time constant for different pre-shear rates in a 0.04 volume fraction nano-clay dispersion in polybutene. The variation of $\tau$ and so the rate of the structure build-up (with concentration and pre-shear rate) can be explained from a micro-structural point of view. The degree of anisotropy increases with concentration and shear rate as was shown by Hobbie *et al.* (2003a ; 2003b), Hobbie (2004), Fry *et al.* (2005), Fry *et al.* (2006) and Hobbie and Fry (2006). However, Table 4-1 reveals a faster structure build-up for higher concentration suspensions and lower pre-shear rates. Consequently, it is difficult to understand whether any change in the degree of anisotropy contributes to the suspension structure build-up. On the other hand, the particle density and so the inter-particle interactions are different at various concentrations. For concentrations as low as 0.5-1 wt% and below the percolation threshold, the density of particles and the physical bonds between nanotubes are low. Upon the application of a weak shear, the particles flocculate and interact more through van der Waals forces. Consequently,

the structure builds-up faster and the percolation threshold shifts to lower concentrations. By increasing the rate of the applied shear, the flocs partially break down and the density of the physical bonds decreases; this is in agreement with the observation of higher percolation thresholds as the pre-shear rate is increased. In such dilute suspensions, the rate of the structure build-up decreases drastically as the pre-shear rate increases. For suspensions with the concentration at the percolation threshold and higher, the structure is strong enough and less sensitive to the flow history; its rate of build-up remains invariant with respect to pre-shear rate.

### 4.3.3 Effect of temperature

As the nanotubes used in this study are not functionalized, only weak van der Waals forces exist between them. On the other hand, Brownian forces that are negligible during flow ( $Pe > 1$ ) may be important in the development of suspensions microstructure upon cessation of shear flow. Different approaches have been proposed to estimate the Brownian forces in the suspensions [Smith *et al.* (1981); Li and Ahmadi (1992)]. A simple way is to use the rotary diffusion time as $Pe/\dot{\gamma}$ from Eq. (4-3) that results in:

$$t_{diffusion} = \frac{1}{D_r} = \frac{\pi \eta_s L^3}{3k_B T\left[\ln(L/d) - 0.8\right]} \tag{4-5}$$

Hence, the characteristic diffusion time decreases with temperature, i.e. a shorter time is required for a particle to travel a certain distance. To ensure the van der Waals forces are not significantly affected by temperature, an estimation of the effect of temperature is carried out using the expression proposed by Buschow *et al.* (2001) in a simplified form for the interaction potential:

$$\Phi = -A_H \, f(a,r) \tag{4-6}$$

where $a$ is the particle diameter, $r$ is the distance between particles and $A_H$ is the Hamaker constant, estimated from the following correlation proposed by Israelachvili (1985) for two bodies of material 1 separated by a solvent 3:

$$A_H = \frac{3}{4} k_B T \left[ \frac{\varepsilon_1 - \varepsilon_3}{\varepsilon_1 + \varepsilon_3} \right]^2 + \frac{3h\upsilon_e}{16\sqrt{2}} \frac{(n_1^2 - n_3^2)^2}{(n_1^2 + n_3^2)^{1/2}} \tag{4-7}$$

In this equation, $k_B$ is the Boltzmann constant, $T$ is the temperature, $n_1$ (taken as about 2.15 for graphite [Tsai and Viers (1987)]) and $n_3$ (1.573 from the supplier's master data sheet) are the relative refractive indices of the particles and the neat epoxy, respectively, $\varepsilon_1$ (2.61 for graphite [Tsai and Viers (1987)]) and $\varepsilon_3$ ( $\sim n_3^2 \approx$ 2.47) are the permittivities of the particles and the pure polymer, respectively, $h$ is the Planck constant and $\upsilon_e$ is the absorption frequency ($1.15 \times 10^{+15}$ $s^{-1}$ for graphite [Tsai and Viers (1987)]). If the temperature is changed from 0 $^oC$ (273 K) to 100 $^oC$ (373 K), $A_H$ will change from $1.765 \times 10^{-19}$ J to $1.770 \times 10^{-19}$ J. This reveals that the Hamaker constant and so the van der Waals forces will not be influenced much by temperature. (It should be noted that in a non-absorbing medium, $\varepsilon_1$ can be approximated by $n_1^2$; however, for graphite, Tsai and Viers (1987) provide no explanation about the relationship between $n_1$ (2.15) and $\varepsilon_1$ (2.61). If $n_1$ is considered to be $\sqrt{\varepsilon_1}$ (1.6155) or $\varepsilon_1$ equals $n_1^2$ (4.6225), the Hamaker constant remains almost invariant when the temperature is changed from 0 to 100 $^oC$).

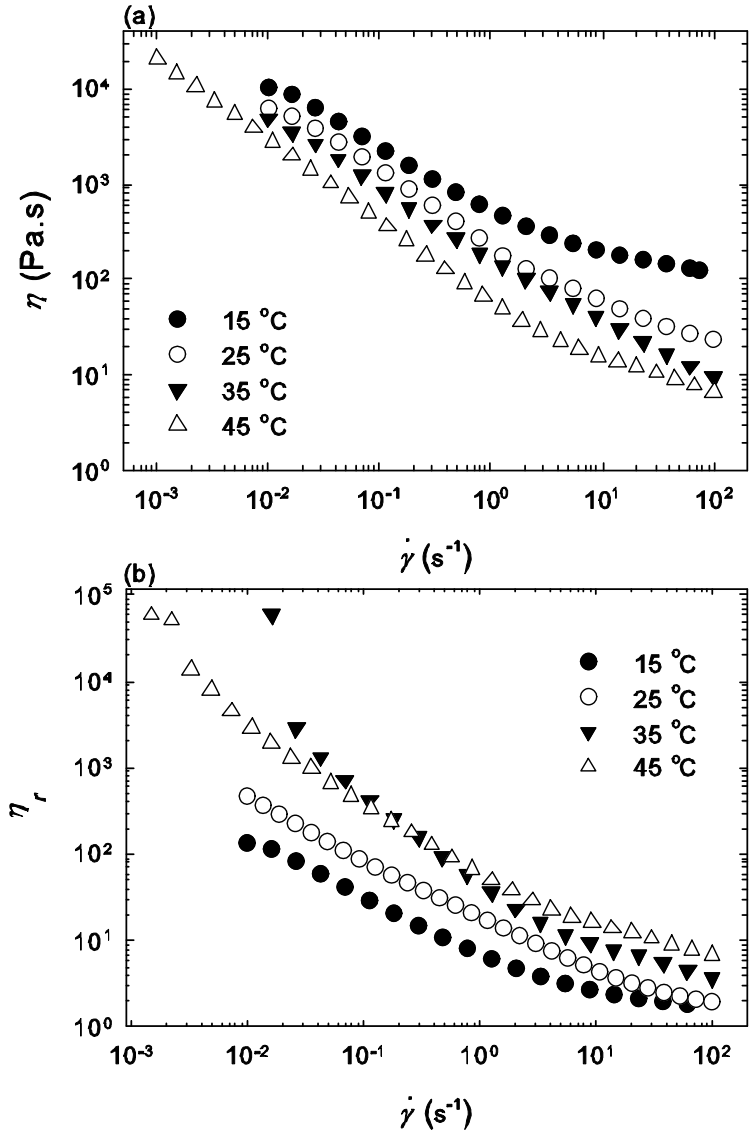


Figure 4-9: Effect of temperature on the steady shear viscosity (a) and the reduced shear viscosity (b) of the 3 wt% MWCNT-epoxy suspension.

The effect of temperature on the steady shear viscosity, $\eta$, and on the reduced shear viscosity, $\eta_r$ (the ratio of the suspension viscosity to the viscosity of the neat epoxy) of a 3 wt% suspension is shown in Figure 4-9. As expected, the shear viscosity in Figure 4-9 (a) decreases as the temperature is increased. At 45 $^{o}$C, it was possible to reach very low shear rates down to

0.001 $s^{-1}$. It can also be observed that the temperature effect is more pronounced at high shear rates where the contribution of the neat polymer to the suspension viscosity is more than that of the particles. It should be noted that the temperature can affect the properties of the neat epoxy and the inter-particle interactions. To eliminate the effect of temperature on the viscosity of the neat epoxy, the reduced shear viscosity of the suspension (viscosity of the suspension divided by the viscosity of the epoxy) is plotted in Figure 4-9 (b). We observe an important increase of the reduced viscosity with temperature revealing more inter-particle interactions in the suspension. This is in agreement with the previous findings of Abbasi *et al.* (2009) for a polycarbonate (PC)-MWCNT composite. From a structural point of view, they argued that the increase in temperature resulted in the breakdown of CNT bundles to individual nanotubes; thus the effective aspect ratio of the nanotubes increased, which resulted in lower percolation thresholds and higher intrinsic viscosities, [$\eta$], at higher temperatures. The intrinsic viscosity can provide valuable information about the contribution of a single particle to the suspension viscosity. The effect of temperature on [$\eta$] of very dilute suspensions was investigated at various temperatures, as did Abbasi *et al.* (2009), to verify if the effective aspect ratio of the nanotubes and so the dispersion quality of the suspensions changed. However, the experimental results were not reliable at such low concentrations and non-conclusive.

The suspensions containing 1 and 3 wt% MWCNTs were used to verify the effect of temperature on the pre-sheared suspensions. The measurements were performed according to the procedure explained in Sec.4.3.2 at different temperatures from 15 to 45 $^{o}$C. The temperature during the pre-shearing was the same as for the structure build-up measurement.

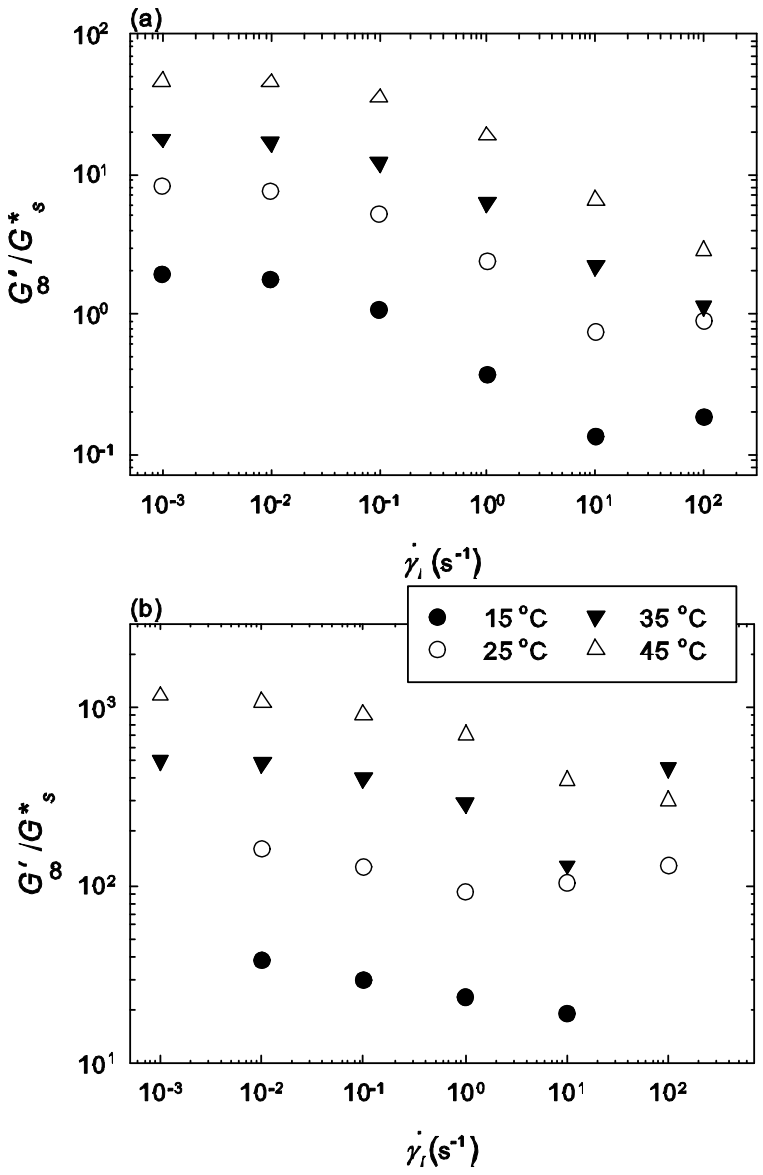


Figure 4-10: Reduced storage modulus as a function of the pre-shear rate for (a) 1 wt% and (b) 3 wt% suspensions at different temperatures. $G'_{\infty}$ is the storage modulus of the suspensions and $G^*_s$ is the complex modulus of the neat epoxy.

Figure 4-10 (a) and (b) report the reduced values of $G'_{\infty}$ with respect to the complex modulus of the neat epoxy ($G^*_s$) for the 1 and 3 wt% suspensions, respectively. Similar to the observations reported in Figure 4-8, at a constant temperature, the reduced storage modulus

decreases with increasing pre-shear rate; however, as the temperature is increased from 15 to 45 $^{o}$C, the reduced storage modulus increases drastically, exhibiting the importance of inter-particle interactions. On the other hand, Abbasi *et al.* (2009) reported that by increasing the temperature, the rigidity of CNTs in PC melt increased and so it became easier to align them by pre-shearing; thus the effect of flow history was less pronounced at higher temperatures. In contrast, for MWCNT-epoxy suspensions, the temperature effect on the reduced modulus was important regardless of pre-shear rate or concentration (see Figure 4-10).

The importance of the Brownian motion on the development of the suspension microstructure at rest is analyzed using the characteristic time, $\tau$, as reported in Figure 4-11. From Figure 4-11 (a) it can be observed that the effect of temperature on $\tau$ is not pronounced for the 1 wt% suspension pre-sheared at low rates ($\dot{\gamma}_i \leq 1\ s^{-1}$); however, at the larger shear rates of 10 and 100 $s^{-1}$ the structure build-up is facilitated as $\tau$ decreases significantly with temperature. We note the strong influence of temperature on $\tau$ for the suspension pre-sheared at large rates. The behaviour for the 3 wt% suspension is compared to that of the 1 wt% in Figure 4-11 (b). The characteristic time is shown to decrease with temperature regardless of pre-shear rate. The $\tau$ values for the 1 wt% suspension are larger than those for the 3 wt% which are almost independent of the pre-shear rate. The faster structure build-up with increased temperature implies that the Brownian forces play an important role at rest. However, it should be mentioned that the temperature increase also results in higher inter-particle interactions as shown in Figure 4-9 and Figure 4-10 previously. Consequently, it is difficult to conclude which of these effects are dominant.

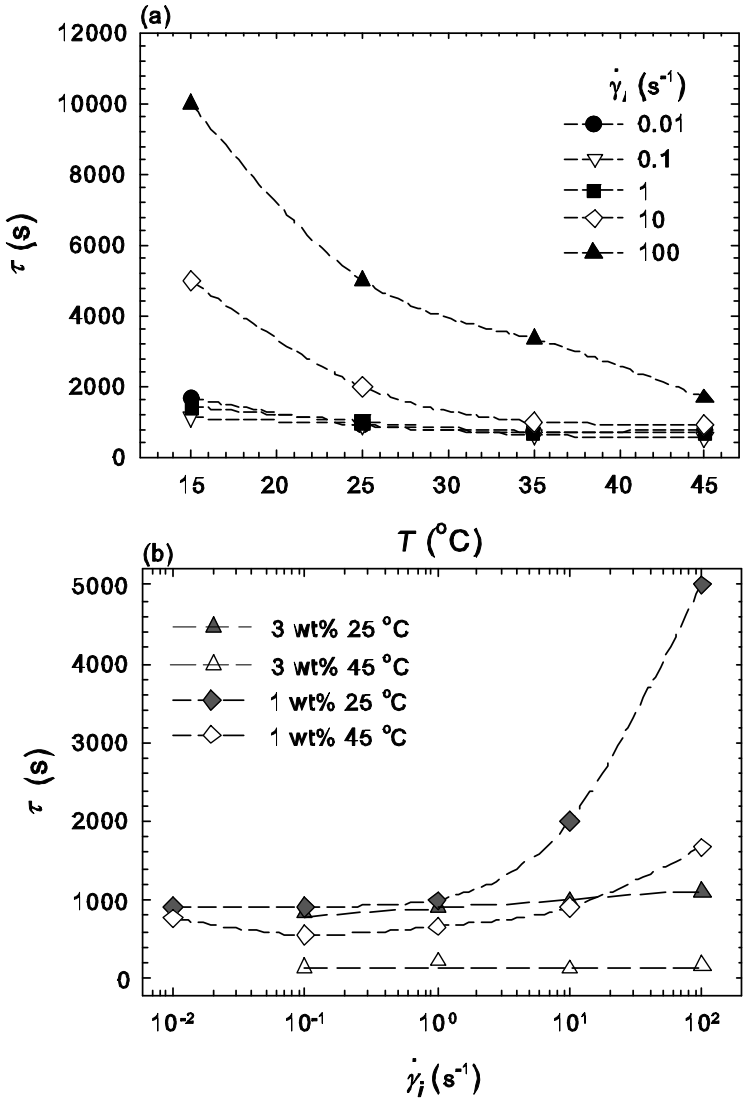


Figure 4-11: Variations of the characteristic time ($\tau$) for (a) 1 wt% suspension as a function of temperature and (b) for 1 wt% and 3 wt% suspensions as a function of the pre-shearing rate.

## 4.4 Summary

The effect of the flow history on the linear viscoelastic properties of CNT-epoxy suspensions as well as on the evolution of the suspensions microstructure after cessation of shear flow has been investigated. The results show a strong impact of the pre-shearing on the microstructure and its evolution. From the frequency sweep experiments, it was observed that the lower was

the pre-shear rate, the higher were the resulting storage and loss moduli and the lower was the rheological percolation threshold; such pre-shearing effects could be ascribed to an increase in the density of the physical bonds between nanotubes induced by low shear flow and the formation of aggregates. By increasing the pre-shear rate, the aggregates are broken down and the particles are re-dispersed in the suspensions, which makes the formation of network more difficult and a higher density of nanotubes is required to form an interconnected network.

The suspension microstructure keeps evolving after cessation of the pre-shearing, characterized by an increase of the storage modulus with time at a constant frequency and strain amplitude. The magnitude of the increase in $G'$ strongly depends on the level of the pre-shear, as reported by Mobuchon *et al.* (2007; 2009), as well as on the concentration and temperature. The qualitative analysis provided in this work reveals that the suspensions microstructure is more sensitive to the flow history at lower concentrations and before the formation of a percolated network. By increasing the temperature, the reduced steady shear viscosity as well as the reduced storage modulus of the suspensions is shown to increase due to more inter-particle interactions.

Contrary to Mobuchon *et al.* (2007) who reported similar kinetics of structure build-up (a single time constant) at different pre-shear rates at a certain concentration, it is shown that the rate of the structure build-up strongly depends on the flow history, concentration and temperature. It decreases dramatically by increasing the pre-shear rate at low concentrations while it remains almost independent with respect to the flow history for high concentration suspensions. However, at a constant pre-shear rate, the development of the structure is accelerated at higher concentrations. By considering the effect of concentration and temperature on the characteristic time of the suspensions, one can conclude that the increase

in inter-particle interactions favours a faster kinetics for the structure build-up. Moreover, since the rate of structure development is facilitated by increasing the temperature regardless of pre-shear rate or concentration, one can conclude that the Brownian forces play an important role on the structure build-up in the absence of shear forces.

## 4.5 Acknowledgements

We are thankful to Dr. Daniel Rosca for technical help in the sample preparation and Dr. S.V. Hoa for providing access to the facilities at Concordia Composite Lab. The authors are grateful to Dr. Michel Moan and Dr. Frederic Bossard for helpful discussions. Funding from NSERC and CRIAQ is gratefully acknowledged.

## 4.6 References

Abbasi, S., P. J. Carreau, A. Derdouri and M. Moan, "Rheological properties and percolation in suspensions of multiwalled carbon nanotubes in polycarbonate," Rheol. Acta 48(9): 943-959 (2009).

Abdalla, M., D. Dean and P. Robinson, *Aligned Carbon Nanotube/Thermoset Nanocomposites: Morphology Development, Rheology and Properties*, (Society for the Advancement of Material and Process Engineering, Covina, CA, 2007), p. 10.

Abdel-Goad, M. and P. Potschke, "Rheological characterization of melt processed polycarbonate-multiwalled carbon nanotube composites," J. Non-Newtonian Fluid Mech. 128(1): 2-6 (2005).

Allaoui, A., S. Bai, H. M. Cheng and J. B. Bai, "Mechanical and electrical properties of a MWNT/epoxy composite," Compos. Sci. Technol. 62(15): 1993-1998 (2002).

Bai, J. B. and A. Allaoui, "Effect of the length and the aggregate size of MWNTs on the improvement efficiency of the mechanical and electrical properties of

nanocomposites-experimental investigation," Composites, Part A 34(8), 689-694 (2003).

Bangarusampath, D. S., H. Ruckdaschel, V. Altstadt, J. K. W. Sandler and M. S. P. Shaffer, *Rheology, Processing and Electrical Properties of Carbon Nanotube/Poly(Ether Ether Ketone) Nanocomposites*, (Society of Plastics Engineers, Brookfield, CT, 2008), pp. 1864-1869.

Bose, S., A. R. Bhattacharyya, A. P. Bondre, A. R. Kulkarni and P. Potschke, "Rheology, electrical conductivity, and the phase behavior of cocontinuous PA6/ABS blends with MWNT: Correlating the aspect ratio of MWNT with the percolation threshold." J. Polym. Sci., Part B: Polym. Phys. 46(15): 1619-1631 (2008).

Buschow, K.H. Jürgen, R.W. Cahn, M.C. Flemings, B. Ilschner, E.J. Kramer and S. Mahajan, *Encyclopedia of Materials - Science and Technology,* (Elsevier, New York, 2001), Vol. 3, p: 2737.

Cipiriano, B. H., T. Kashiwagi, S. R. Raghavan, Y. Yang, E. A. Grulke, K. Yamamoto, J. R. Shields and J. F. Douglas, "Effects of aspect ratio of MWNT on the flammability properties of polymer nanocomposites," Polymer 48(20): 6086-6096 (2007).

Coussot, P., H. Tabuteau, X. Chateau, L. Tocquer and G. Ovarlez, "Aging and solid or liquid behavior in pastes," J. Rheol. 50(6): 975-994 (2006).

Derec, C., G. Ducouret, A. Ajdari and F. Lequeux, "Aging and nonlinear rheology in suspensions of polyethylene oxide-protected silica particles," Phys. Rev. E 67(6), 061403 (2003).

Ding, Y., H. Alias, D. Wen and R. A. Williams, "Heat transfer of aqueous suspensions of carbon nanotubes (CNT nanofluids)," Int. J. Heat Mass Transfer 49(1-2), 240-250 (2006).

Du, F., R. C. Scogna, W. Zhou, S. Brand, J. E. Fischer and K. I. Winey, "Nanotube networks in polymer nanocomposites: Rheology and electrical conductivity," Macromolecules 37(24), 9048-9055 (2004).

Dufresne, A., M. Paillet, J. L. Putaux, R. Canet, F. Carmona, P. Delhaes and S. Cui, "Processing and characterization of carbon nanotube/poly(styrene-co-butyl acrylate) nanocomposites," Mater. Sci. 37(18), 3915–3923 (2002).

Fan, Z. and S. G. Advani, "Rheology of multiwall carbon nanotube suspensions," J. Rheol. 51(4): 585-604 (2007).

Ferec, J., G. Ausias, M.-C. Heuzey and P. J. Carreau, "Modeling fiber interactions in semiconcentrated fiber suspensions," J. Rheol. 53(1), 49-72 (2009).

Fiedler, B., F. H. Gojny, M. H. G. Wichmann, M. C. M. Nolte and K. Schulte, "Fundamental aspects of nano-reinforced composites," Compos. Sci. Technol. 66(16), 3115-3125 (2006).

Fry, D., B. Langhorst, H. Kim, E. Grulke, H. Wang and E. K. Hobbie, "Anisotropy of sheared carbon-nanotube suspensions," Phys. Rev. Lett. 95(3): 038304 (2005).

Fry, D., B. Langhorst, H. Wang, M. L. Becker, B. J. Bauer, E. A. Grulke and E. K. Hobbie, "Rheo-optical studies of carbon nanotube suspensions," J. Chem. Phys. 124(5), 054703 (2006).

Gojny, F. H., M. H. G. Wichmann, B. Fiedler and K. Schulte, "Influence of different carbon nanotubes on the mechanical properties of epoxy matrix composites - A comparative study," Compos. Sci. Technol. 65(15-16), 2300-2313 (2005).

Gojny, F. H., M. H. G. Wichmann, U. Kopke, B. Fiedler and K. Schulte, "Carbon nanotube-reinforced epoxy-composites: enhanced stiffness and fracture toughness at low nanotube content," Compos. Sci. Technol. 64(15), 2363-2371 (2004).

Goodwin, J. W., R. W. Hughes, S. J. Partridge and C. F. Zukoski, "The elasticity of weakly flocculated suspensions," J. Chem. Phys. 85(1), 559-566 (1986).

Hobbie, E. K., "Optical anisotropy of nanotube suspensions," J. Chem. Phys. 121(2), 1029-1037 (2004).

Hobbie, E. K. and D. J. Fry, "Nonequilibrium phase diagram of sticky nanotube suspensions," Phys. Rev. Lett. 97(3): 036101 (2006).

Hobbie, E. K. and D. J. Fry, “Rheology of concentrated carbon nanotube suspensions," J. Chem. Phys. 126(12): 124907 (2007).

Hobbie, E. K., H. Wang, H. Kim, C. C. Han, E. A. Grulke and J. Obrzut, “Optical measurements of structure and orientation in sheared carbon-nanotube suspensions," Rev. Sci. Instrum. 74, 1244-1250 (2003a).

Hobbie, E. K., H. Wang, H. Kim, S. Lin-Gibson and E. A. Grulke, “Orientation of carbon nanotubes in a sheared polymer melt." Phys. Fluids 15(5), 1196-1202 (2003b).

Hu, G., C. Zhao, S. Zhang, M. Yang and Z. Wang, “Low percolation thresholds of electrical conductivity and rheology in poly(ethylene terephthalate) through the networks of multi-walled carbon nanotubes," Polymer 47(1), 480-488 (2006).

Huang, Y. Y., S. V. Ahir and E. M. Terentjev, “Dispersion rheology of carbon nanotubes in a polymer matrix," Phys. Rev. B 73(12), 125422 (2006).

Israelachvili, J. N. *Intermolecular and Surface Forces, with Applications to Colloidal and Biological Systems* (Academic, London,1985).

Kalgaonkar, R. A. and J. P. Jog, “Copolyester nanocomposites based on carbon nanotubes: Reinforcement effect of carbon nanotubes on viscoelastic and dielectric properties of nanocomposites," Polym. Int. 57(1), 114-123 (2008).

Kashiwagi, T., M. Mu, K. Winey, B. Cipriano, S. R. Raghavan, S. Pack, M. Rafailovich, Y. Yang, E. Grulke, J. Shields, R. Harris and J. Douglas, “Relation between the viscoelastic and flammability properties of polymer nanocomposites," Polymer 49(20): 4358-4368 (2008).

Keshtkar, M., M.-C. Heuzey and P. J. Carreau, “Rheological behavior of fiber-filled model suspensions: effect of fiber flexibility," J. Rheol. 53(3), 631-650 (2009).

Kharchenko, S. B., K. B. Migler, J. F. Douglas, J. Obrzut and E. A. Grulke. *Rheology, Processing and Electrical Properties of Multiwall Carbon Nanotube/Polypropylene Nanocomposites*, (Society of Plastics Engineers, Chicago, IL, 2004), pp. 1877-1881.

Kim, Y. J., T. S. Shin, H. D. Choi, J. H. Kwon, Y.-C. Chung and H. G. Yoon, "Electrical conductivity of chemically modified multiwalled carbon nanotube/epoxy composites," Carbon 43(1), 23-30 (2005).

Kinloch, I. A., S. A. Roberts and A. H. Windle, "A rheological study of concentrated aqueous nanotube dispersions," Polymer 43(26), 7483-7491 (2002).

Kota, A. K., B. H. Cipriano, M. K. Duesterberg, A. L. Gershon, D. Powell, S. R. Raghavan and H. A. Bruck, "Electrical and rheological percolation in polystyrene/MWCNT nanocomposites," Macromolecules 40(20), 7400-7406 (2007).

Larson, R.G. *The Structure and Rheology of Complex Fluids* (Oxford University Press, New York, 1999).

Lau, K.-T., M. Lu, C. K. Lam, H. Y. Cheung, F.-L. Sheng and H.-L Li, "Thermal and mechanical properties of single-walled carbon nanotube bundle-reinforced epoxy nanocomposites: The role of solvent for nanotube dispersion," Compos. Sci. Technol. 65, 719-725 (2005).

Lee, S.H., E. Cho, S.H. Jeon and J.R. Youn, "Rheological and electrical properties of polypropylene composites containing functionalized multi-walled carbon nanotubes and compatibilizers," Carbon 45(14), 2810-2822 (2007).

Li, A. and G. Ahmadi, "Dispersion and Deposition of Spherical Particles from Point Sources in a Turbulent Channel Flow," Aerosol Sci. Technol. 16(4), 209-226 (1992).

Lin-Gibson, S., J. A. Pathak, E. A. Grulke, H. Wang and E. K. Hobbie, "Elastic Flow Instability in Nanotube Suspensions," Phys. Rev. Lett. 92(4), 048302 (2004).

Ma, A. W. K., F. Chinesta and M. R. Mackley, "The rheology and modeling of chemically treated carbon nanotubes suspensions," J. Rheol. 53(3), 547-573 (2009).

Ma, W. K. A., F. Chinesta, A. Ammar and M. R. MacKley, "Rheological modeling of carbon nanotube aggregate suspensions," J. Rheol. 52(6), 1311-1330 (2008).

Miyagawa, H., M. J. Rich and L. T. Drzal "Thermo-physical properties of epoxy nanocomposites reinforced by carbon nanotubes and vapor grown carbon fibers," Thermochim. Acta 442(1-2), 67-73 (2006).

Mobuchon, C., P. J. Carreau and M.-C. Heuzey, “Effect of flow history on the structure of a non-polar polymer/clay nanocomposite model system," Rheol. Acta 46(8), 1045-1056 (2007).

Mobuchon, C., P. J. Carreau and M.-C. Heuzey, “Structural analysis of non-aqueous layered silicate suspensions subjected to shear flow," J. Rheol. 53(5), 1025-1048 (2009).

Mobuchon, C., P. J. Carreau, M.-C. Heuzey, M. Sepehr and G. Ausias, “Shear and extensional properties of short glass fiber reinforced polypropylene," Polym. Compos. 26(3), 247-264 (2005).

Nanda, J., C. Maranville, S. C. Bollin, D. Sawall, H. Ohtani, J. T. Remillard and J. M. Ginder, “Thermal conductivity of single-wall carbon nanotube dispersions: Role of interfacial effects," J. Phys. Chem. C 112(3), 654-658 (2008).

Ounaies, Z., C. Park, K. E. Wise, E. J. Siochi and J. S. Harrison, “Electrical properties of single wall carbon nanotube reinforced polyimide composites," Compos. Sci. Technol. 63(11), 1637-1646 (2003).

Park, S. K., S. Hun, Kim and J. T. Hwang. *Thermal Stability and Rheological Properties of Multiwall Carbon Nanotube Reinforced Thermotropic Liquid Crystalline Polymer Nanocomposites* (Society of Plastics Engineers, Brookfield, CT, 2007), pp. 49-53.

Potschke, P., T. D. Fornes and D. R. Paul, “Rheological behavior of multiwalled carbon nanotube/polycarbonate composites," Polymer 43(11), 3247-3255 (2002).

Pujari, S., S. S. Rahatekar, J. W. Gilman, K. K. Koziol, A. H. Windle and W. R. Burghardt, “Orientation dynamics in multiwalled carbon nanotube dispersions under shear flow," J. Chem. Phys. 130(21), 214903 (2009).

Rahatekar, S. S., K. K. K. Koziol, S. A. Butler, J. A. Elliott, M. S. P. Shaffer, M. R. Mackley and A. H. Windle, “Optical microstructure and viscosity enhancement for an epoxy resin matrix containing multiwall carbon nanotubes," J. Rheol. 50(5), 599-610 (2006).

Rong, G., J. Azaiez and C. Bellehumeur, “Rheology of fiber filled polymer melts: role of fiber-fiber interactions and polymer-fiber coupling," Polym. Eng. Sci. 45(3), 385-399 (2005).

Rueb, C. J. and C. F. Zukoski "Viscoelastic properties of colloidal gels," J. Rheol. 41(2), 197-218 (1997).

Sandler, J. K. W., J. E. Kirk, I. A. Kinloch, M. S. P. Shaffer and A. H. Windle "Ultra-low electrical percolation threshold in carbon-nanotube-epoxy composites," Polymer 44(19): 5893-5899 (2003).

Schartel, B., P. Potschke, U. Knoll and M. Abdel-Goad "Fire behaviour of polyamide 6/multiwall carbon nanotube nanocomposites," Eur. Polym. J. 41(5), 1061-1070 (2005).

Schmid, C. F., L. H. Switzer and D. J. Klingenberg "Simulations of fiber flocculation: Effects of fiber properties and interfiber friction," J. Rheol. 44(4), 781-809 (2000).

Sepehr, M., P. J. Carreau, M. Moan and G. Ausias "Rheological properties of short fiber model suspensions," J. Rheol. 48(5), 1023-1048 (2004).

Shen, J., W. Huang, L. Wu, Y. Hu and M. Ye "Thermo-physical properties of epoxy nanocomposites reinforced with amino-functionalized multi-walled carbon nanotubes," Composites, Part A 38(5), 1331-1336 (2007).

Smith, P. W., A. Ashkin and W. J. Tomlinson "Four-wave mixing in an artificial Kerr medium," Opt. Lett. 6(6), 284-286 (1981).

Song, Y.S., “Effect of surface treatment for carbon nanotubes on morphological and rheological properties of poly(ethylene oxide) nanocomposites," Polym. Eng. Sci. 46(10), 1350-1357 (2006).

Song, Y. S. and J. R. Youn "Influence of dispersion states of carbon nanotubes on physical properties of epoxy nanocomposites," Carbon 43(7), 1378-1385 (2005).

Stauffer, D. and A. Aharony, *Introduction to Percolation Theory* (Taylor & Friends, London, 1985).

Switzer, L. H, “Simulating systems of flexible fibers,” Ph.D. thesis, The University of Wisconsin, 2002.

Switzer, L. H. and D. J. Klingenberg, "Rheology of sheared flexible fiber suspensions via fiber-level simulations," J. Rheol. 47(3), 759-778 (2003).

Switzer, L. H. and D. J. Klingenberg, "Flocculation in simulations of sheared fiber suspensions," Int. J. Multiphase Flow 30(1), 67-87 (2004).

Takigawa, T., M. Takahashi, K. Urayama and T. Masuda, "Comparison of model prediction with experiment for concentration-dependent modulus of poly(vinyl alcohol) (PVA) gels near the gelation point," Chem. Phys. Lett. 195(5-6), 509-512 (1992).

Tiwari, M. K., A. V. Bazilevsky, A. L. Yarin and C. M. Megaridis, "Elongational and shear rheology of carbon nanotube suspensions," Rheol. Acta 48, 597–609 (2009).

Tsai, S.C. and B. Viers, "Effects of Liquid Polarity on Rheology of Noncolloidal Suspensions," J. Rheol. 31(6), 483-494 (1987).

Wu, D., L. Wu, W. Zhou, Y. Sun and M. Zhang, "Relations between the aspect ratio of carbon nanotubes and the formation of percolation networks in biodegradable polylactide/carbon nanotube composites," J. Polym. Sci., Part B, Polym. Phys. 48(4), 479-489 (2009).

Xu, D.-H., Z.-G. Wang and J.F. Douglas, "Influence of carbon nanotube aspect ratio on normal stress differences in isotactic polypropylene nanocomposite melts," Macromolecules 41(3), 815-825 (2008).

Yuen, S.-M., C. C. Ma, H. H. Wu, H. C. Kuan, W. J. Chen, S. H. Liao, C. W. Hsu and H. L. Wu, "Preparation and thermal, electrical, and morphological properties of multiwalled carbon nanotube and epoxy composites," J. Appl. Polym. Sci. 103(2), 1272-1278 (2007).

Zhang, Q., S. Rastogi, D. Chen, D. Lippits and P. J. Lemstra, "Low percolation threshold in single-walled carbon nanotube/high density polyethylene composites prepared by melt processing technique," Carbon 44(4), 778-785 (2006).

# CHAPITRE 5 SCALING BEHAVIOUR OF THE ELASTIC PROPERTIES OF NON-DILUTE MWCNT-EPOXY SUSPENSIONS

Fatemeh Khalkhal and Pierre J. Carreau

*Center for Applied Research on Polymers and Composites (CREPEC), Chemical Engineering Department, Ecole Polytechnique of Montreal, QC, Canada*

*C.P. 6079 Suc. Centre-Ville, Montreal, Quebec H3C 3A7*

*Tel:(514)340-4711 ext. 4924*

*Fax:(514)340-2994*

This article has been published online in Rheologica Acta on 13 April 2011 (DOI 10.1007/s00397-010-0527-9).

## Abstract

In this paper, the network structure of multiwalled carbon nanotube (MWCNT)-epoxy suspensions was investigated under the influence of flow history and temperature using the scaling behaviour of the linear viscoelastic properties of the concentrated suspensions above their gel point. It is shown that the suspensions have a self-similar fractal structure with the dimension of about 2.15, characteristic of weakly flocculating suspensions and their elasticity originates from inter and intra-floc links of nanotubes. From the scaling behaviour of the flow induced storage modulus and the critical strain for the limit of linearity, it is shown that the fractal dimension and so the superstructure of the network did not change significantly under the influence of the flow history due to the initial compact structure of the network before pre-shearing. The time-temperature superposition principle was verified for the CNT suspensions and the shift factor was accounted for by an Arrhenius equation. The reduced storage and loss moduli of the suspensions using the complex modulus of the neat epoxy were shown to increase with temperature revealing more inter-particle interactions as the temperature was raised. However, it was impossible to conclude on the changes of the fractal dimensions with temperature.



## Keywords

*Carbon nanotube, rheology, microstructure, scaling theory, flow history, fractal dimension.*

## 5.1 Introduction

Carbon nanotubes (CNTs) show many potential applications since their discovery and have been widely used to reinforce polymers and improve their physical properties, such as electrical conductivity. To control the processing and the final properties of the resulting nano-composites, a great deal of research effort has been devoted to develop structure-property relationships.

Previous studies of the structure in dilute CNT suspensions have focused on the orientation dynamics of nanotubes under flow by employing a variety of light scattering techniques (Hobbie *et al.* 2003a, b; Pujari *et al.* 2009). Fry *et al.* (2005; 2006) established a quantitative relationship between the anisotropy of sheared CNT suspension structure and nanotube concentration and aspect ratio, shear rate and the viscosity of the suspending medium. The state of flocculation (at low shear rates) and de-flocculation (at high shear rates) of CNT suspensions under flow have been probed by rheo-optical techniques by Hobbie and Fry (2006) and Lin-Gibson *et al.* (2004). Their investigations resulted in a universal non-equilibrium phase diagram describing a transition from solid-like networks to flowing nematics under an applied shear stress. Although very helpful information can be obtained from light scattering, they are mainly limited to dilute suspensions whereas the conductive composites are usually prepared at concentrations about the percolation threshold or even higher. In addition, in some cases, the rheological properties originate from length scales different from the ones characterized by the light scattering; consequently, no significant change can be observed by light scattering while rheological properties show a considerable variation (for example see the work of Rahatekar *et al.* (2006)). On the contrary, rheology can be used to characterize the microstructure of suspensions over a wide range of concentrations.

Using rheological measurements, Wu *et al.* (2009) has recently developed a relationship between the aspect ratio of carbon nanotubes and the formation of a percolated network in polylactide-CNT composites. Fan and Advani (2007), Huang *et al.* (2006) and Song and Youn (2005) investigated the effect of the dispersion state of CNTs in different polymer matrices on the rheology of the nano-composites. We have recently (Khalkhal *et al.* 2011) shown that the linear viscoelastic properties of CNT-epoxy suspensions are strongly influenced by the effect of the flow history and the rate of the structure build-up after cessation of pre-shearing was quantified and its dependency on the rate of the pre-shear, the concentration and temperature was investigated.

On the other hand, using models based on scaling theories (Shih *et al.* 1990; Wu and Morbidelli 2001) and fractal theories (Potanin 1991, 1993), some in depth information about the network structure of colloidal suspensions and their evolution under flow can be obtained. Using scaling theories, the origin of the elastic behaviour of the gels can be identified and the extent of their compactness can be quantified. Fractal theories can provide helpful information about the rigidness of the aggregates as well as the mechanisms of aggregate deformation and break up under flow.

In this paper, the network structure of multiwalled carbon nanotube (MWCNT)-epoxy suspensions is investigated under the influence of flow history and temperature using the scaling behaviour of the linear viscoelastic properties of concentrated suspensions above their gel point. Scaling of the steady shear results with the low angular frequency storage modulus of gels resulted in formation of a master curve. Based on fractal theory, it can be assumed that a self-similar fractal network structure is present in the gels. The fractal network dimension (without pre-shearing) is approximated to be 2.15, characteristic of weakly flocculating

suspensions. From scaling of linear viscoelastic (LVE) properties, it is shown that the inter- and intra-floc links of nanotubes contribute to the elasticity of the suspensions. The effect of pre-shearing and temperature on the variation of the fractal dimension is analyzed. This is helpful for describing the rheological properties of highly concentrated CNT suspensions, for which simulations based on fractal theories are impossible.

The article is organized as follows. A background review about the scaling and fractal theories is given in "Theoretical background". In "Materials and their characterization" section, details of experimental techniques and material characterization are described. The results of the rheological measurements and their relation to the scaling and fractal theories are given in "Results and discussion". In "Conclusion" the important findings of the article are highlighted.

## 5.2 Theoretical background

### 5.2.1 Scaling theory

Shih *et al.* (1990) developed a scaling theory for colloidal gels similar to the one for semi-dilute polymeric solutions developed by de Gennes (1979). It was assumed that the network structure of the gel is constituted of closely packed clusters with the fractal dimension $d_f$, which depends on the aggregation mechanism. For fast aggregation, where flocs grow by merging into one another as soon as they collide, $d_f$ = 1.7-1.8 similar to the one for cluster-cluster aggregation and $d_f$ = 2.0-2.2 for slow aggregation or the so-called reaction-limited aggregation, where flocs penetrate to one another partially after collision (Larson 1999). The scaling relation between the average floc size $\xi$ and the particle concentration $\phi$, provided that

the internal concentration of particles $\phi_{\text{int}}$ can be approximated by the overall particle concentration $\phi$, is given by

$$\xi \sim \phi^{\frac{1}{(d_f - d)}} \tag{5-1}$$

where $d$ is the Euclidean dimension. According to this theory, the elastic properties of flocs are dominated by their effective backbone of size $\xi$, where the elastic backbone was approximated to be a linear chain of springs (with a radius of gyration $\xi$), assuming that the aggregates have few loops. Thus, the elastic constant of a floc $K_\xi$ with size $\xi$ can be approximated by

$$K_\xi \sim \frac{K_0}{\xi^{x+2}} \tag{5-2}$$

where $K_0$ is the bending constant between two neighbouring springs and $x$ is the fractal dimension of clusters, which is in the range of 1 and $d_f$ $(1 < x < d_f)$. Consequently, the macroscopic elastic constant of a system with the size $L$ can be written in terms of that of the individual flocs as

$$G' \sim \left[\frac{L}{\xi}\right]^{d-2} K_\xi \tag{5-3}$$

According to Shih *et al.* (1990), the macroscopic elasticity originates whether from intra-floc links (strong-link region) or from the inter-floc links between the particles (weak-link region). The drawback of this model is that, in some cases, it fails by predicting a negative value for the fractal dimension $x$ of clusters. On the other hand, Wu and Morbidelli (2001) defined a

macroscopic elasticity by the contributions from inter and intra-floc links. As a result, $K_\xi$ in Eq. (5-3) should be replaced by $K_{eff}$ given by

$$\frac{1}{K_{eff}} = \frac{1}{K_\xi} + \frac{1}{K_l} \tag{5-4}$$

where $K_\xi$ is the intra-floc elastic constant and $K_l$ is the inter-floc elastic constant and it is independent of the microstructure parameters of the flocs. By approximating $1/(1+K_\xi / K_l)$ with $(K_l / K_\xi)^\alpha$ where $\alpha \in [0,1]$ and substituting this correlation into (5-3) and (5-1), the final correlation for the macroscopic elasticity with particle concentration can be obtained as

$$G' \sim \phi^{\frac{\beta}{d-d_f}} \tag{5-5}$$

where

$$\beta = (d-2) + (x+2)(1-\alpha) \tag{5-6}$$

Similarly, the critical strain for the maximum limit of linearity was approximated by

$$\gamma_c \sim \phi^{-n} \sim \phi^{\frac{d-\beta-1}{d-d_f}} \tag{5-7}$$

For $\alpha = 0$, the correlations (5-5) and (5-7) reduce to that of (Shih *et al.* 1990) for the strong-link region and for $\alpha = 1$, they lead to the ones for weak-link region. By relating the yield stress to the elastic modulus as $\tau_y = G' \gamma_c$, one obtains:

$$\tau_y \sim \phi^{\frac{d-1}{d-d_f}} \tag{5-8}$$

### 5.2.2 Fractal theory

Buscall *et al.* (1987) and Chen and Russel (1991) studied the rheological behaviour of strongly flocculated suspensions and showed that the suspension yield stresses and moduli had a power-law dependence on particle concentration supporting the idea that the networks of the flocculated suspensions have a heterogeneous structure consisting of interconnected fractal aggregates. Potanin (1993) performed computer simulations of the deformation and breakup of colloidal aggregates under shear flow and classified the aggregates into rigid and soft. Rigid aggregates elastically respond to small deformations. This elastic response is characterized by an elastic modulus and a yield stress that are related to each other and are correlated to the radius of gyration ($\xi$) as well as the internal concentration ($\phi_{\text{int}}$) by a power-law given by

$$G' \sim \tau_y \propto \xi^{-\gamma} \propto \phi_{\text{int}}^{\gamma_1} \tag{5-9}$$

where from Eq. (5-1) $\phi_{\text{int}} \sim \xi^{(d_f - d)}$ and thus $\gamma_1$, the power-law exponent relating the storage modulus to the concentration is

$$\gamma_1 = \gamma/(3 - d_f) \tag{5-10}$$

where *d* equals 3. In rigid aggregates, the interaction potential of particles is non-central and is described through a function of angles between neighbouring bonds. On the other hand, the interaction potential of particles is purely central in soft aggregates and depends on the distance between the centers of the neighbouring particles. In addition, the internal structure of the soft aggregates does not respond elastically to small deformations. Sonntag and Russel

(1986, 1987) showed that the radius of gyration of aggregates decrease with shear rate in a power-law manner,

$$\xi \sim \dot{\gamma}^{-m} \tag{5-11}$$

Equating $\eta\dot{\gamma}$ to $\tau_y$, for the rigid aggregates, yields

$$m = m_{rigid} = 1/\gamma \tag{5-12}$$

Furthermore, comparing Eq. (5-5) with Eqs. (5-9) and (5-10), one can conclude that $m_{rigid} = 1/\beta$. For purely rigid aggregates, $m_{rigid}$ is been estimated to be in the range of 0.23-0.29 and for purely soft aggregates, $m_{soft}$ is a value about 0.4-0.5 (Potanin 1993). It should be noted that these values for $m_{rigid}$ and $m_{soft}$ should be considered as lower and upper bounds of *m*; thus, for a typical colloidal suspension, the expected value of *m* is in the range of [0.23, 0.5].

## 5.3 Materials and their characterization

An epoxy Epon 828 (HEXION Speciality Chemicals Inc.) with a density of 1.16 g/mL and viscosity of 12.33 Pa.s (at 25$^{o}$C) was used as the dispersing medium and suspensions of nanotube-epoxy were prepared by mixing in an EXAKT three roll mill (from EXAKT TECHNOLOGIES. INC.) at room temperature. Multiwall carbon nanotubes (MWCNTs) from Cheap Tubes Inc.© were initially characterized by transmission electron microscopy. The details of CNT characterization is described in a previous article (Khalkhal *et al.* 2011). The nanotubes were as long as 0.1-2.2 μm with the average aspect ratio of 45. They were shown to be rigid in the range of the shear rates studied (the effective stiffness of the nanotubes ranges

from $S^{eff} \approx 0.385$ to 3850 when $\dot{\gamma} = 0.01 - 100$ s$^{-1}$ where $S^{eff} = E_Y \pi d^4 / (64 \eta_s \dot{\gamma} L^4)$ according to Switzer and Klingenberg (2003). $E_Y$ (~40 GPa according to Hobbie and Fry (2007)) is the Young modulus of the nanotubes, $d$ (14.86 nm) and $L$ (670 nm) are mean values of the outer diameter and length of the nanotubes, $\eta_s$ is the viscosity of the suspending medium (12.33 Pa.s for the neat epoxy at room temperature) and $\dot{\gamma}$ is the shear rate. The effective stiffness of the MWCNTs is large enough to categorize them among rigid rods).

Samples of CNT-epoxy suspensions were prepared at different concentrations and the details of the mixing process by a three roll mill and sample preparation are presented in a previous article (Khalkhal *et al.* 2011). A Physica MCR501 (Anton Paar) rheometer with a parallel plate geometry (PP50 with the diameter of 49.959 mm) and 1 mm gap was used to perform the rheological measurements at 25$^{o}$C. Temperature was controlled by a Peltier (P-PTD 200) system. Steady shear viscosity measurements were performed at different gaps (0.8, 1 and 1.2 mm) to prove the absence of wall slip effects during the experiments. The reproducibility of the measurements was verified by repeating the experiments several times. The maximum error was calculated to be about ± 15 %.

## 5.4 Results and discussion

Initially, a set of frequency sweep measurements were performed to determine linear viscoelastic (LVE) properties of the suspensions. We observed that the suspensions of 0.5 wt% and 1 wt% exhibited a liquid-like behaviour similar to the neat epoxy and the loss modulus was larger than the storage modulus. At 2 wt%, the storage and loss moduli showed a transition from liquid-like to solid-like behaviour at low angular frequencies, which is an indication of the formation of a percolated CNT network. At the critical concentration of

about 2 wt% and above, the elastic modulus of the suspensions was significantly larger than the viscous one.

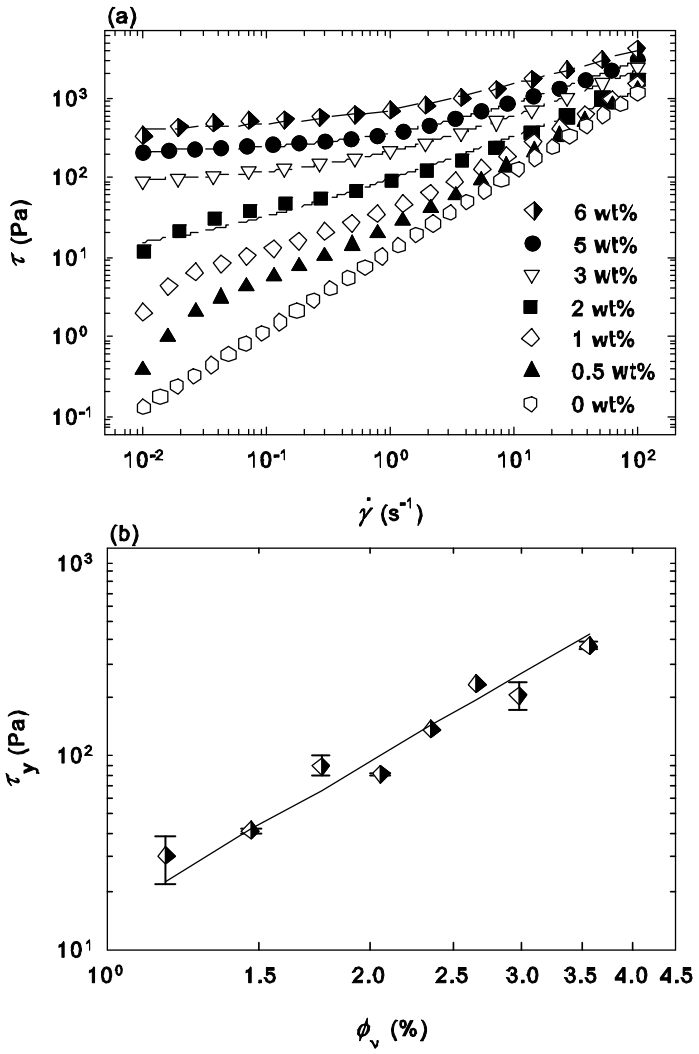


Figure 5-1: (a) Steady-shear measurement of MWCNT suspensions at different concentrations. The lines show the best fits of the data using the Herschel-Bulkley model where the apparent yield stress appears. (b) Scaling behaviour of the apparent yield stress obtained using the Herschel-Bulkley model with volume concentration of MWCNTs. The line shows the best power-law fit.

Consequently, 2 wt% was considered as the rheological percolation threshold. The formation of a percolated network was confirmed by the emergence of an apparent yield stress at about 2

wt% and higher concentration. Figure 5-1 (a) shows the steady shear measurements performed from the low shear of 0.01 $s^{-1}$ to high shear of 100 $s^{-1}$ for a range of concentrations. The results presented in this figure were confirmed to overlap by the steady shear measurement in reverse direction.

The apparent yield stress was estimated from curve fitting using the Herschel-Bulkley model that yields:

$$\tau = \tau_y + a\ \dot{\gamma}^b \tag{5-13}$$

where $\tau_y$ is the apparent yield stress, $a$ is the consistency index and $b$ is the flow behaviour index. The lines in Figure 5-1 (a) show the best fit of the experimental results with the Herschel-Bulkley model. For concentrations lower than 2 wt%, the curve fitting did not converge. Moreover, the apparent yield stress scales with the volume concentration of the suspensions as shown in Figure 5-1 (b). More samples with different concentrations in the range of 2 to 6 wt% were prepared to obtain additional apparent yield stress values and a better power-law fit. The line represents the best power-law fit of the apparent yield stress, which scales with concentration as $\tau_y \sim \phi_v^{2.64\pm0.16}$ ($R^2 = 0.973$).

### 5.4.1 Scaling behaviour of steady-shear results

Using the low frequency storage modulus of gels, Chow and Zukoski (1995) (frequencies in the range of 0.001 to 10 Hz) and Fagan and Zukoski (1997) (at frequency of 1 Hz) showed that a master curve of the steady-shear measurements can be obtained that was weakly dependent on the particle volume fraction, particle size, particle size distribution or the surface potential. To obtain the master curve, the steady-shear stress ($\tau$) should be scaled with the low

angular frequency storage modulus of the gels, $G_0'$ and the shear rate, $\dot{\gamma}$, with $\eta_s / G_0'$, where $\eta_s$ is the viscosity of the suspending medium and $\eta_s / G_0'$ is the characteristic time of the suspension. Figure 5-2 shows the steady-shear results scale with the low angular frequency (1 rad/s) storage modulus of the CNT suspensions at 2 wt% and higher concentrations. From this figure, it is clear that the results are weakly dependent on concentration. This weak dependence suggests that the network structure of the suspensions is self-similar above the percolation threshold and is constituted of closely packed clusters (flocs) that have a fractal nature.

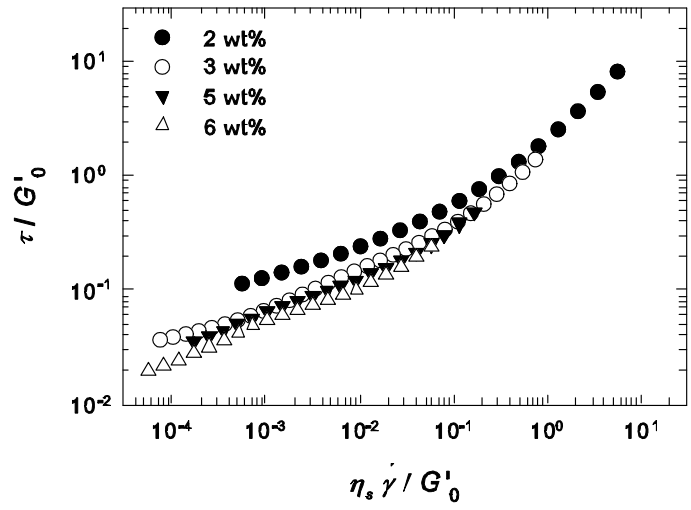


Figure 5-2: Scaling behaviour of steady shear data with low angular frequency (1 rad/s) storage modulus of the suspensions.

In the following sub-sections, the fractal structure of the suspensions is analyzed more quantitatively and the effect of flow history and temperature are investigated.

### 5.4.2 Scaling behaviour of linear viscoelastic properties

We assume that the aggregates were initially rigid, so their behaviour can be characterized by the storage modulus and yield stress that scale with the concentration of particles. The maximum strain for the limit of linearity, $\gamma_c$, was considered as the strain above which $G'/G'_0 < 0.9$, where $G'_0$ is the plateau storage modulus in the linear region. The scaling behaviour of $\gamma_c$ as well as the storage modulus (before pre-shearing) at the low angular frequency of 1 rad/s ($G'_0$) with the volume concentration was verified above the gel point of 1.17 vol% (2 wt%) as shown in Figure 5-3. The scaling behaviour of the elastic properties of the suspensions with concentration supports the fact that the suspensions have a space filling network, i.e. they are formed by individual aggregates (clusters) growing into one another and filling the space. The experimental data were fitted with power-law correlations and the best fits are shown as dashed lines in Figure 5-3. From Figure 5-3 (a), the storage modulus scales with concentration as $G'_0 \sim \phi_v^{\gamma_1}$, where $\gamma_1$ is equal to 3.74 ($R^2$ = 0.988) and from Figure 5-3 (b), $\gamma_c \sim \phi_v^{-n}$, where $n$ is equal to 1.378 ($R^2$ = 0.795). Using Eqs. (5-5)-(5-7) the fractal dimension $d_f$ was estimated to be 2.15, revealing that the network structure of CNT suspensions is among the slowly flocculating suspensions (Larson 1999). A very similar value of $d_f$ was calculated using Eq. (5-8) with $\tau_y \sim \phi_v^{2.64\pm0.16}$. Hobbie and Fry (2006, 2007) reported a fractal dimension of 2.45 for MWCNTs dispersed in low-molecular-mass polyisobutylene (PIB) showing the presence of a slightly denser network structure than our CNT suspensions. The slightly larger value could be due to more entanglements of longer nanotubes used in their study ($L$~10 μm with $L/d$ ~ 200) compared to the short nanotubes used in this study ($L$~0.1-2.2 μm, with $\langle L/d \rangle$ ~ 45). On the other hand, Chatterjee and Krishnamoorti (2007) reported a fractal dimension of

$2.1 \pm 0.3$ for single walled carbon nanotubes (SWCNTs) with an effective $L/d \sim 650$ dispersed in polyethylene oxide (PEO), which is similar to the value obtained for our MWCNT suspensions.

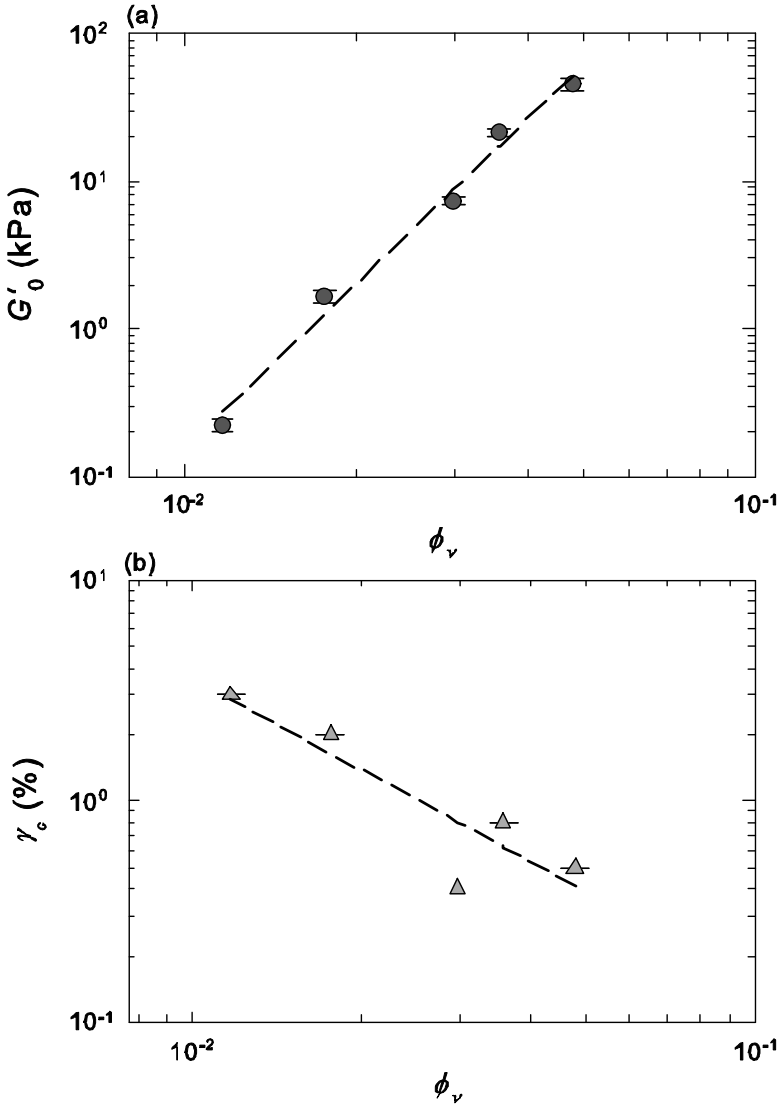


Figure 5-3: Scaling behaviour of (a) the elastic modulus and (b) the critical strain before pre-shearing as a function of volume concentration of MWCNTs.

From Figure 5-3 (b), $\gamma_c$ decreases as the volume concentration increases. This means that although the inter-particle interactions increase with concentration and a stronger network

forms, the structure becomes more fragile as the concentration increases. In the case of SWCNTs in PEO, Chatterjee and Krishnamoorti (2007) observed a similar decrease in $\gamma_c$ with concentration. Using the Shih *et al.* (1990) theory, they reported that the suspension elasticity originates mainly from short-range interactions between carbon nanotubes and the multiple connections in the percolating network. However, using the scaling theory of (Shih *et al.* 1990), the fractal backbone dimension *x* was calculated to be negative in our case, which does not have a physical meaning. On the other hand, Wu and Morbidelli (2001) introduced the parameter $\alpha$ that was calculated from Eq. (5-6) to be about 0.3-0.4 when the fractal backbone dimension *x* is in the range of 1.0-1.3, revealing the fact that in CNT suspensions used here the elasticity of the network is a contribution of the inter and intra-floc links between nanotubes. Moreover, from Eq. (5-5) and Eq. (5-7), $\beta$ was calculated to be 3.17 from which *m* equals 0.32. This value is in the range of $m_{rigid} \sim 0.23-0.29$ and $m_{soft} \sim 0.4-0.5$ reported by Potanin (1993) using computer simulations. It is very similar to the experimental value of 0.35 reported by Sonntag and Russel (1986, 1987) for polystyrene lattices. Mobuchon *et al.* (2009) obtained different values of 0.22 and 0.42 for non-polar and polar nano-clay model suspensions, respectively. This stresses that the aggregates in the CNT network are partly rigid and partly soft and so the interaction potential of the particles is a combination of central (which depends on the distance between the centers of the neighbouring particles) and non-central (which depends on angles between the adjacent bonds) components (Potanin 1993).

The evolution of the structure of colloidal suspensions under flow has been described by fractal theories (Potanin 1991,1993; Potanin *et al.* 1995) from which the deformation and break up of aggregates can be modeled. However, due to high computational cost, these

models are restricted to a very limited number of particles, which means that only the behaviour of dilute systems can be modeled. As a result of this drawback, it is impossible to compare the rheological behaviour of our CNT suspensions above their gel point using these simulation models.

### 5.4.3 The effect of flow history

In order to investigate the variation of the network structure of the suspensions under flow, the samples were pre-sheared at different rates until steady-state was reached, followed by a low angular frequency small amplitude oscillatory shear at very small deformations in the linear viscoelastic region (0.0118, 0.01, 0.0025 and 0.00174 for 0.5wt%, 1wt%, 5wt% and 6wt% respectively and 0.0072 for 2wt% and 3wt%) for sufficient time (5000 s) to approach a quasi-equilibrium state. From the scaling behaviour of the linear viscoelastic properties of the pre-sheared suspensions, the fractal dimension was estimated using the scaling theories and its variation with the pre-shear rate is explained in the light of the fractal theories.

The variation of the limit for the linear viscoelastic region with flow history was initially verified. The effect of the pre-shear rate was analyzed on the strain sweep results of the suspensions at different concentrations and pre-shear rates, followed by 5000 s rest to ensure the results were not affected by a fast structural evolution right after pre-shearing. Figure 5-4 presents the results for the strain sweep of a 3 wt% suspension pre-sheared at 1 $s^{-1}$ and 100 $s^{-1}$ carried out at 0.1 rad/s and 10 rad/s, respectively. The *y*-axis data of the pre-sheared suspension at 1 $s^{-1}$ was multiplied by a factor 5 for a better representation.

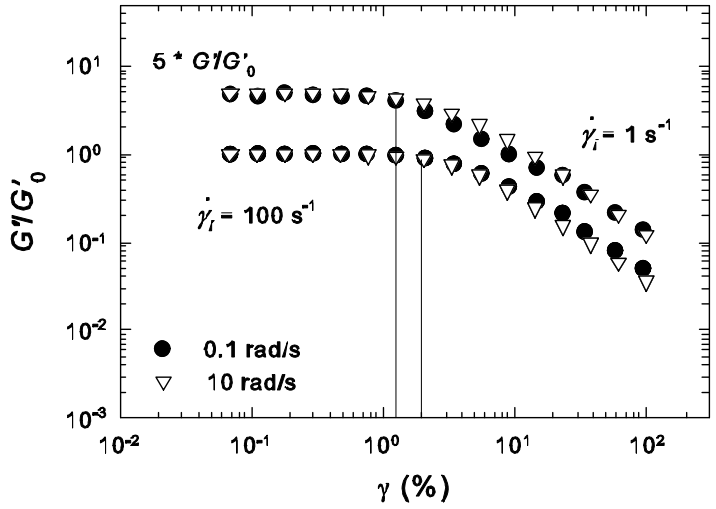


Figure 5-4: Strain sweep of reduced elastic modulus carried out at 0.1 rad/s and 10 rad/s after pre-shear rates of 1 $s^{-1}$ and 100 $s^{-1}$ for a 3 wt% MWCNT suspension in epoxy ( $G_0'$ is the storage modulus of the linear zone).

From this figure, $\gamma_c$ for the 3 wt% suspension is shown to increase from 1.27 % to 2 % when the pre-shear rate, $\dot{\gamma}_i$ , increases from 1 to 100 $s^{-1}$. This means the structure is more fragile after pre-shearing at lower rate of 1 $s^{-1}$. A similar result was obtained at other concentrations. However, the effect of pre-shearing on $\gamma_c$ was more significant at lower concentrations. These results will be used shortly to scale $\gamma_c$ with concentration via power-law correlations and to estimate the variation of $d_f$ with pre-shear rate.

The effect of pre-shearing on the small amplitude oscillatory shear (SAOS) data at 1 rad/s and strain amplitude of 0.0072 for the 3 wt% suspension is shown in Figure 5-5. The solid lines show the best exponential fits of the experimental data with the following correlation from (Khalkhal *et al.* 2011).

$$G'(t) = G'_i + (G'_\infty - G'_i)[1 - \exp(-t/\tau)] \quad (5\text{-}14)$$

where $G'_i$ and $G'_\infty$ are the storage modulus right after pre-shearing (at $t$ = 0) and 5000 s after cessation of pre-shearing, respectively and $\tau$ is a characteristic time. Some data have been eliminated to clarify the curves. For the sake of brevity, the structure build-up curves for other concentrations are not presented, but have been used for further analysis. More details about the effect of the flow history can be found in Khalkhal *et al.* (2011).

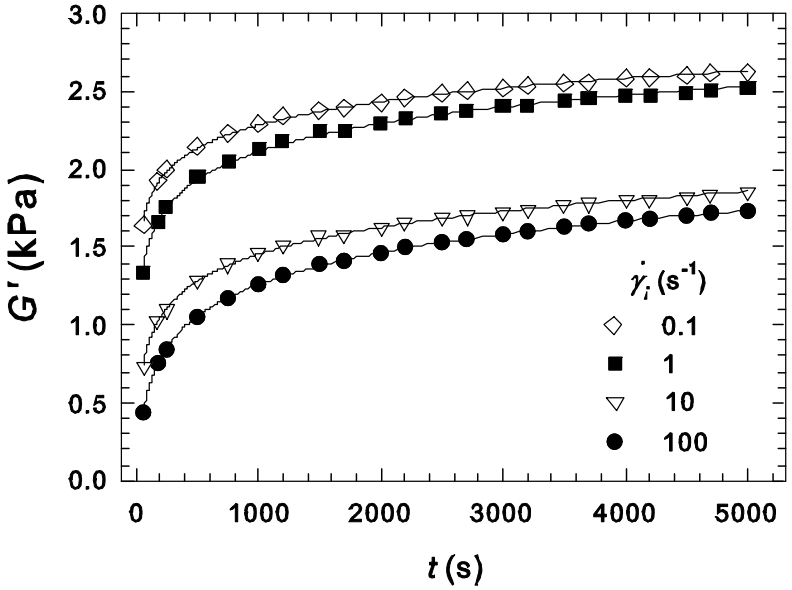


Figure 5-5: Increases of the elastic modulus for 3 wt% MWCNT-epoxy suspensions with time after cessation of shear flow for different pre-shear rates. The SAOS measurements were carried out at 1 rad/s and at a strain amplitude of 0.0072.

Figure 5-5 reveals that the suspension storage modulus evolves after cessation of shear flow. The elastic modulus of the 3 wt% suspension strongly depends on the rate of the pre-shear and it increases as the rate of the applied pre-shear decreases. Moreover, the storage modulus and so the suspension structure build up very fast shortly after cessation of pre-shearing and then more slowly to reach an equilibrium value at 5000 s or longer. In a previous article (Khalkhal

*et al.* 2011), it has been shown that pre-shearing at low rates results in the formation of a denser structure and more entanglements between nanotubes while pre-shearing at high rates breaks down some interconnections between nantotubes and their clusters. This results in the formation of an interconnected network at lower concentrations when suspensions are pre-sheared at low rates while the percolation threshold shifts to higher concentrations by pre-shearing at high rates. Figure 5-5 shows a similar effect on the structure where pre-shearing at lower rates of 0.1 and 1 $s^{-1}$ resulted in more entanglements and higher elastic modulus. However, by increasing the rate of pre-shear to 10 $s^{-1}$, some interconnections between clusters and nanotubes broke down at the expense of lower elasticity of the suspension.

The storage modulus at equilibrium (i.e. 5000 s) is denoted by $G'_\infty$, which is a function of concentration and pre-shear rate as shown in Figure 5-6. The dashed lines are the best power-law fits of $G'_\infty$ with the pre-shear rate that yields:

$$G'_\infty = \kappa \ \dot{\gamma}_i^{-\varepsilon} \tag{5-15}$$

where $\kappa$ and $\varepsilon$ are constants that depend on concentration.

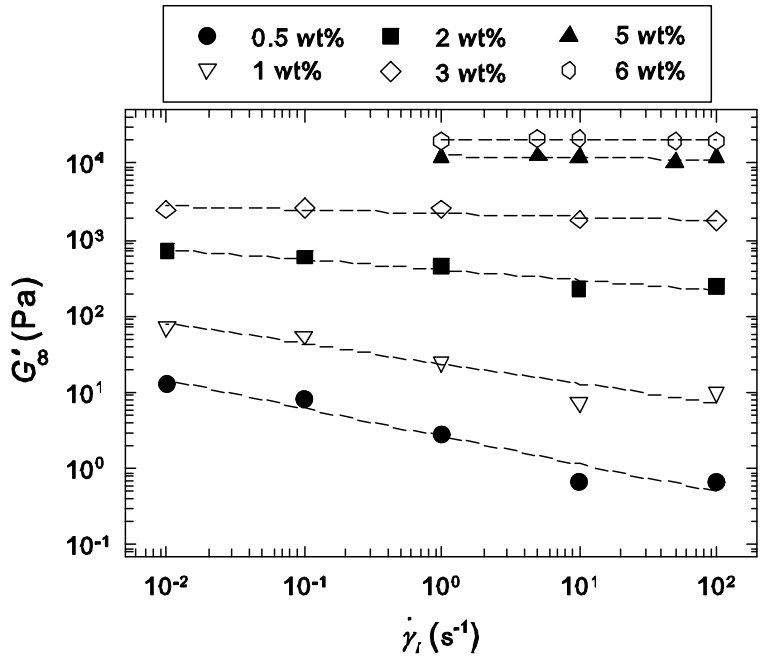


Figure 5-6: Dependence of the storage modulus on pre-shear rate for the pre-sheared MWCNT suspensions followed by 5000 s rest ($G'_\infty$). SAOS measurements were carried out at 1 rad/s in the linear region.

The error for the best fit was calculated using the normalized standard deviation that can be defined as $\sigma_N = \sqrt{\sum \left\{ \left[ (G'_\infty)_{\text{exp}} - (G'_\infty)_{\text{model}} \right] / (G'_\infty)_{\text{exp}} \right\}^2 / N}$ (where $N$ is number of experimental data) and is a more suitable parameter in this case than $R^2$ to estimate the error correctly. It is worth to note that $\varepsilon$ varies from 0.365 at 0.5 wt% (with $\sigma_N = 0.358$) to 0.003 at 6 wt% (with $\sigma_N = 0.035$). Hence, the dependence of $G'_\infty$ on the flow history becomes less pronounced by increasing concentration.

Considering Eq. (5-15), the storage modulus can be interpolated at other pre-shear rates in the range of 0.01 to 100 s$^{-1}$ having $\varepsilon$ and $\kappa$ from curve fitting; this is how $(G'_\infty)_{\text{model}}$ was calculated.

The steady-shear results can be rescaled using $\left(G'_{\infty}\right)_{\text{model}}$ instead of $\left(G'_{0}\right)$ similarly as done for Figure 5-2. The results reported in Figure 5-7 show a master curve of the steady-shear results that is almost independent on the concentration over a wider range of concentrations compared to Figure 5-2, from 0.5 wt% to 6 wt%. Note that the only large departures from the master curve are observed for the low concentration suspensions at the lowest shear rates. This reveals that $G'_{\infty}$ can predict most of the structural changes and hence is a suitable parameter for characterizing the structure of MWCNT suspensions. However, to quantify the fractal structure of the suspensions and to verify its variation under the influence of flow history (and temperature), the scaling behaviour of the LVE properties of the suspensions is considered for concentrations above the percolation threshold only.

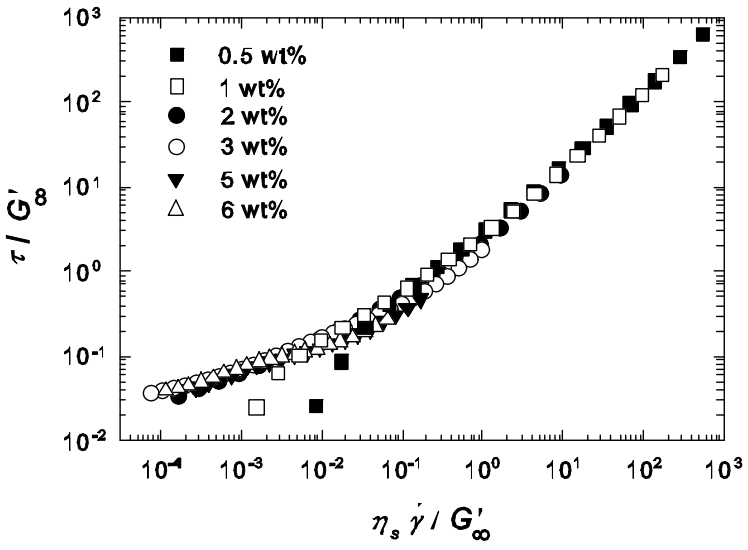


Figure 5-7: Scaling behaviour of steady-shear data with the low angular frequency storage modulus of the pre-sheared suspensions $\left(G'_{\infty}\right)$ obtained from interpolation using Eq. (5-15).

The scaling behaviour of $G'_\infty$ and the critical strain for the limit of linearity, $\gamma_c$, with the volume concentration is now verified. It should be noted that the variation of $G'_\infty$ with the pre-shear rate, $\dot{\gamma}_i$, results in a variation of the percolation threshold with pre-shearing from near 1 wt% at 0.1 $s^{-1}$ to 2.5 wt% at 100 $s^{-1}$ as mentioned previously (Khalkhal *et al.* 2011). As a result, to estimate the fractal dimension correctly, the scaling behaviour of the pre-sheared suspensions was verified just above the percolation threshold for each pre-shear rate. Figure 5-8 presents the variations of $G'_\infty$ and $\gamma_c$ with volume concentration of MWCNTs. The lines show the best power-law fits with the experimental data. From Figure 5-8 (a), the slope is shown to increase gradually with increasing pre-shear rate revealing a stronger dependence of $G'_\infty$ on the flow history. However, as seen from Figure 5-8 (b) the slope of $\gamma_c$ with volume concentration does not change significantly, but the absolute value of $\gamma_c$ increases drastically with pre-shearing. The power-law exponents from the best fits are summarized in Table 5-1, where $G'_\infty \sim \phi_v^{\gamma_1}$ and $\gamma_c \sim \phi_v^{-n}$. The estimated $R^2$ values are in the range of 0.989 to 0.998 for $\gamma_1$ and 0.916 to 0.997 for $n$.

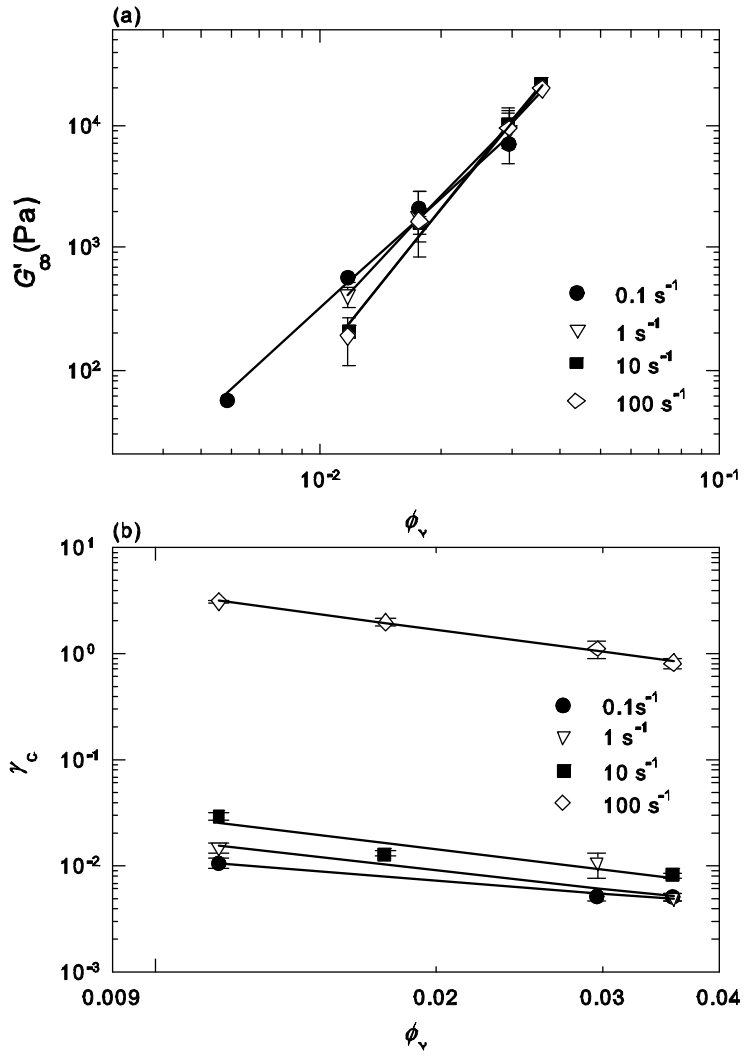


Figure 5-8: Scaling behaviour of (a) the elastic modulus and (b) the critical strain after pre-shearing at different rates followed by 5000 s rest as a function of volume concentration of MWCNTs.

Table 5-1: Exponents from the scaling behaviour of the LVE properties and fractal dimension as a function of pre-shear rate.

| $\dot{\gamma}_i(\mathrm{s}^{-1})$ | $\gamma_1$ | $n$ | $d_f$ | $m$ | $\alpha$ |
|---|---|---|---|---|---|
| 0.100 | $3.00 \pm 0.08$ | $0.69 \pm 0.27$ | $2.13 \pm 0.14$ | $0.38 \pm 0.04$ | 0.47-0.52 |
| 1.00 | $3.42 \pm 0.14$ | $0.96 \pm 0.28$ | $2.19 \pm 0.09$ | $0.36 \pm 0.03$ | 0.41-0.46 |
| 10.0 | $4.10 \pm 0.08$ | $1.10 \pm 0.12$ | $2.33 \pm 0.02$ | $0.37 \pm 0.01$ | 0.42-0.48 |
| 100 | $4.11 \pm 0.33$ | $1.18 \pm 0.02$ | $2.31 \pm 0.15$ | $0.36 \pm 0.01$ | 0.40-0.45 |

From this table, it can be observed that the exponents $\gamma_1$ and $n$ increase with pre-shear rate revealing a much stronger dependence of $G'_\infty$ and $\gamma_c$ to the volume concentration as the pre-shear rate is increased. From Eqs. (5-5)-(5-7) the fractal dimension can be determined and the values are also reported in Table 5-1. Although, the exponents $\gamma_1$ and $n$ significantly increase with pre-shear rate, the fractal dimension, $d_f$ increases only slightly from 2.13 at 0.1 to 2.31 at 100 $s^{-1}$ pre-shear rates. A similar increase in the fractal dimension of a colloidal suspension was reported by Potanin (1993) and Potanin *et al.* (1995) that was related to the breakdown of the primary aggregates and the formation of secondary aggregates that contract as the pre-shear rate increase and form a more compact structure with larger $d_f$. However, for initially dense aggregates with $d_f > 2.0$, the extent of the increase in the $d_f$ was not very significant, which is the case for the CNT suspensions used here with an initial $d_f$ of about 2.15. Our results reveal that although the suspensions structure is sensitive to the flow history, the superstructure of the network is not influenced considerably and the variation of $d_f$ with pre-shear rate remains within the experimental error. Consequently, one should consider the

fractal dimension of the pre-sheared suspensions to be in the range of $2.13 \pm 0.14$ to $2.31 \pm 0.15$.

The power-law exponent for the variation of the radius of gyration of aggregates ($\zeta$) with the shear rate under the influence of flow history, $m$, was also determined for the suspensions to be in the range of 0.36-0.38 and in the limit between $m_{rigid}$ and $m_{soft}$, clarifying the importance of both central and non-central components of the interaction potential of particles in the pre-sheared suspensions. In addition, considering a typical range of 1.0-1.3 for $x$, the fractal backbone dimension, $\alpha$ was estimated from Eq. (5-6) and is presented in Table 5-1. It is shown that $\alpha$ varies between 0.40-0.52 revealing that the elasticity of the pre-sheared suspensions stems from inter and intra-floc links between nanotubes (Wu and Morbidelli 2001).

### 5.4.4 The effect of temperature

To investigate the effect of temperature on the suspensions microstructure, the variation of the limit for the linear viscoelastic region as well as the linear viscoelastic results at different concentrations was verified when the temperature was varied from 15 to 45 $^{o}$C. It should be noted that although the range of temperatures used was limited, its influence on the LVE results was significant. To ensure the sample had a uniform temperature after being loaded into the rheometer, it was kept in quiescent conditions for 10 min before running any experiments.

Initially, the maximum strain for the limit of linearity was determined for each concentration at different temperatures. The results are summarized in Table 5-2. It can be observed that for each suspension, $\gamma_c$ decreased with temperature revealing the formation of a more fragile

structure as the temperature increased. However, the influence of temperature on $\gamma_c$ was more pronounced at lower concentrations.

Table 5-2: Variations of $\gamma_c$ (%) with temperature at various concentrations

| ***c* (wt%)** | ***T* = 15 °C** | ***T* = 25 °C** | ***T* = 35 °C** | ***T* = 45 °C** |
|---|---|---|---|---|
| 2 | 2.41 | 1.94 | 1.46 | 1.01 |
| 3 | 1.72 | 1.26 | 0.96 | 0.78 |
| 5 | 0.67 | 0.64 | 0.48 | 0.60 |
| 6 | 0.79 | 0.58 | 0.38 | 0.43 |

The effect of temperature on the LVE properties was determined for the suspensions as well as the neat epoxy. The complex viscosity, storage and loss moduli of the suspensions decreased with temperature as expected. However, to eliminate the influence of temperature on the viscosity of the matrix, the results were reduced using the norm of the complex modulus of the neat epoxy at each temperature. The reduced storage and loss moduli for a 2 wt% suspension reported in Figure 5-9 show a drastic increase with temperature; however, this effect is more pronounced on the reduced storage modulus. A similar behaviour was observed at other concentrations revealing the effect of increasing interaction between CNTs with temperature on the rheology of the suspensions.

Abbasi *et al.* (2009) observed that the reduced complex viscosity of polycarbonate-MWCNT nano-composites increased with temperature revealing more inter-particle interactions, which is also in agreement with our results. However, in contrast to the results of this work, they reported increases of $\gamma_c$ and cohesive energy ($E_c = 0.5\gamma_c^2 G_0'$, the work required to break-up

the elastic structure) with temperature, revealing the formation of stronger network. From a structural point of view, they argued that the increase in temperature results in the breakdown of CNT bundles to individual nanotubes; thus the effective aspect ratio of nanotubes increased, which resulted in lower percolation thresholds and higher intrinsic viscosities at higher temperatures.

The time-temperature superposition was verified for the suspensions in the temperature range of 15 to 45 $^{o}$C using the reduced storage modulus data. Since the neat epoxy is Newtonian, the reduced storage modulus corresponds to the contribution of CNTs. The results are reported in Figure 5-10. The angular frequency was multiplied by a shift factor, $a_T$ taken the reference temperature at 15 $^{o}$C. The *y*-axis for the 6 wt% suspension was multiplied by a factor 10 to avoid overcrowding with the one for the 5 wt%. This figure shows that the time-temperature superposition principle, which is valid for pure polymers, is also valid for the CNT suspensions. This is in accordance with our previous observation (Khalkhal *et al.* 2011) for collapsing the steady-shear viscosity data of a CNT suspension on a master curve for a similar temperature range. Note from Figure 5-10 (a), the angular frequency is extended by more than two decades, down to $10^{-3}$ rad/s compared to $10^{-1}$ rad/s in Figure 5-9, which was practically inaccessible at high concentrations. Moreover, the reduced storage modulus for the 5 wt% suspension is almost a decade larger than the one for the 3 wt% suspension (and similarly, the reduced storage modulus of the 3 wt% suspension was almost a decade larger than the one for the 2 wt%) at similar angular frequencies that can be associated to more inter-particle interactions due to the increase in concentration. However, the reduced modulus for the 5 wt% and 6 wt% suspensions are almost similar. Figure 5-10 (b) reports the shift factor $a_T$, as a function of $1/T$. From this figure, there is only a small variation of $a_T$ with concentration, which shows that the increase of the CNT interactions with temperature is almost independent

of concentration. $a_T$ is shown to scale exponentially with $1/T$ (straight line in Figure 5-10 (b)), revealing the fact that the time-temperature superposition is accounted for by an Arrhenius correlation:

$$a_T = \exp[\frac{E_a}{R}(\frac{1}{T} - \frac{1}{T_0})] \quad (5\text{-}16)$$

where $E_a$ is the activation energy, $R$ is the gas constants (8.314 J/(mol K)) and $T_0$(K) is the reference temperature which is considered to be 15 $^oC$ (288 K). Using Eq. (5-16), an average $E_a$ is calculated from curve fitting in Figure 5-10 (b), which is equal to 129.7 kJ/mol ($R^2$ = 0.979). This is the energy required for the molecules to move against the internal flow barriers caused by friction between the neighbouring molecules.

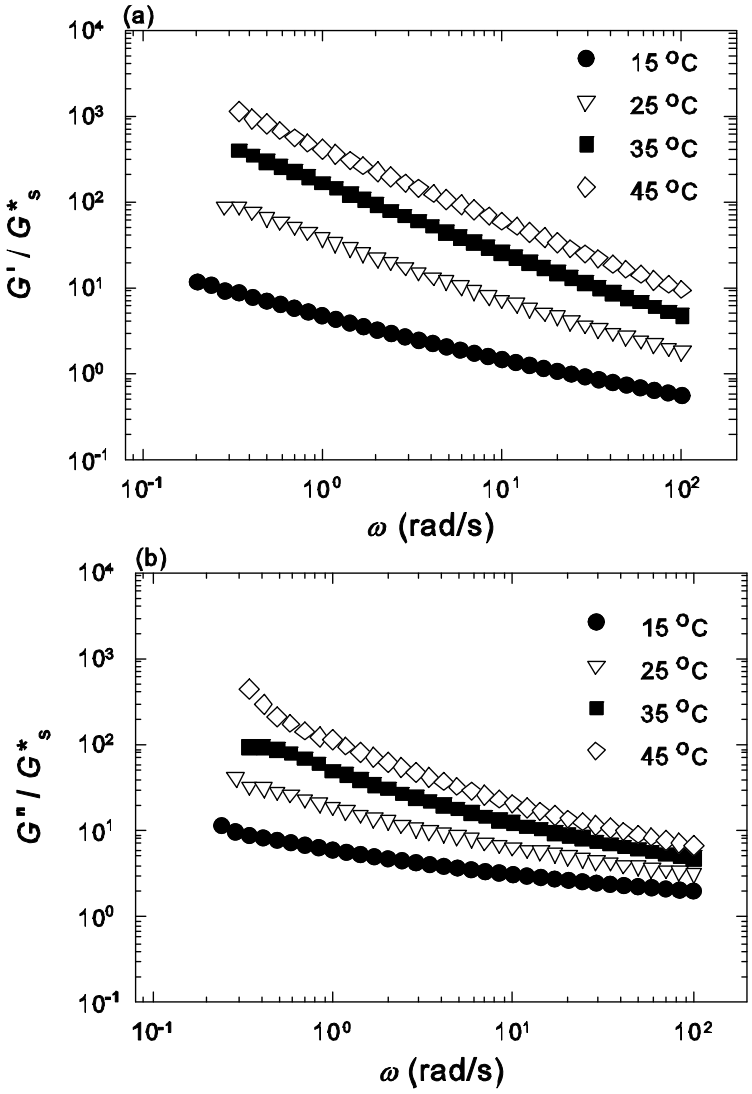


Figure 5-9: The effect of temperature on the frequency sweep results of a 2 wt% MWCNT-epoxy suspension (a) reduced storage modulus (b) reduced loss modulus. $G^*_s$ is the norm of the complex modulus of the neat epoxy.

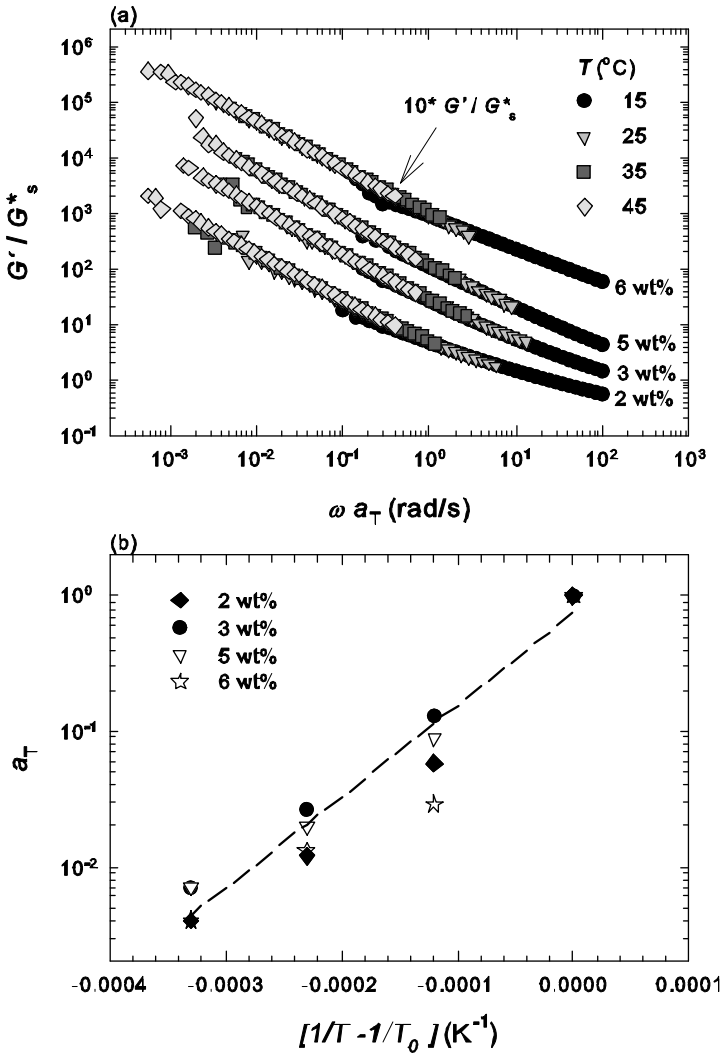


Figure 5-10: (a) Time-temperature superposition for reduced storage modulus of MWCNT suspensions in epoxy; $G^*_s$ is the norm of the complex modulus of the neat epoxy (b) variation of the shift factor $a_T$ with absolute temperature at various concentrations.

For non pre-sheared suspensions, the scaling behaviour of the low angular frequency storage modulus $G'_0$ at 1 rad/s and the maximum strain for the limit of linearity $\gamma_c$ was verified at different temperatures and the power-law exponents $\gamma_1$ (from $G'_0 \sim \phi_v^{\gamma_1}$) with $R^2$ = 0.930 to 0.999 and $n$ with $R^2$ = 0.923 to 0.997 were obtained and reported in Table 5-3. From these

exponents the fractal dimension $d_f$ was calculated as a function of temperature using Eqs. (5-5)-(5-7). The results show the variations of $d_f$ with temperature; however, the variations do not show a clear trend and the differences in the fractal dimensions remain in the range of the experimental error. Moreover, the exponent $m$ varies from 0.29 to 0.38 and remains within the limit of soft and rigid aggregates. $\alpha$ was also calculated to be within [0,1] revealing that the suspensions elasticity originates from both inter and intra-floc links.

Table 5-3: Variations of the scaling exponents with temperature

| $T$ ($^o$C) | $\gamma_1$ | $n$ | $d_f$ | $m$ | $\alpha$ |
|---|---|---|---|---|---|
| 15 | $2.740 \pm 0.167$ | $1.167 \pm 0.274$ | $1.72 \pm 0.09$ | $0.29 \pm 0.04$ | 0.17-0.25 |
| 25 | $3.442 \pm 0.058$ | $1.131 \pm 0.084$ | $2.13 \pm 0.01$ | $0.34 \pm 0.01$ | 0.34-0.40 |
| 35 | $2.922 \pm 0.391$ | $1.223 \pm 0.051$ | $1.77 \pm 0.25$ | $0.29 \pm 0.02$ | 0.19-0.26 |
| 45 | $2.868 \pm 0.060$ | $0.707 \pm 0.158$ | $2.07 \pm 0.04$ | $0.38 \pm 0.02$ | 0.45-0.50 |

From the results reported on the effect of temperature, one can conclude that the inter-particle interactions increase with temperature as shown in Figure 5-9; however it is impossible to clarify whether the superstructure becomes more open or compact with temperature. This could be due to the limited temperature range of this system (only 30 $^o$C temperature difference) although the linear viscoelastic properties of the suspensions were significantly influenced by temperature in this range.

## 5.5 Conclusion

The scaling behaviour of linear viscoelastic properties of MWCNT-epoxy suspensions was investigated with and without pre-shearing history. Initially, the suspensions fractal dimension $d_f$ was approximated to be about 2.15, characteristic of slowly flocculating suspensions where flocs gradually penetrate one another to some extent after collision. In addition, the elasticity of the network structure of the suspensions was shown to originate from the contribution of inter and intra-floc links between nanotubes.

From the master curve of the steady-shear results normalized with the low angular frequency storage modulus of the pre-sheared suspensions, $G'_\infty$, it was concluded that $G'_\infty$ that varies with the pre-shear rate and concentration can account for most of the structural changes during flow and thus is a suitable parameter for characterizing the structure of CNT suspensions. The power-law exponents of $G'_\infty$ and $\gamma_c$ demonstrated a significant increase with applied pre-shear rate; however, the resulting $d_f$ and so the superstructure of the network of the suspensions exhibited only a small variation with flow history that was related to the initially dense structure of the suspensions before pre-shearing ($d_f \sim 2.15$). As one of the applications of CNT suspensions is in preparing conductive nano-composites, it is important to preserve the network structure of the suspensions during processing.

The power-law exponent $m$ revealing the variation of the radius of gyration of the aggregates with the applied shear rate ($\xi \sim \dot{\gamma}^{-m}$) was found to be in the range of 0.36-0.38 and in the limit for $m_{rigid}$ and $m_{soft}$ obtained theoretically by Potanin (1993) and similar to the experimental values obtained by Sonntag and Russel (1986, 1987). This shows that the interaction potential of nanotubes is a combination of central and non-central components.

Finally, the effect of temperature on the scaling behaviour of the suspensions was verified with no pre-shear history except for the sample loading into the instrument. It was observed that the reduced storage and loss moduli of the suspensions increased with temperature, suggesting more interactions between CNTs. Moreover, the time-temperature superposition principle was verified for the CNT suspensions and the shift factor was found to obey an Arrhenius equation. However, the estimated fractal dimension had large errors that made it difficult to identify whether the superstructure of the suspensions change as influenced by temperature.

## 5.6 Acknowledgements

We are thankful to Dr. Daniel Therriault for providing access to the three roll mill at the composite lab in the mechanical engineering department of Ecole Polytechnique. Funding from Natural Sciences and Engineering Research Council of Canada (NSERC) and Consortium for Research and Innovation in Aerospace in Quebec (CRIAQ) is gratefully acknowledged.

## 5.7 References

Abbasi S, Carreau PJ, Derdouri A, Moan M (2009) Rheological properties and percolation in suspensions of multiwalled carbon nanotubes in polycarbonate. Rheol Acta 48(9):943-959

Buscall R, McGowan IJ, Mills PDA, Stewart RF, Sutton D, White LR, Yates GE (1987) Rheology of strongly-flocculated suspensions. J Non-Newton Fluid Mech 24(2):183-202

Chatterjee T, Krishnamoorti R (2007) Dynamic consequences of the fractal network of nanotube-poly(ethylene oxide) nanocomposites. Phys Rev E Stat Nonlinear Soft Matter Phys 75(5):050403

Chen M, Russel WB (1991) Characteristics of flocculated silica dispersions. J Colloid Interface Sci 141(2):564-577

Chow MK, Zukoski CF (1995) Nonequilibrium behaviour of dense suspensions of uniform particles: Volume fraction and size dependence or rheology and microstructure. J Rheol 39(1):33-59

de Gennes PG (1979) Scaling concepts of polymer physics. Cornell University Press, Ithaca

Fagan ME, Zukoski CF (1997) Rheology of charge stabilized silica suspensions. J Rheol 41(2):373-397

Fan Z, Advani SG (2007) Rheology of multiwall carbon nanotube suspensions. J Rheol 51(4):585-604

Fry D, Langhorst B, Kim H, Grulke E, Wang H, Hobbie EK (2005) Anisotropy of sheared carbon-nanotube suspensions. Phys Rev Lett 95(3):038304

Fry D, Langhorst B, Wang H, Becker ML, Bauer BJ, Grulke EA, Hobbie EK (2006) Rheo-optical studies of carbon nanotube suspensions. J Chem Phys 124(5):054703

Hobbie EK, Fry DJ (2006) Non-equilibrium phase diagram of sticky nanotube suspensions. Phys Rev Lett 97(3):036101

Hobbie EK, Fry DJ (2007) Rheology of concentrated carbon nanotube suspensions. J Chem Phys 126(12):124907

Hobbie EK, Wang H, Kim H, Han CC, Grulke EA, Obrzut J (2003a) Optical measurements of structure and orientation in sheared carbon-nanotube suspensions. Rev Sci Instrum 74(3 I):1244-1250

Hobbie EK, Wang H, Kim H, Lin-Gibson S, Grulke EA (2003b) Orientation of carbon nanotubes in a sheared polymer melt. Phys Fluids 15(5):1196-1202

Huang YY, Ahir SV, Terentjev EM (2006) Dispersion rheology of carbon nanotubes in a polymer matrix. Phys Rev B: Condens Matter 73(12):125422

Khalkhal F, Carreau PJ, Ausias G (2011) Effect of flow history on linear viscoelastic properties and the evolution of the structure of multiwalled carbon nanotube suspensions in an epoxy. J Rheol 55(1):153-175

Larson RG (1999) The structure and rheology of complex fluids. Oxford University Press, New York

Lin-Gibson S, Pathak JA, Grulke EA, Wang H, Hobbie EK (2004) Elastic flow instability in nanotube suspensions. Phys Rev Lett 92(4):48302

Mobuchon C, Carreau PJ, Heuzey MC (2009) Structural analysis of non-aqueous layered silicate suspensions subjected to shear flow. J Rheol 53(5):1025-1048

Potanin AA (1991) On the mechanism of aggregation in the shear flow of suspensions. J Colloid Interface Sci 145(1):140-157

Potanin AA (1993) On the computer simulation of deformation and breakup of colloidal aggregates in shear flow. J Colloid Interface Sci 157:399-410

Potanin AA, De Rooij R, Van den Ende D, Mellema J (1995) Microrheological modeling of weakly aggregated dispersions. J Chem Phys 102(14):5845-5853

Pujari S, Rahatekar SS, Gilman JW, Koziol KK, Windle AH, Burghardt WR (2009) Orientation dynamics in multiwalled carbon nanotube dispersions under shear flow. J Chem Phys 130(21):214903

Rahatekar SS, Koziol KKK, Butler SA, Elliott JA, Shaffer MSP, Mackley MR, Windle AH (2006) Optical microstructure and viscosity enhancement for an epoxy resin matrix containing multiwall carbon nanotubes. J Rheol 50(5):599-610

Shih W-H, Shih WY, Seong-Il K, Jun L, Alsay IA (1990) Scaling behaviour of the elastic properties of colloidal gels. Phys Rev A 42(8):4772-4779

Song YS, Youn JR (2005) Influence of dispersion states of carbon nanotubes on physical properties of epoxy nanocomposites. Carbon 43(7):1378-1385

Sonntag RC, Russel WB (1986) Structure and breakup of flocs subjected to fluid stresses : I. Shear experiments. J Colloid Interface Sci 113(2):399-413

Sonntag RC, Russel WB (1987) Structure and breakup of flocs subjected to fluid stresses: II. Theory. J Colloid Interface Sci 115(2):378-389

Switzer III LH, Klingenberg DJ (2003) Rheology of sheared flexible fibre suspensions via fiber-level simulations. J Rheol 47(3):759-778

Wu H, Morbidelli M (2001) A model relating structure of colloidal gels to their elastic properties. Langmuir 17(4):1030-1036

Wu D, Wu L, Zhou W, Sun Y, Zhang M (2009) Relations between the aspect ratio of carbon nanotubes and the formation of percolation networks in biodegradable polylactide/carbon nanotube composites. J Polym Sci B Polym Phys 48(4):479-489

# CHAPITRE 6 CRITICAL SHEAR RATES AND STRUCTURE BUILD-UP AT REST IN MWCNT SUSPENSIONS

Fatemeh Khalkhal and Pierre J. Carreau

*Center for Applied Research on Polymers and Composites, Chemical Engineering Department, Ecole Polytechnique of Montreal, Quebec, Canada*

*C.P. 6079 Suc. Centre-Ville, Montreal, Quebec H3C 3A7*

*Tel:(514)340-4711 ext. 4924*

*Fax:(514)340-2994*

This article has been submitted to the Journal of Non-Newtonian Fluid Mechanics.

# Abstract

In this paper, we quantitatively analyze the extent of structure build-up at rest in carbon nanotubes (CNTs) dispersed in an epoxy by a set of transient flow measurements. Stress overshoots appeared at very small deformations during forward and reverse flow measurements by providing some rest time between the two consecutive flows in opposite directions, during which the suspensions structure was reconstructed. The rest time required to build-up the structure completely was much longer than the values reported in literature (about 1h). Moreover, unlike fibre suspensions or some nano-composites, it was shown that the Brownian motion plays an important role in the structure build-up of the CNT suspensions in the absence of flow. We observed critical shear rates at low and intermediate concentrations above which some nanotube entanglements broke down; this resulted in lower elasticity of the suspensions and partial structure build-up at rest during transient flow reversal measurements. This phenomenon and the possible mechanisms of structure evolution during flow and rest were further investigated by comparing the experimental results with the predictions of a structural model.

**Keywords**: carbon nanotube, stress overshoot, structure build-up, rheology, nano-composite, structural model

## 6.1 Introduction

To make multi-functional nano-composites, it is important to control their structure. A great deal of research has been devoted to establish a relationship between the micro-structure and the macroscopic properties of composites. In particular, rheology has been employed to evaluate the structural changes during processing. Small amplitude oscillatory shear (SAOS) measurements are commonly used as they are non-destructive. However, to extend the rheological analysis to larger deformations, transient measurements have been used by many researchers.

Since CNTs have a fibre-like shape and dimensions in the order of nanometres, they may have similar behaviour to fibre suspensions in one hand and nano-composites on the other hand. Therefore, it is necessary to compare their properties with both groups. The transient behaviour of fibre suspensions and nano-composites has been studied experimentally and theoretically. Overshoots have been observed and related mainly to fibre orientation in flow direction [1] while the breakdown of a percolated network and/or orientation of nano-particles in flow direction has been reported as the main mechanisms for the emergence of stress overshoots; as an example, one can refer to transient results reported for polybutylene terephthalate (PBT)-MWCNT [2], PBT-montmorillonite nano-composites [3], polypropylene (PP)/clay nano-composites [4-6], organoclay in poly[butylene succinate-co-adipate] (PBSA) [7] and carbon nano-fibres (CNFs) in polystyrene (PS) [8]. A set of flow reversal experiments are usually performed to examine the extent of structure build-up at rest. If no rest time is provided between both consecutive transient measurements, no stress overshoot is observed in the reverse direction in nano-composites [2-4, 6-9]; however, in fibre suspensions, reverse overshoots were reported under similar conditions and were related to fibre tumbling [10]. On

the other hand, stress overshoots appeared in nano-composites after providing some rest time between the two consecutive experiments in forward and reverse directions and the overshoot magnitude increased with rest time. The complete structure build-up, which is characterized by the extent of the reverse stress (or viscosity) overshoot approaching a similar value to the one in forward direction, took about 1000 s [11] and 1200 s [4] in PP/organoclay nano-composites and 1800 s in PBSA/organoclay [7]. A similar behaviour has been reported in fibre suspensions during shorter rest time of 1 min in glass fibre suspensions dispersed in Newtonian and non-Newtonian fluids [12] and 200 s and 1000 s in short glass fibre suspensions dispersed in polybutene (PB) and in a Boger fluid [10], respectively. During rest, it has been shown that fibres lose their orientation partially or completely due to the relaxation of polymer molecules [10], which resulted in the emergence of reverse stress overshoots. In nano-composites, the dis-orientation of nano-particles due to the relaxation of the polymer matrix [4, 7, 11] and the reconstruction of network [2, 3, 5, 6] due to attraction between particles and not to Brownian forces have been reported as possible mechanisms for the evolution of the suspension structure at rest.

Recently, we have shown [13] how the flow history affects the structure and linear viscoelastic (LVE) properties of CNT suspensions. Moreover, the suspensions structure develops upon cessation of shear flow with a certain rate that strongly depends on the rate of pre-shearing (especially in more dilute systems) and the inter-particle interactions. The higher is the rate of pre-shear, the slower is the kinetics of structure build-up. With increasing concentration or temperature, the inter-particle interactions increase and result in faster structure development. In this paper, we investigate the evolution of structure of CNTs dispersed in an epoxy via a set of transient flow reversal experiments. Unlike previous

investigations in the literature which are mainly limited to a single concentration or relatively low shear rates, various concentrations and two different shear rates are considered. We observe critical shear rates above which some nanotube entanglements breakdown and reduce the suspension elasticity. The extent of structure build-up at rest is quantified in the vicinity of the critical shear rates by comparing the magnitude of stress overshoots in opposite directions. Surprisingly, unlike fibre suspensions or nano-composites, the structure build-up at rest is limited to a certain extent when the rate of applied shear is larger than the critical one. At lower shear rates (below the critical shear rate), the structure develops completely but during much longer rest times compared to the values reported in literature. These phenomena as well as the possible mechanisms for the structure evolution during flow and rest are further investigated by comparing the experimental results with predictions of a structural model.

The article is organized as follows. Initially the materials are introduced and the sample preparation method along with a summary of the detail experimental procedure is reported in Sec.6.2. A structural model used to compare our experimental results is presented in Sec.6.3. In the next section, the critical shear rates are quantified using non-destructive SAOS measurements. The results of the transient flow measurements are reported in the following section in the vicinity of critical shear rates. In Sec.6.6, a brief sensitivity analysis of the fitting parameters on the model predictions is performed. The results are compared with predictions of the structural model in the subsequent section and are more elaborated from a structural point of view. A short discussion is presented in Sec.6.8 followed by the concluding remarks in Sec.6.9.

## 6.2 Materials and rheological measurements

An epoxy Epon 828 (supplied by Hexion Specialty Chemicals, Inc.) with a density of 1.16 g/mL and viscosity of 12.33 Pa.s (at 25$^{o}$C) was used as the dispersing medium and suspensions of nanotube-epoxy were prepared by mixing in an EXAKT three roll mill (from Exakt Technologies Inc.) at room temperature. Multiwalled carbon nanotubes (MWCNTs) from Cheap Tubes Inc.© were initially characterized by transmission electron microscopy. The nanotubes were as long as 0.1-2.2 μm with the average aspect ratio of 45. More details about sample preparation and characterization as well as CNTs characterization are given in a previously published article [13].

A Physica MCR501 (Anton Paar) rheometer with a parallel plate geometry (PP50 with the diameter of 50 mm) and 1 mm gap was used to perform the rheological measurements at 25$^{o}$C. This geometry was previously shown to generate reliable data in other filled polymers [10, 14, 15]. The temperature was controlled by a Peltier (P-PTD 200) system. Steady-shear viscosity measurements were performed at different gaps (0.8, 1 and 1.2 mm) to prove the absence of wall slip effects during the experiments. The transient stress growth experiments were repeated several times for samples of the same concentration. At each concentration, different samples may give slightly different results. We shall notify that the differences are more pronounced at the beginning of the stress growth measurements. However, the relative values of the stress overshoots in opposite directions remain almost invariant ($<\pm 1\%$ to $\pm 9\%$) at similar rest times. The overall discrepancy between different measurements was within $\pm 7\%$ to $\pm 16\%$ range. The shear rate and strain were evaluated at the rim of the geometry, i.e. for a radial position equal to 25 mm.

As we have shown previously [13], the flow history strongly influences the rheological properties of the suspensions. Hence, it is important to consider a similar pre-conditioning for all samples in order to minimize the effect of flow history on the results. Samples were initially pre-sheared at 0.5 $s^{-1}$ in clock wise (CW) direction until steady state conditions were reached (64 s for 2 wt% and 3 wt% and 75 s for 5 wt%). Then a rest time (1200 s for 2 wt% and 2400 s for 3 wt% and 5 wt%) was given and the stress relaxation was monitored to avoid the effect of residual stresses at the beginning of the next experiments. The final values of the stress at the end of the rest time were less than 5% of the steady state values after start-up at 0.5 $s^{-1}$. This was considered as a pre-shearing stage for all suspensions. After pre-shearing, a stress growth experiment was performed in counter clock-wise (CCW) direction at two different shear rates of 1 $s^{-1}$ and 10 $s^{-1}$ up to steady state conditions (437 s and 65 s, respectively) at 2 wt%, 3 wt% (269 s and 65 s, respectively) and (75 s and 65 s, respectively) 5 wt%; after different rest times from 0 s to 1 h, the suspensions response was monitored by transient measurements in reverse (CW) direction. At 5 wt%, the first normal stress difference could be measured at the shear rate of 10 $s^{-1}$ according to a similar procedure just explained for measuring the stress growth. However, at other shear rate of 1 $s^{-1}$ or other concentrations, the results were poorly reproducible; therefore, they are not reported here.

## 6.3 Structural model

A structural model was proposed by Yziquel *et al.* [16] that describes the nonlinear behaviour of concentrated suspensions. This model was used to compare the experimental results with model predictions. A structural parameter, $\xi$, is introduced to describe the evolution of suspension structure more quantitatively. $\xi$, represents the number of physical bonds between the particles which is normalized with the maximum possible number of bonds and so varies

between 0 for completely destroyed structure and 1 for completely structured suspensions. A more careful quantitative way to analyze the structural evolution is via confocal microscopy. This technique was earlier used by Mobuchon *et al.* [17] who showed the rheological properties of model clay suspensions is controlled by the aggregate size. However, the same technique could not be used in the model carbon nanotube suspensions due to their opaque structure even in very dilute concentrations.

In the Yziquel model [16], the flow properties of the suspensions are assumed to be controlled by a simultaneous breakdown and build-up of the structure. The shear stress is described by a modified form of the upper convected Jeffreys model as follows [16]:

$$\frac{\delta}{\delta t}\left[\frac{\sigma}{G(\xi)}\right]+\frac{\sigma}{\eta(\xi)}=\left(1+\frac{\eta_\infty}{\eta(\xi)}\right)\dot{\gamma}+\eta_\infty\frac{\delta}{\delta t}\left(\frac{\dot{\gamma}}{G(\xi)}\right) \tag{6-1}$$

where, $\delta/\delta t$ is the upper convected derivative, $\sigma$ is the shear stress, $t$ is time, $\dot{\gamma}$ is the shear rate and $\eta_\infty$ is the viscosity of destroyed structure. $G(\xi)$ and $\eta(\xi)$ are the structured modulus and viscosity, which are defined in Eq. (6-2) and Eq. (6-3), respectively.

$$G(\xi)=G_0\xi+G_\infty \tag{6-2}$$

where, $G_\infty$ is the elastic modulus of destroyed structure and $G_\infty + G_0$ (when $\xi = 1$) is the equilibrium value of the elastic modulus of the structure.

$$\eta(\xi)=\frac{\eta_0}{f(\xi)} \tag{6-3}$$

where, $\eta_0$ is a characteristic viscosity and $f(\xi)$ is an empirical structural function defined as:

$$f(\xi)=\left(\frac{1}{\xi}-1\right)^{(1-n)/(1+n)} \tag{6-4}$$

where, $n$ is an empirical power-law coefficient. The evolution of the structure is defined by the evolution of structural parameter, $\xi$, in the following form:

$$\frac{\lambda_0}{k_1}\frac{\partial \xi}{\partial t} = (1-\xi) - \frac{{\lambda_0}^2}{\eta_0}\frac{k_2}{k_1}\xi\left|\sigma : \dot{\gamma}\right| \tag{6-5}$$

where, $\lambda_0 = \eta_0/(G_0 + G_\infty)$ is a characteristic time related to the particle interactions. $k_1$ and $k_2$ are two kinetic constants that control the rate of the structure build-up (the first term on the right hand side of Eq. (6-5)) and the structure breakdown (the second term on the right hand side of Eq. (6-5)), respectively. Eq. (6-5) is a balance between the structure build-up, which is assumed to be controlled by Brownian motion only and the structure breakdown, which is controlled by the rate of energy dissipated ($\left|\sigma : \dot{\gamma}\right|$) by the flow process. The model has seven parameters including $\eta_0$, $\eta_\infty$, $G_0$, $G_\infty$, $k_1$, $k_2$ and $n$.

A simplified form of Eq. (6-1) was introduced by Letwimolnun *et al.* [4] where $G(\xi)$ was put outside the convected derivative. This simplified model has shown its ability to predict the transient behaviour of organoclay nano-composites only for relatively low shear rates. In the following analysis, the original model of Yziquel *et al.* [16], i.e. Eq. (6-1), is retained.

## 6.4 Critical shear rates

As a common knowledge, flow history can affect the rheological properties of suspensions. In previously published articles [13, 18], we have quantified the effect of the flow history on the structure of MWCNTs and the linear viscoelastic properties of the suspensions. It has been shown that meta-stable structures form upon cessation of shear flow, the properties of which strongly depend on the rate of pre-shearing. The lower is the rate of pre-shear, the higher is the resulting storage modulus. This effect is more pronounced at lower concentrations where

the suspensions structure is more fragile due to less inter-particle interactions [13]. Pre-shearing results in the formation of more entanglements between nanotubes when applied at low rates and partial breakdown of some clusters and nanotube entanglements at higher shear rates. This argument was supported by the quantitative measurement of the percolation threshold, which shifted from near 1 wt% when the samples were pre-sheared at 0.01 $s^{-1}$ to 2.5 wt% after pre-shearing at 100 $s^{-1}$. Hence, there should be a critical pre-shear rate at each concentration above which some entanglements breakdown. In this section, this shear rate is quantified.

One way to verify the extent of the structural change and so the LVE properties under the influence of flow history, is to compare the storage modulus of suspensions before pre-shearing ($G'_{ref}$) and the storage modulus of the pre-sheared suspensions ($G'_{\infty}$) at similar conditions. $G'_{ref}$ was measured for different concentrations at the angular frequency of 1 rad/s in LVE region and is reported in Table 6-1; the samples were kept under quiescent conditions for 30 min after being loaded into rheometer to relax before measuring $G'_{ref}$. $G'_{\infty}$ was measured 5000 s after cessation of pre-shearing at various rates and concentrations. More details on how to obtain $G'_{\infty}$ is given elsewhere [13]. It has been shown that $G'_{\infty}$ is a strong function of pre-shear rate especially at lower concentrations and scales with the applied pre-shear rate ($\dot{\gamma}_i$) in a power-law form [18] as:

$$G'_{\infty} = \kappa \, \dot{\gamma}_i^{-\varepsilon} \tag{6-6}$$

where, $\kappa$ and $\varepsilon$ are constants and strongly depend on concentration of nanotubes. $G'_{\infty}$ should not be mistaken with $G_{\infty}$, the elastic modulus of the destroyed structure, in the Yziquel model. The power-law exponent values of Eq. (6-6) are summarized in Table 6-1. If the two storage

moduli ($G'_{ref}$ and $G'_{\infty}$) are compared at similar deformations (0.0118, 0.01 and 0.0025 for 0.5wt%, 1wt% and 5wt% respectively and 0.0072 for 2wt% and 3wt%) in LVE region and angular frequency of 1 rad/s, one can examine the extent of structural change under the influence of flow history. The results are shown in Figure 6-1 where $G'_{\infty}$ is plotted as a function of pre-shear rate ($\dot{\gamma}_i$). The solid lines exhibit the best power-law fit of Eq. (6-6). The horizontal dashed lines represent $G'_{ref}$ at each concentration. From this figure, it can be observed that by increasing the applied pre-shear rate, $G'_{\infty}$ drops at lower concentrations while it remains almost intact with respect to the pre-shear rate at the high concentration of 5 wt%. The two storage moduli crossover at a certain shear rate for suspensions containing less than 3 wt% MWCNTs; the shear rate at the crossover point is arbitrarily called the critical shear rate ($\dot{\gamma}_c$), which is equal to 1.7 $s^{-1}$ for 0.5 wt%, 3 $s^{-1}$ for 1 wt% and 7 $s^{-1}$ for 2 wt%.

Table 6-1: Power-law exponents from the best fit of Eq. (6-6) with experimental data and $G'_{ref}$ (Pa) for various concentrations at 1 rad/s in LVE region.

| $\phi$ (wt%) | $\kappa$ (Pa.s$^{-\varepsilon}$) | $\varepsilon$ | $G'_{ref}$ (Pa) |
|---|---|---|---|
| 0.5 | 2.67 | 0.3652 | 2.20 |
| 1.0 | 23.8 | 0.2612 | 17.9 |
| 2.0 | 403 | 0.1355 | 310 |
| 3.0 | 2213 | 0.0475 | 1640 |
| 5.0 | 12517 | 0.0236 | 9800 |

It should be noted that it is difficult to consider a precise value for $\dot{\gamma}_c$ as the structure and so $G'_{ref}$ can be easily affected by sample loading into the geometry. For the suspensions

containing 3 wt% and 5 wt% MWCNTs, the two storage moduli do not crossover in Figure 6-1; though, at 10 $s^{-1}$, their difference is about 200 Pa (or 12 % difference) for suspensions of 3 wt% and becomes less at higher pre-shear rates. In case of the 5 wt% suspension, $G'_{ref}$ is 2264 Pa less than $G'_{\infty}$ (or 21% difference). Considering the experimental error of ±15% for LVE results reported in Figure 6-1, a critical shear rate of approximately 10 $s^{-1}$ is estimated for the suspension containing 3 w% MWCNTs, although both storage moduli do not cross over in Figure 6-1. However, the difference between both moduli remains larger than the experimental error for the 5 wt% suspension; hence, there is no critical shear rate at this concentration.

From Figure 6-1, it is clear that $G'_{\infty}$ is larger than $G'_{ref}$ as long as the rate of the pre-shear is lower than $\dot{\gamma}_c$ while $G'_{ref}$ dominates $G'_{\infty}$ at higher shear rates. This reveals that after pre-shearing at low rates and below the critical shear rate ($\dot{\gamma}_i < \dot{\gamma}_c$) the suspension structure builds-up if sufficient time (e.g. 5000 s in this case) is provided. Indeed, pre-shearing at low rates leads to the formation of more entanglements between nanotubes and provides more elasticity to the suspensions. However, at high pre-shear rates ($\dot{\gamma}_i > \dot{\gamma}_c$), some entanglements breakdown and result in lower elasticity. Hence, 5000 s was not enough for the suspensions to develop their structures. In the following section, we analyze the evolution of structure at rest quantitatively by a set of transient flow measurements at two different rates near the critical shear rates.

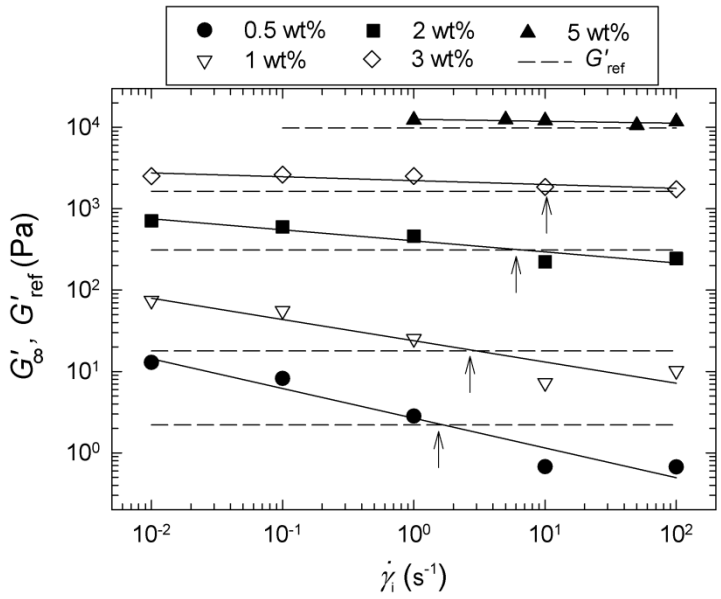


Figure 6-1: Storage modulus of the pre-sheared ( $G'_\infty$ , symbols) suspensions at various concentrations (measured in LVE region and angular frequency of 1 rad/s) plotted as a function of the pre-shear rate. For the non-pre-sheared samples $G'_{ref}$ , are reported as the dashed lines. The arrows show an estimation of the critical shear rate.

## 6.5 Transient results

A set of transient measurements were performed at various concentrations according to the procedure explained in Sec.6.2 at two shear rates of 1 $s^{-1}$ and 10 $s^{-1}$. The first stress growth experiment was performed in CCW direction followed by a rest time from 1 s to 1 h and a second measurement at similar shear rate in CW direction. The results for the 2 wt% and 5 wt% suspensions are presented in Figure 6-2 and Figure 6-3, respectively. The results for the neat epoxy are also indicated for reference.

Initially, a clear stress overshoot is observed in CCW direction, which levels off to a steady-state value at about 10 s in all cases. The extent of the CCW stress overshoots increases with increasing concentration and shear rate from 118 Pa at 2 wt% to 319 Pa at 3 wt% and 901 Pa at 5 wt% at 1 $s^{-1}$ and from 491.3 Pa at 2 wt% to 1147 Pa at 3 wt% and 2341 Pa at 5 wt% at 10

$s^{-1}$. If the flow direction is reversed 1 s after the CCW measurement, no stress overshoot is observed regardless of concentration or shear rate. This means there is no tumbling of nanotubes when the flow direction was reversed, as was imparted by Sepehr *et al.* [10] for fibre suspensions. By increasing the rest time between the two experiments in the CW direction, stress overshoots emerge and their extent increases with increasing rest time. In all cases, the stress overshoots appear at very small deformations ($\gamma \sim 0.1$-$0.5$) compared to the values reported for fibre suspensions ($\gamma \sim 10$ [10, 19] and $\gamma \sim 4$ [20]) or other nano-composites ($\gamma \sim 0.5$-$1$ [6], $\gamma \sim 1.7$ [4], $\gamma \sim 1$-$2$ [3], $\gamma \sim 2$-$4$ [9] and $\gamma \sim 2$ [2, 7]). The reason for this difference is not clear. Similarly, at shear rates of 5 $s^{-1}$ and 30 $s^{-1}$, the stress overshoots appeared at $\gamma = 0.3$ and $\gamma = 0.63$, respectively. It should be noted that the time resolution of the Physica-MCR501 rheometer is 0.01 s and the results were reproducible. Some suspicious data were eliminated at very short times in Figs. 2 to 4.

From Figure 6-2 (a), it was observed that for an applied shear rate of 1 $s^{-1}$ the structure build-up of a 2 wt% suspension during rest was completed after almost 1 h, as evidenced by the overlap of the stress overshoots in CCW and CW directions. However, upon the application of a higher shear rate of 10 $s^{-1}$, the structure build-up was limited after long rest time of 1 h or even longer (see Figure 6-2 (b)). This has not been reported previously in the literature and needs to be further investigated. A similar behaviour was observed for suspensions containing 1 wt% and 3 wt% MWCNTs under similar shear rates but the results are not shown here for the sake of brevity. At concentrations lower than 1 wt%, the transient results were poorly reproducible and were not used for further analysis. Similarly as is shown in Figure 6-3, the suspension containing 5 wt% MWCNTs exhibits CCW and CW stress overshoots at both shear rates and the extent of structure development is almost complete after 1 h rest,

regardless of the applied shear rate. In all cases, the neat epoxy exhibited a Newtonian behaviour.

As mentioned earlier, the mechanism for the emergence of stress overshoot is due to fibre orientation or breakdown of the nano-composite structure and nano-particles orientation in flow direction. CNTs orientation could influence transient results, but at high concentrations of 2 to 5wt%, it could not be examined. If the orientation of MWCNTs in the flow direction is the major mechanism for stress overshoots, the extent of orientation should increase with shear rate [7]. Consequently, more time would be required to disorient the particles at rest and reconstruct the structure. On the other hand, the hydrodynamic interactions in semi-dilute suspensions [21] and the mechanical contacts between the particles in concentrated suspensions [22] become important, which make the orientation dynamics of suspensions more complicated. Unfortunately, the theoretical models (e.g. fibre direct simulation) that predict the flow induced orientation of particles in polymer matrices are limited to very dilute systems. In addition, light scattering techniques are not helpful in the range of concentrations studied here due to opaqueness of the suspensions. We believe that the transient behaviour is mostly controlled by the size of the aggregates as characterized by the value of the elastic modulus, measured after cessation of shear flow; hence, the breakdown of structure during transient flow and reconstruction of structure at rest imparted by [2, 3, 5, 6] in nano-composites seem to be the more plausible mechanisms for the structural evolution. The structural kinetic model of Yziquel *et al.* [16] is employed in the next section to analyze the transient results and explain the evolution of structure during flow and at rest more quantitatively. In general, structural thixotropic models such as the one used in this work, are

applicable to a wide range of concentrations and predict transient results at least qualitatively well.

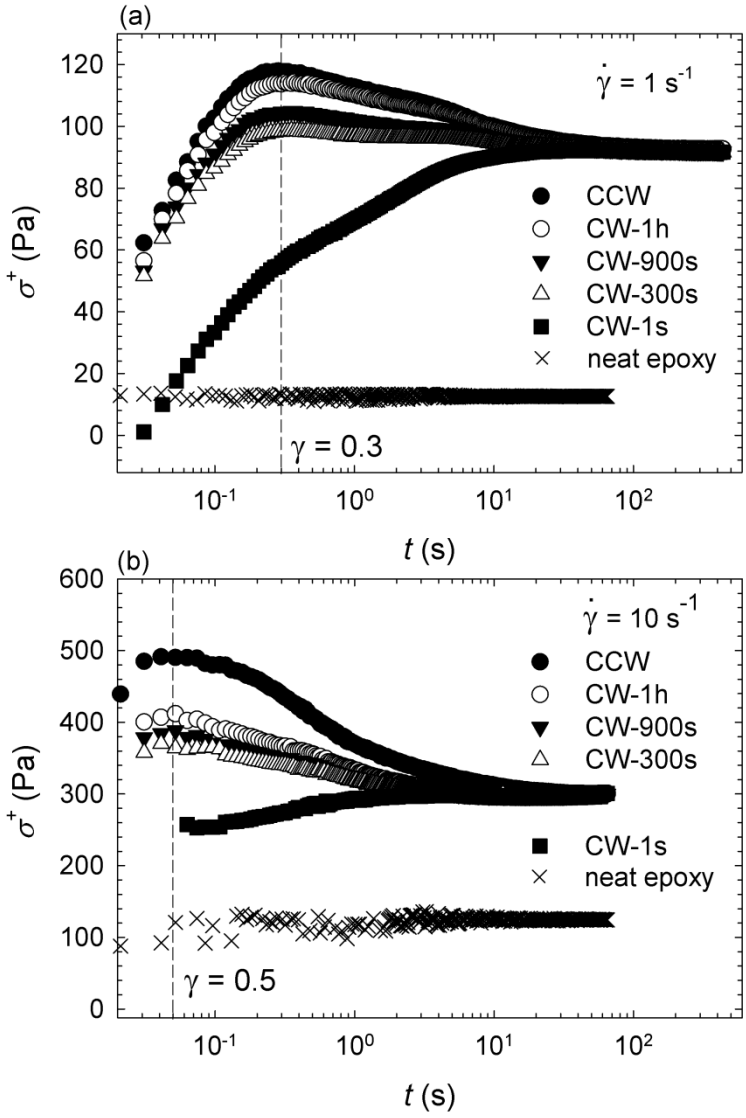


Figure 6-2: Transient stress data for a 2 wt% MWCNT suspension in an epoxy at shear rates of (a) 1 $s^{-1}$ and (b) 10 $s^{-1}$. The result for neat epoxy is shown for the reference.

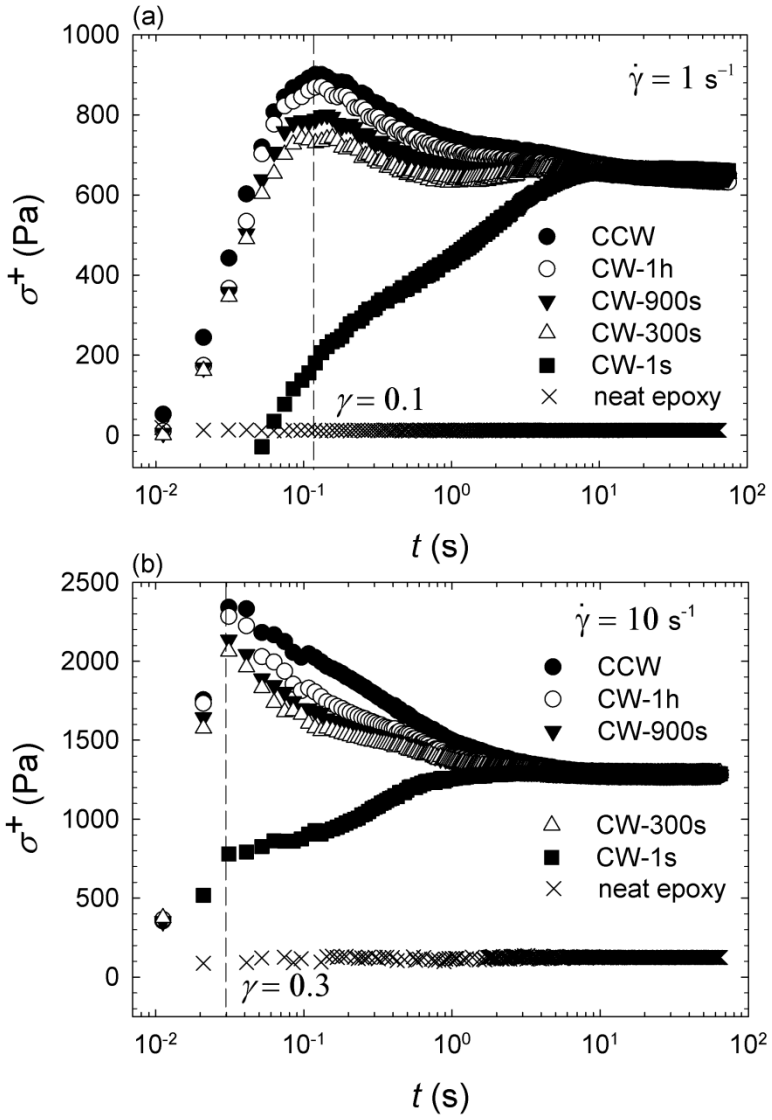


Figure 6-3: Transient stress data for a 5 wt% MWCNT suspension in an epoxy at shear rates of (a) 1 $s^{-1}$ and (b) 10 $s^{-1}$. The results for the neat epoxy are shown for reference.

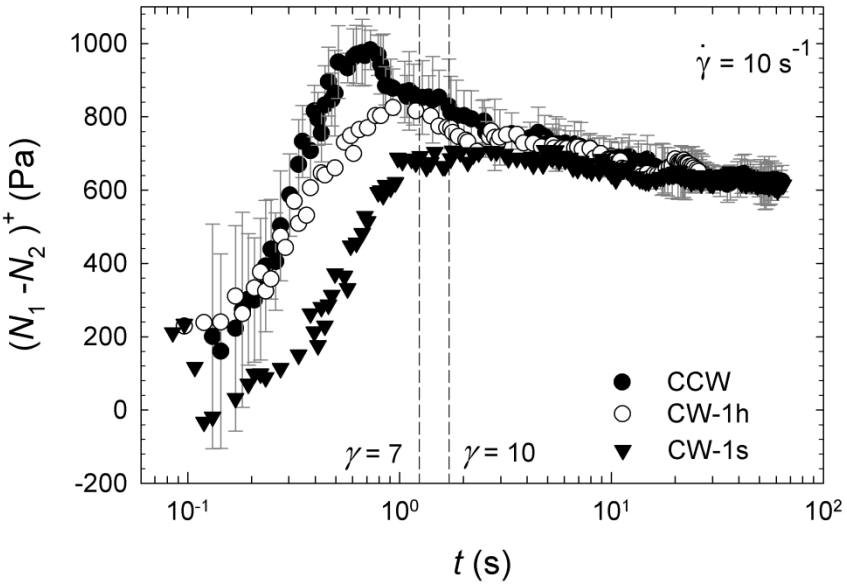


Figure 6-4: Transient normal stress difference for a 5 wt% MWCNT suspension in an epoxy under an applied shear rate of 10 $s^{-1}$.

Figure 6-4 shows the transient results for the normal stress difference of the 5 wt% suspension for an applied shear rate of 10 $s^{-1}$. A clear overshoot is observed in the CCW direction at a much larger deformation ($\gamma \sim 7$) than the stress overshoot ($\gamma \sim 0.3$ in Figure 6-3 (b)). Moreover, it should be noted that the difference between the normal stress difference overshoot and its steady-state value (400 Pa) is much less than the one for stress overshoot (1100 Pa). As is shown in this figure, large scatter in the data exist at the beginning of the experiments. In the CW direction, overshoots appear after some rest time but at a larger deformation of about $\gamma \sim 10$. The emergence of the overshoot in ($N_1$-$N_2$) at larger deformations than the stress overshoots is similar to the observations for fibre suspensions [10, 20] and clay nano-composites [7]. The results in reverse direction are shown only for 1 s and 1 h rest to avoid overcrowding the figure. It is not very clear whether a CW overshoot appears when there is 1 s rest, but unlike the previously reported results in Figure 6-3 (b) for the transient

stress, the relaxation of the normal stress difference is much slower than the shear stress, since the reverse overshoot is far from the CCW overshoot after 1 h rest. A non-zero normal stress difference in this suspension is due to the presence of nanotubes, since the neat epoxy is purely Newtonian.

## 6.6 Model simulation and prediction

In this section, the sensitivity of the structural model to several fitting parameters is analyzed. $\eta_\infty$ and $n$ are obtained from the steady-shear data and $\eta_0$ is calculated from $G_0$, $G_\infty$, $k_1$ and $k_2$. In all cases, $G_0$ = 561 Pa, $G_\infty$ = 0 Pa, $k_1$ = 0.130, $k_2$ = 7.80, $n$ = 0.290 and $\eta_\infty$ = 15.1 Pa.s, unless otherwise mentioned. It should be noted that $\eta_\infty$ controls the high-shear viscosity of the suspensions. $n$ and $G_\infty$ (which is set to zero) do not have a great influence on the prediction of the stress growth results. Figure 6-5 demonstrates the sensitivity of the model prediction to the fitting parameters, $G_0$, $k_1$ and $k_2$. From (a), it can be observed that, the steady state stress increases with increasing $k_1$ when $k_2$ is constant. On the other hand, the difference between the stress overshoot and the steady-state value decreases as $k_1$ increases (or $k_2/k_1$ decreases). In addition, the rate of the stress relaxation at rest and the relaxation plateau increase with increasing $k_1$ (results not shown here). By keeping $k_2/k_1$ invariant, the steady-state stress remains intact while the extent of the stress overshoot decreases with increasing $k_1$ as shown in Figure 6-5 (b). Similarly, if $G_0+G_\infty$ is kept constant while $G_0$ and $G_\infty$ change, the steady-shear stress remains invariant while the extent of the stress overshoot decreases by increasing $G_0$ (the results not shown here).

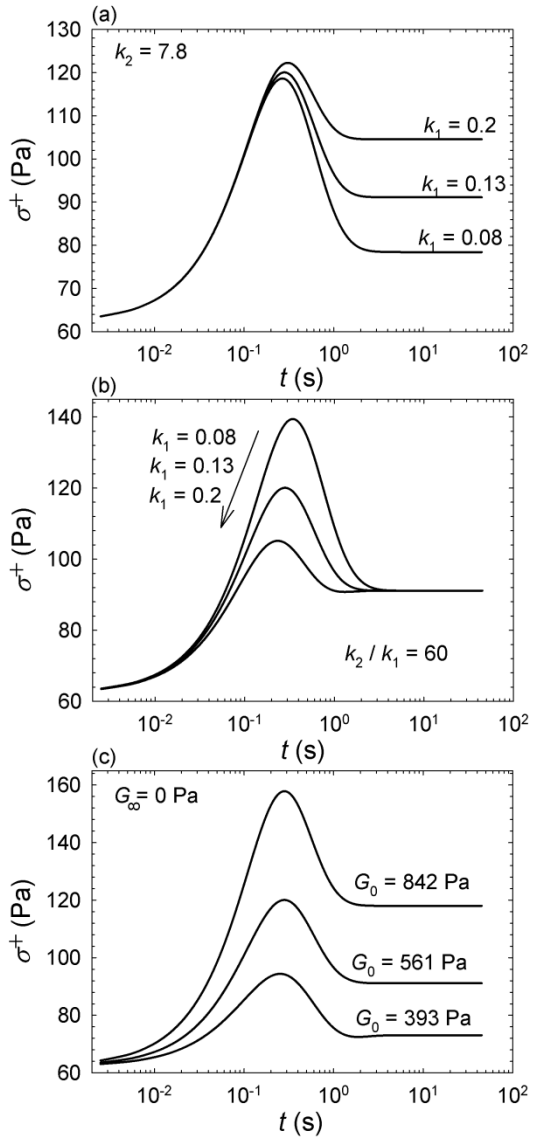


Figure 6-5: Sensitivity analysis on the fitting parameters for stress growth results. (a) Variable $k_1$ and constant $k_2$. (b) Variable $k_1$ and constant $k_2/k_1$. (c) Variable $G_0$ and $G_\infty$= 0. The arrow in (b) shows the direction of increasing $k_1$.

In Figure 6-5 (c), $G_\infty$ is maintained equal to zero; by increasing $G_0$ the steady-state stress increases while the difference between the stress overshoot and steady-state stress slightly increases. Moreover, by increasing $G_0$ the stress relaxation accelerates (results not shown). From the results reported in Figure 6-5, it can be concluded that $G_0+G_\infty$ and $k_2/k_1$ control the

steady-state shear stress. By increasing $G_0+G_\infty$ and/or decreasing $k_2/k_1$, the steady-state stress increases significantly. The extent of overshoot during flow decreases with increasing $k_1$, provided that $k_2/k_1$ is maintained constant. Moreover, $k_1$ controls the thixotropic behaviour of suspensions. The rate of structure build-up at rest and the stress relaxation plateau increase with increasing $k_1$.

## 6.7 Result comparison with model predictions

In this section, the experimental transient stress growth measurements reported in previous section are compared with the predictions of the Yziquel *et al.* [16] structural model. Initially, the steady shear results were compared with the model predictions and the results are presented in Figure 6-6. According to the model, the steady-shear viscosity is defined by:

$$\eta(\dot{\gamma}) = \frac{\sigma_{12}}{\dot{\gamma}} = \eta_\infty + \left[ \eta_0 \left( \lambda_0 \sqrt{\frac{k_2}{k_1}} \right)^{n-1} \right]^{\frac{2}{n+1}} \left( \eta(\dot{\gamma})\dot{\gamma} \right)^{\frac{n-1}{n+1}} \tag{6-7}$$

with a limiting high shear viscosity of $\eta_\infty$; $n$ is the power-law exponent and $\eta_0(\sqrt{k_2/k_1}\lambda_0)^{n-1}$ can be referred to $m$ hereafter for simplicity. Eq. (6-7) is an implicit equation in terms of $\eta(\dot{\gamma})$ and should be solved in an iterative procedure. If $\eta_\infty << \eta(\dot{\gamma})$, Eq. (6-7) simplifies to the following form:

$$\eta(\dot{\gamma}) = \eta_0 (\sqrt{\frac{k_2}{k_1}} \lambda_0 \dot{\gamma})^{n-1} + \eta_\infty \tag{6-8}$$

From Figure 6-6, the model can predict the steady shear viscosity well with a single set of parameters at each concentration.

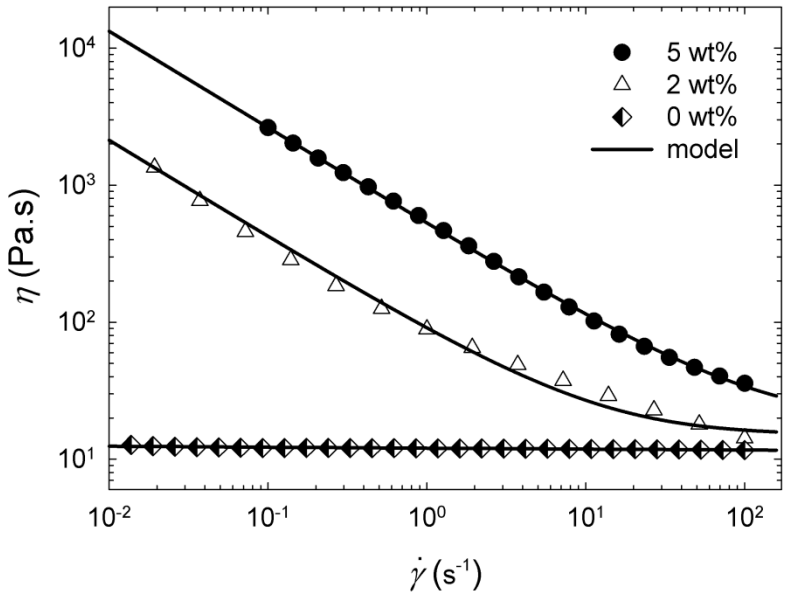


Figure 6-6: Steady-shear viscosity results for the 0 wt%, 2 wt% and 5 wt% suspensions. The lines show the model predictions.

Using Eq. (6-7), the three parameters, $m$, $n$ and $\eta_\infty$, were obtained from a minimization procedure based on the mean squared errors. The fitting parameters for the steady shear results are reported in Table 6-2 for 2 wt% and 5 wt% suspensions. It should be noted that $\eta_\infty$ is the high shear viscosity at each concentration, which is slightly higher than the viscosity of neat epoxy (~12.33 Pa.s). By keeping $\eta_\infty$, $m$ and $n$ constant, the fitting parameters will be reduced to $G_0$, $G_\infty$, $k_1$ and $k_2$ for transient measurements. $\eta_0$ can be estimated from $m$ and the other four fitting parameters. It should be noticed that finding the best fit is non-trivial and the model convergence strongly depends on the initial guess for the fitting parameters. In all cases, the initial value of $\xi$ was assumed to equal 1 at the beginning of the CCW start-up. As mentioned earlier in Sec.6.3, $G_\infty$ is the elastic modulus of the destroyed structure and $G_0 + G_\infty$ is the equilibrium (frequency independent) storage modulus of the structure. Since the pure epoxy is a Newtonian fluid, it doesn't have a significant elasticity; therefore, $G_\infty$ could be set

to zero for simplicity. For a 5 wt% suspension, $G_0 + G_\infty$ (from Table 6-2) equals $G'_{ref}$ (~9800 Pa) and is very close to the pre-sheared storage modulus ($G'_\infty \sim 10^4$ Pa) in Figure 6-1. Moreover, a single set of parameters could be used for this suspension to predict the transient results qualitatively. On the contrary, for the 2 wt% suspension, two different sets of parameters should be used. At the low shear rate of 1 $s^{-1}$, the estimated value for $G_0 + G_\infty$ (~526 Pa) is comparable to $G'_\infty$ (~ 500 Pa) in Figure 6-1; however, at the higher shear rate of 10 $s^{-1}$, it deviates from $G'_\infty$ (~ 225 Pa after pre-shearing at 10 $s^{-1}$ in Figure 6-1) and $G'_{ref}$ (~310 Pa from Table 6-1). This could be due to the fact that the frequency independent value of the storage modulus is inaccessible from the experiments at this concentration. If $G_\infty$ is set equal to zero at 10 $s^{-1}$, an undershoot appears right before the emergence of the steady state, which is not possible to eliminate. In addition, an abnormal stress overshoot appeared in the stress relaxation curve, which has no physical meaning. By setting $G_\infty$ equal to 12 Pa, the undershoot in the stress growth and the overshoot in the stress relaxation are eliminated.

Table 6-2: Model parameters used to predict the steady shear viscosity and stress growth results.

| **2 wt%** | $\eta_0$ [Pa.s] | $\eta_\infty$ [Pa.s] | $G_0$ [Pa] | $G_\infty$ [Pa] | $k_1$ | $k_2$ | $n$ | $m$ [Pa. $s^n$] |
|---|---|---|---|---|---|---|---|---|
| Steady shear | … | 15.1 | … | … | … | … | 0.290 | 81.1 |
| Stress growth at 1 $s^{-1}$ | 106 | 15.1 | 561 | 0 | 0.130 | 7.79 | 0.290 | 81.1 |
| Stress growth at 10 $s^{-1}$ | 526 | 15.1 | 800 | 12.0 | 0.003 | 1.40 | 0.290 | 81.1 |
| **5 wt%** | $\eta_0$ [Pa.s] | $\eta_\infty$ [Pa.s] | $G_0$ [Pa] | $G_\infty$ [Pa] | $k_1$ | $k_2$ | $n$ | $m$ [Pa.$s^n$] |
| Steady shear | … | 17.0 | … | … | … | … | 0.300 | 521 |
| Stress growth at 1 $s^{-1}$ | 51.6 | 17.0 | 9800 | 0 | 0.009 | 0.450 | 0.300 | 521 |
| Stress growth at 10 $s^{-1}$ | 51.6 | 17.0 | 9800 | 0 | 0.009 | 0.450 | 0.300 | 521 |

Note that $k_1$, which controls the rate of structure build-up by the Brownian motion, should not depend on concentration or shear rate; however, from Table 6-2, different values of $k_1$ were obtained from curve fitting of the 2 and 5 wt% suspensions and even at the two different shear rates for the 2 wt% suspension. This suggests that the role of the Brownian motion in the structure reconstruction is not as simple as described by the kinetic equation in Eq. (6-5). Similarly, $k_2$ was not unique for different concentrations and shear rates for the 2 wt% suspension, revealing the fact that the role of the viscous dissipation in breaking down the structure is more complex than proposed in Eq. (6-5).

Figure 6-7 compares the stress growth data for the 2 wt% suspension with the model predictions. From this figure, it can be observed that the model can qualitatively predict the experimental results. However, the model predicts a small reverse overshoot at the shear rate of 1 $s^{-1}$ in (a) when only 1 s rest time is considered. By increasing the rest time, the predicted reverse overshoots increase as experimentally observed. The predicted time for a complete structure build-up is much shorter and the forward and reverse overshoots are comparable in Figure 6-7 (a) after 300 s rest. The predicted CW results overlap the CCW stress growth results after 300 s and longer rest times. However, at the higher shear rate of 10 $s^{-1}$, the rate of structure build-up seems to be slower since the reverse stress overshoot does not approach a similar value as the CCW overshoot after 300 s as shown in Figure 6-7 (b). This is evident from the experiments and model predictions. The reason for this will be explained shortly from a structural point of view. In addition, the steady-shear stress is underestimated at 10 $s^{-1}$; the difference, which originates from the discrepancy in experimental results, remains within the experimental error.

From Figure 6-7, the strain ( $\gamma = \dot{\gamma} t$ ) at maximum stress appears at a slightly smaller value in the experiments than the model prediction. This is the case at other concentrations. The reason for the emergence of the experimental stress overshoots at very small deformations is not clear. Also, from the results reported in Figure 6-7, the model predicts a shorter time required to reach steady state, by almost a decade compared to the experimentally observed time. A similar behaviour is observed for the 5 wt% suspension in Figure 6-8, except that in this case the suspensions structure develops completely after 1 h rest during the experiments and 300 s from the model predictions. The model predictions in CW direction overlap the CCW predictions after 300 s rest. Similar to the 2 wt% suspension, the reverse overshoots are overestimated. The model underestimates the steady-state stress but the difference stems from the experimental error. Figure 6-9 presents the predictions of the model for the first normal stress difference of the 5 wt% suspension at 10 $s^{-1}$ using the parameters reported in Table 6-2. Some data were eliminated from the curve for more clarity. It is shown that the overshoots in the normal stress difference are overestimated. The predictions of the model for CCW and CW after 1 h overlap but the strain at the maximum normal stress difference and the steady-state value are underestimated, the differences considerably exceeding the experimental error in this case.

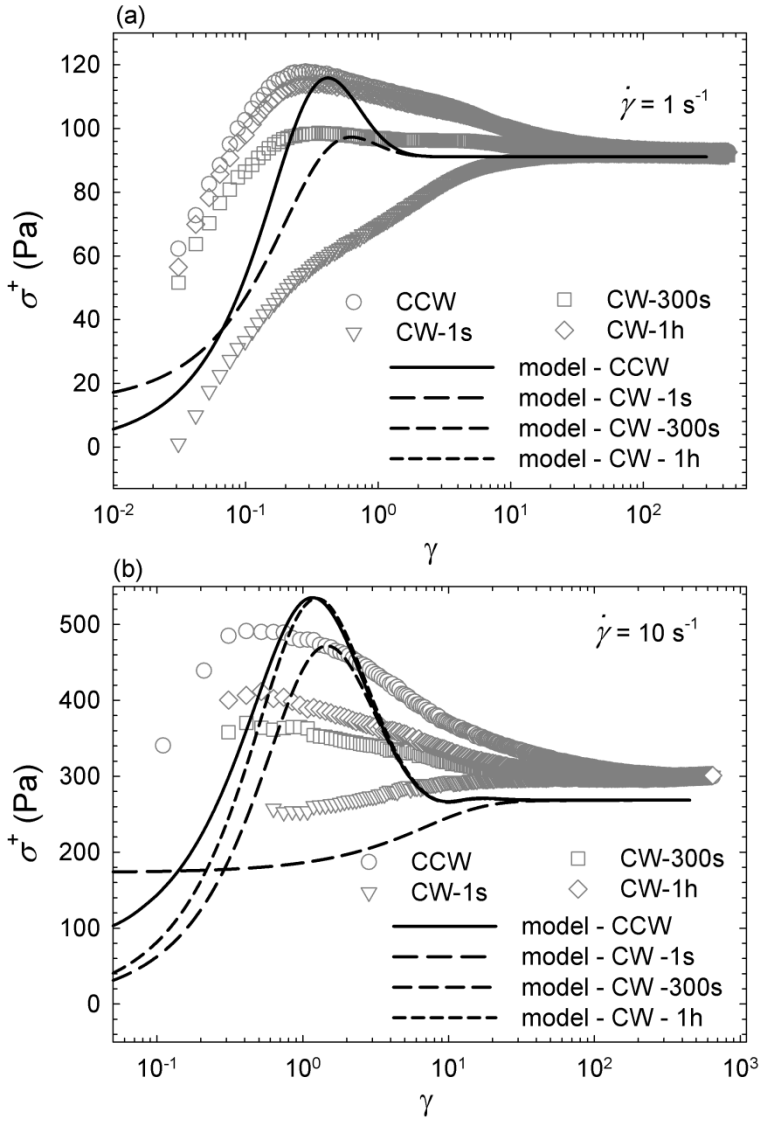


Figure 6-7: Shear stress growth data for the 2 wt% suspension under an applied shear rate of (a)1 $s^{-1}$ and (b)10 $s^{-1}$. The lines show the model predictions.

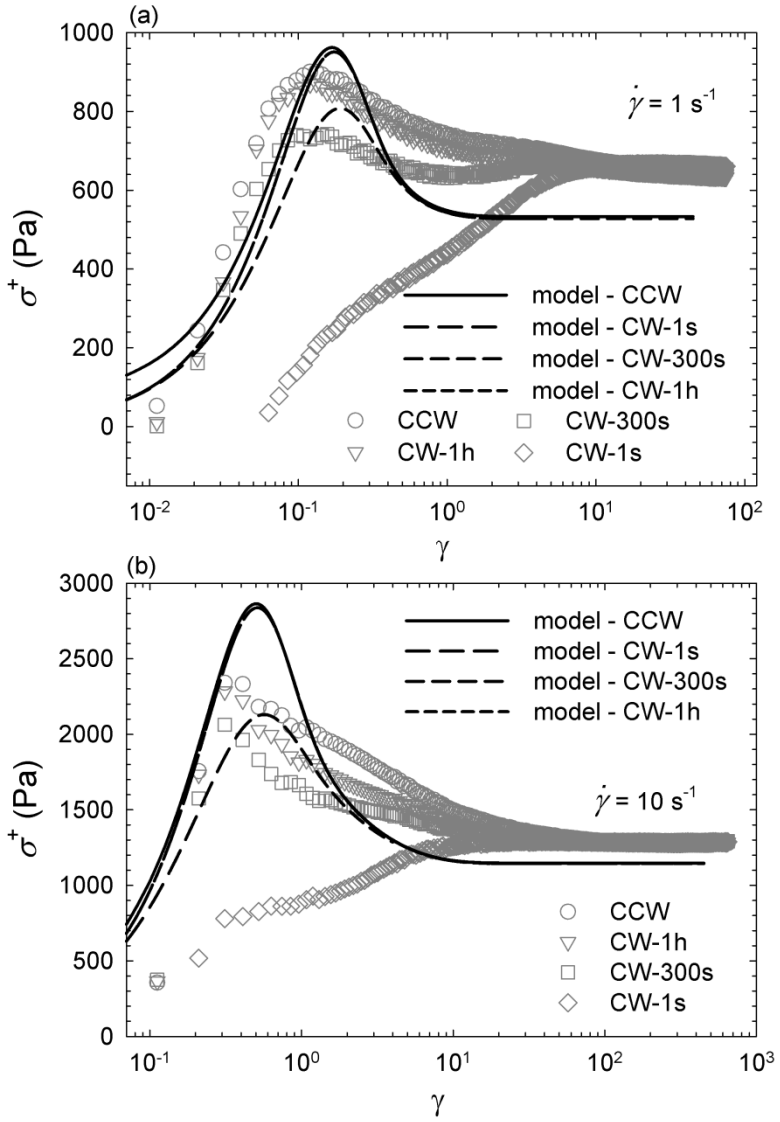


Figure 6-8: Shear stress growth data for the 5 wt% suspension under an applied shear rate of (a) 1 $s^{-1}$ and (b) 10 $s^{-1}$. The lines show the model predictions.

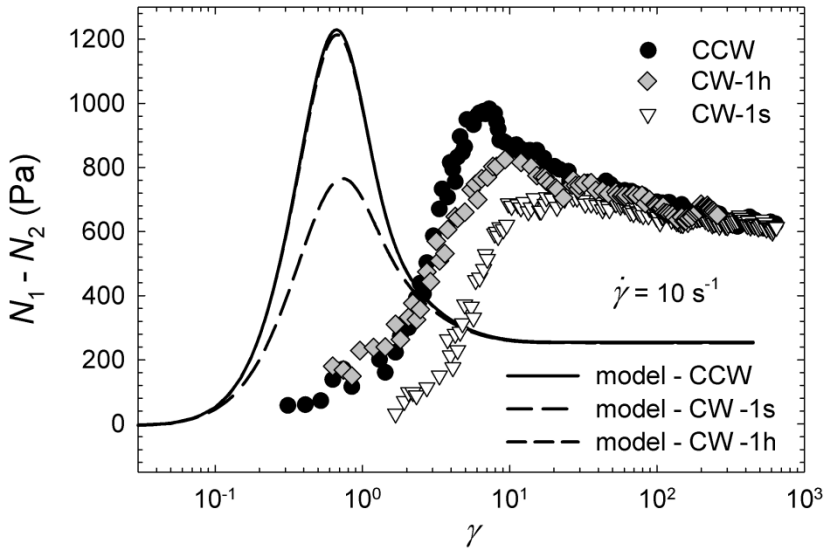


Figure 6-9: First normal stress difference as a function of strain in a stress growth experiment at 10 $s^{-1}$ for the 5 wt% suspension. The lines show the model predictions.

The results presented in Figure 6-7 and 6-8 can be analyzed from a structural point of view by considering the evolution of the structural parameter $\xi$ with time during flow and rest. The results are presented in Figure 6-10 based on the parameters of Table 6-2. According to the kinetic equation (Eq. (6-5)), the rate of variation of $\xi$ with time is controlled by the balance between the structure build-up and breakdown during flow. The coefficients $k_2$ and $k_1$ control the rate of structure breakdown and build-up respectively and the ratio $k_2/k_1$ can evaluate the extent of the structure breakdown to build-up relatively. During flow, the structure breaks down due to flow induced viscous dissipation and $\xi$ drops from an initial value of 1 to a lower value at steady state. In the absence of flow ($\dot{\gamma} = 0$), the structure reconstructs and $\xi$ can be expressed in an exponential form after solving Eq. (6-5) that yields:

$$\xi = 1 - c_2 \ \exp\ (-k_1 t / \lambda_0) \tag{6-9}$$

where the constant $c_2$ equals (1- $\xi_{CCW}$) and $\xi_{CCW}$ is the steady-state value of the structural parameter at the end of CCW. According to this equation, $k_1/\lambda_0$ determines the kinetics for the structure build-up at rest.

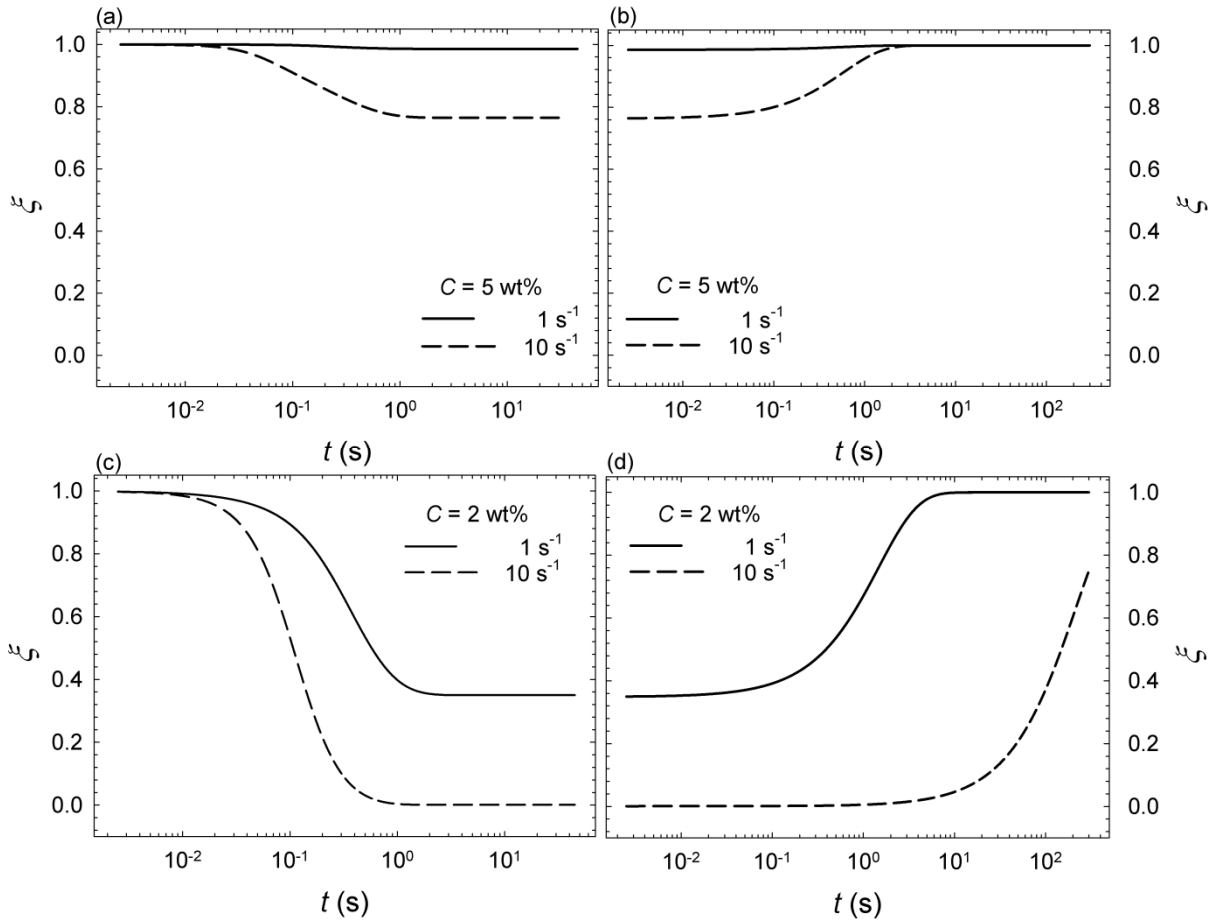


Figure 6-10: Evolution of the structural parameter ($\xi$) during (a,c) CCW flow and (b,d) rest for the 5 wt% (a,b) and the 2 wt% (c,d) suspensions.

Figure 6-10 (a) reveals the breakdown of the structure from an initial value of $\xi = 1$ to 0.98 at 1 $s^{-1}$ and 0.78 at 10 $s^{-1}$ under steady-state conditions, when the suspension contains 5 wt% MWCNTs. In addition, the rate of structure breakdown is faster for the larger applied shear rate. Figure 6-10 (b) reports the evolution of $\xi$ during rest when the structure reconstructs. It

can be observed that after a short time of about 3 s, $\xi$ approaches 1 in an exponential trend after cessation of start-up. Similarly, Figure 6-10 (c) and (d) exhibit the structure breakdown and reconstruction for the 2 wt% suspension. However, the extent of breakdown during flow is more severe since $\xi$ approaches to 0.36 at 1 $s^{-1}$ and almost 0 at 10 $s^{-1}$ under steady-state conditions. In quiescent conditions, the destroyed structure reconstructs completely and $\xi$ evolves from $\xi = 0.36$ to $\xi = 1$ after 7 s for pre-shearing at 1 $s^{-1}$ while it develops partially from $\xi = 0$ to $\xi = 0.76$ after 300 s rest for pre-shearing at 10 $s^{-1}$. The partial structure build-up in the latter case could be due to a more severe structure breakdown during flow and slower kinetics of structure build-up at rest.

From Figure 6-10, the extent of structure breakdown is much less at higher concentration of 5 wt% (regardless of the applied shear rate); this is evident from the fitting parameters where $k_2$ decreases by increasing the concentration in Table 6.2. For the 5 wt% suspension $k_2/k_1$ remains relatively small at about 50 for both shear rates, which explains the less severe structure breakdown in Figure 6-10 (a) in comparison to the 2 wt% suspension where $k_2/k_1$ increases from 59.9 at 1 $s^{-1}$ to 467 at 10 $s^{-1}$. The relatively large ratio of $k_2/k_1$ in the latter case can explain the reason for the more sever structure breakdown when increasing the shear rate as shown in Figure 6-10 (c). Since the suspension structure is more fragile at lower concentrations due to lower inter-particle interactions, the rate of energy dissipated by the flow process is more significant at the lower concentration of 2 wt% and increases with increasing shear rate. This could also be the reason why different sets of fitting parameters should be used to fit the transient results for the 2 wt% suspension under different shear rates.

During rest, $k_1/\lambda_0$ varies from 0.68 at 1 $s^{-1}$ to 0.0046 at 10 $s^{-1}$ for the 2 wt% suspension; thus, much slower kinetics of structure build-up is evident by increasing the shear rate. In

comparison, $k_1/\lambda_0$ is relatively higher for 5 wt% suspension and is about 1.7; this explains much faster kinetics of structure build-up for higher concentration of 5 wt% in Figure 6-10 (b).

## 6.8 Discussion

In section 6.4, we defined a critical pre-shear rate for each concentration above which some entanglements breakdown; if the suspensions were pre-sheared at low rates below the critical one, they would exhibit higher elasticity as they formed a more developed structures compared to the non-pre-sheared ones. However, upon the application of larger shear rates, the suspension would become less elastic as a result of the partial breakdown of some nanotube entanglements. The critical shear rates were reported to be about 7 $s^{-1}$ for 2 wt% and 10 $s^{-1}$ for 3 wt% within the experimental error of ±15%. No critical shear rate was obtained for the suspension containing 5 wt% MWCNTs. Moreover, the structure evolution was analyzed during rest upon cessation of flow in the vicinity of the critical shear rates at 1 and 10 $s^{-1}$. It was shown that the extent of the reverse stress overshoot depended on the rest time during which the suspensions structure reconstructed. The magnitude of the structure build-up at rest can be quantified by plotting the relative value of the stress overshoots in CCW and CW directions as a function of rest time as is reported in Figure 6-11. Since 1 $s^{-1}$ is below the critical shear rate, the suspension structure should develop at rest after a very long time of the order of 1 h as evidenced in Figure 6-11 (a), where the relative stress overshoots emerge to 1. Since the structure breakdown is not significant during flow, the structure development starts shortly after the cessation of flow until it reconstructs completely after 3 s for the 5 wt% suspension and 7 s for the 2 wt% suspension as is predicted by the model. This is also the case at the shear rate of 10 $s^{-1}$ for the suspension containing 5 wt% MWCNTs illustrated in Figure

6-11 (b); in contrast, the extent of the structure build-up is limited to approximately 80% for the suspensions containing 3 wt% and 2 wt% MWCNTs; even though, by providing much longer rest times (> 1 h), the extent of the CW stress overshoot did not change (results are not presented here). This reveals that some part of the structure (entanglements between nanotubes) is broken-down during flow and providing very long rest time is insufficient to develop the structure completely. However, the model predicts a complete structure reconstruction after almost 900 s rest (see Figure 6-11 (b)). Moreover, the severe structure breakdown during flow and the slow kinetics of structure build-up are the reasons why the structure reconstruction starts much later for the 2 wt% suspension under an applied shear rate of 10 $s^{-1}$ (no reverse overshoot appears before 30 s rest) compared to other cases presented in Figure 6-11.

The results presented in Figure 6-11 reveal the fact that the suspensions structure can be thoroughly reconstructed under quiescent conditions within the experimental time if the applied shear rate is below the critical shear rate. Moreover from Figure 6-11, it can be observed that most (about 80%) of the structure build-up occurs after 300 s rest regardless of the concentration or the applied shear rate (the model predicts a much shorter time). On the other hand, the rotary diffusion time of one particle that can be calculated from the following correlation [23]:

$$\frac{1}{D_r} = \frac{\pi \eta_s L^3}{3k_B T\left[\ln(L/d) - 0.8\right]} \tag{6-10}$$

is estimated to be 314 s at room temperature (25 $^{o}$C). In Eq. (6-10), $\eta_s$ is the viscosity of the neat epoxy (12.3 Pa.s), $L$ (~ 670 nm) and $d$ (14.9 nm) are the average length and diameter of nanotubes, $k_B$ is the Boltzmann constant and $T$ is the absolute temperature. It should be noted

that Eq. (6-10) is more suitable for dilute systems. In the semi-dilute regime, $D_r$ could be rescaled to $D_r / \phi^2$ [23], where $\phi$ is the volume concentration of particles, revealing the fact that at higher concentrations, the rotary diffusion time is even shorter. Since, the Peclet number ( $Pe = \dot{\gamma} / D_r$ ) is much larger than 1 at the shear rates of 1 and 10 $s^{-1}$ (about 314 and 3140, respectively), Brownian forces are negligible during flow; however, in the absence of flow, they can play a role in randomizing nanotubes and can facilitate the structure build-up of suspensions. Since the rest time required for most of the structure build-up (~300 s) is very similar to the Brownian rotary diffusion time (~314 s), Brownian forces are a possible mechanism for structure development in the absence of flow. This is in contradiction with the previously reported results in literature for some nano-composites [2, 3, 6] where Brownian forces were reported not to play a significant role under quiescent conditions.

The trend for the evolution of the relative stress overshoots at rest is similar for the suspensions containing 2, 3 and 5 wt% as shown in Figure 6-11 (a) and for the 2 wt% and 3 wt% suspensions in Figure 6-11 (b). From the results reported in Figure 6-11, a thorough structure reconstruction takes 1 h during the experiments, which is longer than the rotary diffusion time; hence, Brownian forces cannot be the only mechanism involved. On the other hand, carbon nanotubes are non-functionalized and only van der Waals forces are present between CNTs; thus, other colloidal forces should be neglected. While the rate of structure build-up strongly depends on inter-particle interactions [13], the loss of some entanglements diminishes the rate of structure build-up and leads to incomplete structure development, whereas the presence of a highly entangled structure (e.g. at 5 wt%) yields to a complete structural reconstruction under quiescent conditions. Consequently, a contribution of both Brownian forces and inter-particle interactions are important in the development of the

structure at rest. On the other hand, CNT suspensions are among the slowly flocculating ones that form a self-similar fractal structure near and above the gel point with a fractal dimension of 2.15 [18]; this may explain the slow kinetics for the structure reconstruction (~ 1 h).

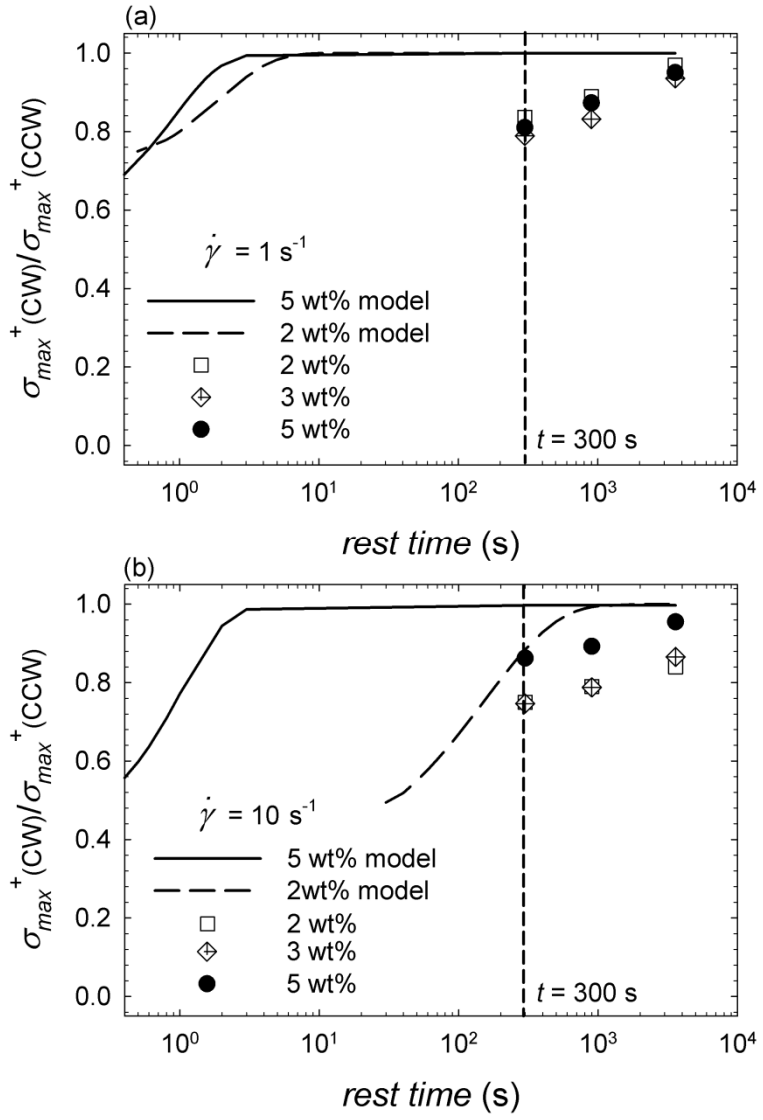


Figure 6-11: Extent of structure build-up at rest for the 2 wt%, 3 wt% and 5 wt% suspensions of MWCNTs in epoxy for applied shear rates of (a) 1 $s^{-1}$ and (b) 10 $s^{-1}$. The symbols are experimental data and the lines show the model predictions. The vertical dashed line marks the rest time at 300 s.

Since Brownian motion is the sole mechanism for structure build-up in the model (see Eq. (6-5)), the model predicts a much faster structure reconstruction at rest; hence, it overestimates the reverse overshoots and predicts a much shorter time required to reach steady state. When the applied shear rate is larger than the critical rate, the model predicts a relatively much longer rest time for a complete structure development (~ 900 s).

## 6.9 Summary

A critical shear rate was defined at low and intermediate concentrations beyond which the suspension elasticity decreased and the extent of structure build-up was limited due to a partial breakdown in nanotube entanglements during flow. On the contrary, when the applied shear rate was below the critical rate, the structure reconstructed completely under quiescent conditions. The extent of structure build-up at rest was quantified by a set of transient flow reversal measurements in the vicinity of critical shear rates. From the experimental results, it was concluded that the transient behaviour of MWCNT suspensions is similar to that of other nano-composites and is different from fibre suspensions since no reverse stress overshoot appeared when no rest time was provided between the CCW and CW flows, during the experiments. The extent of structure build-up was shown to increase with rest time and was quantified by considering the relative value of the stress overshoot in opposite directions. It was observed that most (about 80%) of the structure reconstructed during the first 300 s of rest, which is equivalent to the rotary diffusion time ($1/D_r$ ~314 s). This suggests that Brownian motion plays an important role in the structure build-up of the CNT suspensions in the absence of flow. However, from the experimental results, the rest time required to develop the structure completely was much longer (about 1 h) than 300 s, probably due to the slowly

flocculating nature of the nanotube suspensions, which revealed that other mechanisms should be involved during the evolution of structure in quiescent conditions. On the other hand, the rate of structure build-up increases with increasing inter-particle interactions and the formation of more entanglements between nanotubes [13]; hence, inter-particle interactions contribute as well to the reconstruction of structure in the absence of flow.

Finally, the stress growth results were compared with the predictions of Yziquel *et al.* [16] structural model. It was shown that the model can qualitatively predict the experimental results as well as a partial structure development at shear rates above the critical shear rate. However, the reverse overshoots and the rest time required for a complete structure build-up were overestimated.

## 6.10 Acknowledgements

Funding from Natural Sciences and Engineering Research Council of Canada (NSERC) and Consortium for Research and Innovation in Aerospace in Quebec (CRIAQ) is gratefully acknowledged.

## 6.11 References

[1] H.M. Laun, Orientation effects and rheology of short glass fiber-reinforced thermoplastics, Colloid. Polym. Sci., **262** (1984) 257-269.

[2] D. Wu, L. Wu and M. Zhang, Rheology of multi-walled carbon nanotube/poly(butylene terephthalate) composites, J. Polym. Sci., Part B: Polym. Phys., **45** (2007) 2239-2251.

[3] D. Wu, C. Zhou, Z. Hong, D. Mao and Z. Bian, Study on rheological behaviour of poly(butylene terephthalate)/montmorillonite nano-composites, Eur. Polym. J., **41** (2005) 2199-2207.

[4] W. Letwimolnun, B. Vergnes, G. Ausias and P.J. Carreau, Stress overshoots of organoclay nanocomposites in transient shear flow, J. Non-Newtonian Fluid Mech., **141** (2007) 167-179.

[5] J. Li, C. Zhou, G. Wang and D. Zhao, Study on rheological behaviour of polypropylene/clay nano-composites, J. Appl. Polym. Sci., **89** (2003) 3609-3617.

[6] M.J. Solomon, A.S. Almusallam, K.F. Seefeldt, A. Somwangthanaroj and P. Varadan, Rheology of polypropylene/clay hybrid materials. Macromolecules, **34** (2001) 1864-1872.

[7] H. Eslami, M. Grmela and M. Bousmina, Structure build-up at rest in polymer nanocomposites: Flow reversal experiments, J. Polym. Sci., Part B: Polym. Phys., **47** (2009) 1728-1741.

[8] C. Kagarise, J. Xu, Y. Wang, M. Mahboob, K.W. Koelling and S.E. Bechtel, Transient shear rheology of carbon nanofiber/polystyrene melt composites, J. Non-Newtonian Fluid Mech., **165** (2010) 98-109.

[9] D. Wu, L. Wu, W. Zhou, Y. Sun and M. Zhang, Relations between the aspect ratio of carbon nanotubes and the formation of percolation networks in biodegradable polylactide/carbon nanotube composites, J. Polym. Sci., Part B: Polym. Phys., **48** (2010) 479-489.

[10] M. Sepehr, P. J. Carreau, M. Moan and G. Ausias, Rheological properties of short fiber model suspensions. J. Rheol., **48** (2004) 1023-1048.

[11] A. Lele, M. Mackley, G. Galgali and C. Ramesh, In situ rheo-x-ray investigation of flow-induced orientation in layered silicate-syndiotactic polypropylene nano-composite melt, J. Rheol., **46** (2002) 1091-1110.

[12] E. Ganani and R.L. Powell, Rheological properties of rodlike particles in a Newtonian and a non-Newtonian fluid, J. Rheol., **30** (1986) 995-1013.

[13] F. Khalkhal, P.J. Carreau and G. Ausias, Effect of flow history on linear viscoelastic properties and the evolution of the structure of multiwalled carbon nanotube suspensions in an epoxy, J. Rheol., **55** (2011) 153-175.

[14] J. Ferec, M.C. Heuzey, G. Ausias and P.J. Carreau, Rheological behavior of fiber-filled polymers under large amplitude oscillatory shear flow. Journal of Non-Newtonian Fluid Mechanics, 151 (2008) 89-100.

[15] M. Keshtkar, M.-C. Heuzey and P.J. Carreau, Rheological behavior of fiber-filled model suspensions: effect of fiber flexibility. Journal of Rheology, 53 (2009) 631-650.

[16] F. Yziquel, P.J. Carreau, M. Moan and P.A. Tanguy, Rheological modeling of concentrated colloidal suspensions, J. Non-Newtonian Fluid Mech., **86** (1999) 133-155.

[17] C. Mobuchon, P.J. Carreau and M.C. Heuzey, Structural analysis of non-aqueous layered silicate suspensions subjected to shear flow. Journal of Rheology, 53 (2009) 1025-1048.

[18] F. Khalkhal and P.J. Carreau, Scaling behaviour of the elastic properties of non-dilute MWCNT-epoxy suspensions, Rheol. Acta, (2011), DOI: 10.1007/s00397-010-0527-9.

[19] A.S.A. Ramazani, A. Ait-Kadi and M. Grmela, Rheology of fibre suspensions in viscoelastic media: Experiments and model predictions, J. Rheol., **45** (2001) 945-962.

[20] M. Keshtkar, M.C. Heuzey, P.J. Carreau, M. Rajabian and C. Dubois, Rheological properties and microstructural evolution of semi-flexible fibre suspensions under shear flow, J. Rheol., **54** (2010) 197-222.

[21] M.P. Petrich, D.L. Koch and C. Cohen, An experimental determination of the stress-microstructure relationship in semi-concentrated fiber suspensions, J. Non-Newtonian Fluid Mech., **95** (2000) 101-133.

[22] M.P. Petrich and D.L. Koch, Interactions between contacting fibres, Phys. Fluids, **10** (1998) 2111-2113.

[23] R.G. Larson, The structure and rheology of complex fluids, Oxford University Press. New York, 1999

# CHAPITRE 7 GENERAL DISCUSSION AND CONCLUSION

This thesis explored the mechanisms involved in the formation of structure in model CNT suspensions under the influence of concentration, temperature and pre-shear rate. The MWCNTs used in this study has been initially characterized as rigid rods in the wide range of shear rates studied. Suspensions of MWCNT-epoxy were prepared using a three-roll-mill over a wide range of concentrations. A set of rheological methods, scaling and fractal theories and a structural thixotropic model was used to characterize the suspensions structure and its evolution to determine the effect of the variation of those parameters.

Initially, it has been quantitatively shown that flow history strongly influenced the linear viscoelastic properties of the suspensions. Application of low shear forces induced more inter-particle entanglements whereas pre-shearing at high rates caused the distortion of structure and opened up some nanotube entanglements. This was deduced from the fact that the onset for the formation of an interconnected carbon nanotube network shifted to lower concentrations as the pre-shear rate decreased. The rheological percolation threshold was determined to be about 2.5 wt% after pre-shearing at 100 $s^{-1}$ whereas applying a low pre-shear at 0.01 $s^{-1}$ led to the percolation threshold value of about 1 wt%.

Evidenced by measuring the storage modulus of the suspensions at a constant low frequency and strain amplitude in the linear viscoelastic region, the evolution of structure did not stall upon cessation of shear flow. The measured moduli were shown to develop exponentially in time at each concentration. Different metastable structures formed after sufficient elapsed time upon cessation of pre-shearing. The formed metastable structures were distinguishable by various storage moduli in dilute and semi-dilute concentration regimes which were inversely related to the rate of pre-shearing. However, for more concentrated suspensions, the formed

metastable structures demonstrated an approximately similar storage modulus after pre-shearing at different rates. These observations revealed that the suspensions structure was more sensitive to the effect of flow history at relatively low and intermediate concentrations. This was due to the fact that in these concentration regimes, the inter-particle interactions were not strong enough; thus the fragile structure of the suspensions was more prone to be affected by the external shear forces. However, at high concentrations the particles interacted through sufficiently large hydrodynamic and friction forces; hence, a highly entangled structure formed which was more resistant to the impact of external shear fields and pre-shearing had a little influence on their structures as well as their macroscopic properties.

Further analysis on the effect of flow history on the formed metastable structures exhibited that the elastic modulus of these structures were scaled with the rate of pre-shearing in a power-law form as $G'_{\infty} = \kappa \dot{\gamma}_i^{-\varepsilon}$, the parameters of which strongly depended on the concentration. As a result, by scaling the steady shear results of the suspensions using this correlation, a master curve formed over a wide range of concentrations below and above the gel point; this evidently showed the importance of the storage modulus of metastable structures as a characterizing element, which represented the parameters involved in the evolution of structure.

By comparing the storage moduli of the suspensions before pre-shearing (except for sample loading into the instrument), $G'_{ref}$, with the ones obtained for the metastable structures, $G'_{\infty}$, it was shown that a corresponding critical shear rate existed at low and intermediate concentrations above which some nanotube entanglements broke down leading to a lower suspension elasticity. The critical shear rate was quantified by plotting these two moduli against the applied pre-shear rate; the pre-shear rate corresponding to the crossing point was

called the critical shear rate, $\dot{\gamma}_c$, and ranged between 1.7 $s^{-1}$ at 0.5 wt% to 10 $s^{-1}$ at 3 wt% within the experimental error of ±15%. At higher concentrations, no critical shear rate was observed due to the presence of strong nanotube entanglements. By pre-shearing at shear rates lower than the critical one ($\dot{\gamma}_i < \dot{\gamma}_c$), more entanglements formed between nanotubes leading to a higher elasticity in the formed metastable structures ($G'_\infty > G'_{ref}$). On the contrary, application of higher shear forces ($\dot{\gamma}_i \geq \dot{\gamma}_c$) resulted in partial breakdown of structure and consequently the elasticity of metastable structures decreased ($G'_\infty \leq G'_{ref}$).

The extent of structure build-up and breakdown in the vicinity of critical shear rates was quantified by a set of transient flow reversal experiments. It was observed that the structure build-up was complete if the applied shear rate was below the critical ones. This was characterized by approaching the reverse stress overshoot to a similar value of that in forward direction after a sufficient rest time. Upon the application of higher shear rates, the structure partially developed due to the disentanglement of some nanotubes. At higher concentrations, the stress overshoots in opposite directions overlapped after a sufficient rest time regardless of the rate of the applied shear.

The rate of structure build-up and formation of metastable structures after cessation of pre-shearing was characterized by determining the characteristic time of the system as a function of the concentration, pre-shearing rate and temperature. The characteristic time was shown to decrease with concentration exhibiting a faster structure reconstruction. However, its variation with respect to the pre-shear rate strongly depended on the concentration. In dilute suspensions, it dramatically augmented with the rate of pre-shearing, revealing a slower rate of structure reconstruction while it remained almost intact in more concentrated suspensions.

The other parameter affecting the rate of structure build-up was temperature. However, studying the effect of temperature was more complicated since both the inter-particle interactions and the rheological properties of the polymer matrix were sensitive to the variation of temperature. Hence, for a comprehensive interpretation of the results, it was essential to distinguish between these two phenomena. By normalizing the shear viscosity as well as the storage and loss moduli of the suspensions with the corresponding values for the neat polymer at each temperature, the effect of the inter-particle interactions was more highlighted. The normalized values were shown to increase with temperature reflecting the increase of inter-particle interactions. The same conclusion reached by observing the similar trend of the normalized storage modulus of the metastable suspensions with the norm of the complex modulus of the neat epoxy at each temperature.

Variation of temperature affected the characteristic time of the formation of metastable structures. It was observed that the rate of formation of metastable structures increased with temperature regardless of the concentration or pre-shear rate. This was in-line with the observations of a faster rate of structure build-up with increasing concentration at a constant temperature. From both of these observations it was concluded that the inter-particle interactions had a crucial role in the formation of the metastable structures. On the other hand, the rotary diffusion time decreased with temperature; that evidently showed the important role of Brownian forces in the structure build-up of CNT suspensions in the absence of flow. This was also in conjunction with the fact that the characteristic time of metastable dilute suspensions at high pre-shear rates declined with temperature to a much larger extent compared to the case of low pre-shear rates. This means that in the absence of high inter-particle interactions (where the structure was distorted by pre-shearing at high rates), the rate of structure reconstruction increased with temperature as highly influenced by Brownian

forces. As a result, in the wide range of concentrations, pre-shear rates and temperatures, the Brownian motion and the inter-particle interactions were two important mechanisms in the development of metastable structures.

The relative importance of Brownian forces and the inter-particle interactions in structure development was further investigated through a set of transient flow reversal experiments in the vicinity of critical shear rates. It was observed that most of the structure build-up occurred during the first 300 s of rest after cessation of transient flow in the forward direction; this time was comparable to the rotary diffusion time, $1/D_r$ of about 314 s in dilute systems and even shorter ($D_r' \sim D_r / \phi^2$) in semi-dilute suspensions. However, a complete structure build-up took much longer (~1 h) revealing the fact that Brownian forces cannot be the only mechanism involved in quiescent. On the other hand, as discussed earlier, the lack of sufficient inter-particle interactions due the application of high shear rates ($\dot{\gamma} \geq \dot{\gamma}_c$) and structure distortion, resulted in a partial structure build-up in transient flow reversal experiments. Hence, Brownian forces in conjunction with inter-particle interactions were necessary to reconstruct the structure of the pre-sheared nanotube suspensions in the absence of flow.

Using the thixotropic structural model of Yziquel *et al.* (1999), the transient behaviour of the nanotube suspensions were compared with predictions of this model. As a result of this investigation, the model qualitatively predicted the experimental results as well as a partial structure development at shear rates above the critical one. However, the reverse overshoots and the rest time required for a complete structure build-up were overestimated.

Further interpretation of the structural behaviour of the suspensions in the light of scaling theories imparted fruitful information about the nature of the nanotubes network. It was demonstrated that the nanotube suspensions formed a self-similar network structure near and

above their gel point which was assumed to be formed by closely packed fractal flocs. The fractal nature of the network was evidenced by observing the scaling behaviour of low-frequency plateau storage modulus of the suspensions and the strain for the maximum limit of linearity, $\gamma_c$, with the concentration in a power-law form. Using the scaling exponents of the corresponding power law correlations, the fractal dimension of the suspensions was estimated to be about 2.15 in the range for slowly flocculating suspensions. This explained why the shelf time of the suspensions was limited to few months. In view of the scaling theory, the elasticity of the networks originated from both the inter- and intra-floc links.

From this stand view, the complex behavior of rheological properties of the flow-induced metastable structures was investigated. It was shown that the power-law exponents of $G'_\infty$ and $\gamma_c$ with respect to concentration enhanced significantly with the applied pre-shearing rate. However, the resulting fractal dimensions only slightly changed from 2.13 to 2.31 after pre-shearing at 0.1 $s^{-1}$ and 100 $s^{-1}$ respectively. In fact, the small difference between the fractal dimensions of the metastable structures remained within the experimental error so the superstructure of the network of the suspensions exhibited only a small variation with the flow history; this was associated with the initially compact structure of the suspensions before pre-shearing ($d_f \sim 2.15$). The lower sensitivity of the fractal dimension of the suspensions to the flow history was in agreement with the invariant storage modulus of the metastable structures, which was barely influenced by the rate of pre-shearing near and above the gel point. In addition, the power-law exponent *m* relating the variation of the radius of gyration ($\xi$) of the aggregates with the applied shear rate ($\xi \sim \dot{\gamma}^{-m}$) was found to be in the range of 0.36–0.38 and in the limit for the theoretical values for the rigid and soft aggregates. This illustrated that

nanotubes aggregates were partially soft and partially rigid and their interaction potential was a combination of central and non-central components.

At the last stage, the effect of temperature on the scaling behaviour of the suspensions was characterized. The reduced storage moduli of the suspensions increased with temperature whereas $\gamma_c$ decreased revealing the formation of a more fragile structure. This is in contradiction with Abbasi *et al.* (2009) who reported the increase of $\gamma_c$ with temperature and formation of a stronger network and a better dispersion of CNTs in nano-composite. In this sense, the decrease of $\gamma_c$ with temperature could be an indication of more aggregation upon increasing temperature. Yet, no phase separation occurred since the time-temperature superposition was valid over the temperature range studied. The power-law exponents of the storage modulus and $\gamma_c$ and so the estimated fractal dimensions had large errors that made it difficult to identify whether the superstructure of the suspensions changed as influenced by temperature; this could be due to a limited range of accessible temperatures to only 30 $^{o}$C.

# RECOMMENDATIONS

The findings of this investigation are based on model suspensions and can be used in other systems, regardless of the type and properties of particles or the polymer matrix, the suspensions concentration, the temperature or the preparation technique. In this research, the physics behind the structure formation has been elaborated under the simultaneous influence of flow history, concentration and temperature and has brought about some questions that need to be tackled by further research.

Fig 4-10, shows the effect of temperature and flow history on normalized storage modulus of metastable structures. From this figure, it can be observed that at each temperature, by increasing the pre-shear rate, the reduced storage modulus decreased; however, above the pre-shear rate of 10 $s^{-1}$, there was a sudden increase in the reduced storage modulus which was more significant at lower temperatures of 15 and 25 $^{o}$C. Given the fact that at high shear rates and lower temperatures, the sample undergoes a much higher stress, the reason for this observation remains unclear and needs to be more examined by considering a wider range of temperatures. Since, the range of accessible temperature in this study was limited between 15 to 45 $^{o}$C due to the type of epoxy, it is suggested to use a more thermally stable polymer matrix that can be examined over a wider temperature range for further investigations.

Another issue observed in experimental results was the emergence of stress overshoots at very small strains compared to the model predictions (e.g. see Fig 6-7 for a 2 wt%). However, the Yziquel *et al.* (1999) model predicted the presence of overshoots at strains in the range of 1, which was comparable to other nano-composites such as PP-clay nanocomposites (Letwimolnun *et al.* (2007) ( $\gamma \sim 1.7$), PBT-montmorillonite nano-composites (Wu *et al.*

(2005)) ($\gamma$ ~ 1-2). The reason for the appearance of experimental stress overshoots at very small deformations is not clear and needs to be more investigated.

The conducted research has clearly shown the impact of inter-particle interactions on the structural evolution of the model nanotube suspensions from the experimental stand view. This effect should be explicitly considered as a governing entity in a structural thixotropic model. This is, however, unclear how to do it.

The predictive thixotropic models that take into account the inter-particle interactions as a governing mechanism in the reversible build-up and breakdown of suspension structure are those developed at a microscopic level such as the ones in de Rooij *et al.* (1993) and Potanin (1993). The scope of application of these microstructural models is restricted to very dilute suspensions. On the other hand, the existing thixotropic structural models such as the ones developed by Yziquel *et al.* (1999) and Dullaert and Mewis (2006) are applicable over a wide range of concentrations and to some extent a wide range of shear rates. These models have been used to predict the steady shear results and the thixotropic behaviour of a variety of flocculating suspensions. The kinetic equations involved in these models are composed of two terms representing the flow-induced structure breakdown and the structure build-up due to Brownian forces. However, as a partial contribution of this thesis, the importance of the inter-particle interactions in the structure reconstruction of the suspensions has been shown. In order to incorporate the effect of inter-particle interactions, one need to modify the kinetic equations in these models by adding an explicit term to the structure build-up term, representing the impact of inter-particle interactions. As a result the new model is expected to address the shortcomings of the existing models associated with the overestimation of the predicted results as reported in Chapter 6.

Another interesting point that can be addressed in the model is its inadequacy in predicting the transient normal stress differences. As shown in Chapter 6 (see Fig 6-9), the model overestimates the normal stress difference overshoots and underestimates the strain at the maximum normal stress difference and the steady state value. We believe that the transient behaviour of the carbon nanotube suspensions is mostly controlled by the size of the aggregates as characterized by the value of the elastic modulus, measured after cessation of shear flow. However, the orientation of the particles may influence these results. Unfortunately, the existing theoretical (e.g. fibre direct simulation) and experimental (e.g. light scattering) techniques to simulate and characterize the orientation dynamics of particles is limited to very dilute transparent suspensions. By developing new experimental techniques that are applicable over a wider range of concentrations, an in-depth knowledge about the orientation (of individual particles or aggregates) dynamics of more concentrated suspensions can be achieved; this needs to be eventually incorporated in the existing models and address the current shortcomings in predicting transient results especially normal stress differences.

# BIBLIOGRAPHY

Abbasi, S., Carreau, P.J., Derdouri, A. and Moan, M. (2009) "Rheological properties and percolation in suspensions of multiwalled carbon nanotubes in polycarbonate." Rheologica Acta **48**(9): 943-959.

Abbasi, S., Carreau, P.J. and Derdouri, A. (2010) "Flow induced orientation of multiwalled carbon nanotubes in polycarbonate nanocomposites: Rheology, conductivity and mechanical properties." Polymer **51**(4): 922-935.

Abdel-Goad, M. and Potschke, P. (2005) "Rheological characterization of melt processed polycarbonate-multiwalled carbon nanotube composites." Journal of Non-Newtonian Fluid Mechanics **128**(1): 2-6.

Allaoui, A., Bai, S., Cheng, H.M. and Bai, J.B. (2002) "Mechanical and electrical properties of a MWNT/epoxy composite." Composites Science and Technology **62**(15): 1993-1998.

Barnes, H.A. (1997) "Thixotropy-a review." Journal of Non-Newtonian Fluid Mechanics **70**(1-2): 1-33.

Bose, S., Bhattacharyya, A.R., Kodgire, P.V., Misra, A. and Potschke, P. (2007) "Rheology, morphology, and crystallization behavior of melt-mixed blends of polyamide6 and acrylonitrile-butadiene-styrene: Influence of reactive compatibilizer premixed with multiwall carbon nanotubes." Journal of Applied Polymer Science **106**(5): 3394-3408.

Chaplain, V., Mills, P. and Djabourov, M. (1994) "Elastic properties of networks of fractal clusters." Colloid and Polymer Science **272**(8): 991-999.

Cipiriano, B.H., Kashiwagi, T., Raghavan, S.R., Yang, Y., Grulke, E.A., Yamamoto, K., Shields, J.R. and Douglas, J.F. (2007) "Effects of aspect ratio of MWNT on the flammability properties of polymer nanocomposites." Polymer **48**(20): 6086-6096.

de Rooij, R., Potanin, A. A., van den Ende, D. and Mellema, J. (1993) "Steady shear viscosity of weakly aggregating polystyrene latex dispersions." Journal of Chemical Physics **99**(11): 9213-9223.

Du, F., Scogna, R.C., Zhou, W., Brand, S., Fischer, J.E. and Winey, K.I. (2004) "Nanotube networks in polymer nanocomposites: Rheology and electrical conductivity." Macromolecules **37**(24): 9048-9055.

Dullaert, K. and Mewis, J. (2006) "A structural kinetics model for thixotropy." Journal of Non-Newtonian Fluid Mechanics **139**(1-2): 21-30.

Fan, Z. and Advani, S.G. (2007) "Rheology of multiwall carbon nanotube suspensions." J. Rheology **51**(4): 585-604.

Fry, D., Langhorst, B., Kim, H., Grulke, E., Wang, H. and Hobbie, E.K. (2005) "Anisotropy of sheared carbon-nanotube suspensions." Physical Review Letters **95**(3): 038304.

Fry, D., Langhorst, B., Wang, H., Becker, M.L., Bauer, B.J., Grulke, E.A. and Hobbie, E.K. (2006) "Rheo-optical studies of carbon nanotube suspensions." Journal of Chemical Physics **124**(5): 054703.

Gojny, F.H., Wichmann, M.H.G., Kopke, U., Fiedler, B. and Schulte, K. (2004) "Carbon nanotube-reinforced epoxy-composites: enhanced stiffness and fracture toughness at low nanotube content." Composites Science and Technology **64**(15): 2363-2371.

Hobbie, E.K. and Fry, D.J. (2006) "Nonequilibrium phase diagram of sticky nanotube suspensions." Physical Review Letters **97**(3), 036101.

Hobbie, E.K. and Fry, D.J. (2007) "Rheology of concentrated carbon nanotube suspensions." Journal of Chemical Physics **126**(12): 124907.

Hobbie, E.K., Wang, H., Kim, H., Han, C.C., Grulke, E.A. and Obrzut, J. (2003) "Optical measurements of structure and orientation in sheared carbon-nanotube suspensions." Review of Scientific Instruments **74**(3 I): 1244-1250.

Hong, S. and Myung, S. (2007) "Nanotube Electronics: A flexible approach to mobility." Nature Nanotechnology **2**(4): 207-208.

Huang, Y.Y., Ahir, S.V. and Terentjev, E.M. (2006) "Dispersion rheology of carbon nanotubes in a polymer matrix." Physical Review B (Condensed Matter and Materials Physics) **73**(12): 125422-1.

Keshtkar, M., Heuzey, M.-C. and Carreau, P.J. (2009) "Rheological behavior of fiber-filled model suspensions: effect of fiber flexibility." Journal of Rheology **53**(3): 631-650.

Kim, J.A., Seong, D.G., Kang, T.J. and Youn, J.R. (2006) "Effects of surface modification on rheological and mechanical properties of CNT/epoxy composites." Carbon **44**(10): 1898-1905.

Kim, J.Y., Han, S.I. and Hong, S. (2008) "Effect of modified carbon nanotube on the properties of aromatic polyester nanocomposites." Polymer **49**(15): 3335-3345.

Kinloch, I. A., Roberts, S.A. and Windle, A. H. (2002) "A rheological study of concentrated aqueous nanotube dispersions." Polymer **43**(26): 7483-7491.

Kota, A.K., Cipriano, B.H., Duesterberg, M.K., Gershon, A.L., Powell, D., Raghavan, S.R. and Bruck, H.A. (2007) "Electrical and rheological percolation in polystyrene/MWCNT nanocomposites." Macromolecules **40**(20): 7400-7406.

Larson, R.G. (1999) *The structure and rheology of complex fluids.* New York: Oxford University Press.

Lau, K.-T., Lu, M., Lam, C.K., Cheung, H.Y., Sheng, F.-L. and Li, H.-L (2005) "Thermal and mechanical properties of single-walled carbon nanotube bundle-reinforced epoxy nanocomposites: The role of solvent for nanotube dispersion." Composites Science and Technology **65**(5 SPEC ISS): 719-725.

Lee, S.H., Cho, E., Jeon, S.H. and Youn, J.R. (2007) "Rheological and electrical properties of polypropylene composites containing functionalized multi-walled carbon nanotubes and compatibilizers." Carbon **45**(14): 2810-2822.

Letwimolnun, W., Vergnes, B., Ausias, G. and Carreau, P.J.(2007) Stress overshoots of organoclay nanocomposites in transient shear flow, J. Non-Newtonian Fluid Mech., **141** (2-3), 167-179.

Lin-Gibson, S., Pathak, J.A., Grulke, E.A., Wang, H. and Hobbie, E.K. (2004) "Elastic Flow Instability in Nanotube Suspensions." Physical Review Letters **92**(4): 48302.

Mewis, J. (1979) "Thixotropy-a general review." Journal of Non-Newtonian Fluid Mechanics **6**(1): 1-20.

Mobuchon, C., Carreau, P.J. and Heuzey, M.-C. (2009) "Structural analysis of non-aqueous layered silicate suspensions subjected to shear flow." Journal of Rheology **53**(5): 1025-1048.

Montes, S., White, J.L. and Nakajima, N. (1988) "Rheological behavior of rubber carbon black compounds in various shear flow histories." Journal of Non-Newtonian Fluid Mechanics **28**(2): 183-212.

Nanda, J., Maranville, C., Bollin, S.C., Sawall, D., Ohtani, H., Remillard, J.T. and Ginder, J.M. (2008) "Thermal conductivity of single-wall carbon nanotube dispersions: Role of interfacial effects." Journal of Physical Chemistry C **112**(3): 654-658.

Narine, S.S. and Marangoni, A.G. (1999) "Fractal nature of fat crystal networks." Physical Review E **59**(2): 1908-1920.

Negi, A.S. and Osuji, C.O. (2010) "Physical aging and relaxation of residual stresses in a colloidal glass following flow cessation." Journal of Rheology **54**(5): 943-958.

Pignon, F., Magnin, A., Piau, J-M., Cabane, B., Lindner, P. and Diat, O. (1997) "Yield stress thixotropic clay suspension investigations of structure by light, neutron, and X-ray scattering." Physical Review E (Statistical Physics, Plasmas, Fluids, and Related Interdisciplinary Topics) **56**(3): 3281-3289.

Potanin, A.A., De Rooij, R., Van den Ende, D. and Mellema, J. (1995) "Microrheological modeling of weakly aggregated dispersions." Journal of Chemical Physics **102**(14): 5845-5853.

Potanin, A.A. (1991) "On the mechanism of aggregation in the shear flow of suspensions." Journal of Colloid and Interface Science **145**(1): 140-157.

Potanin, A.A. (1993) "On the computer simulation of deformation and breakup of colloidal aggregates in shear flow." Journal of Colloid and Interface Science **157**(2): 399-410.

ahatekar, S. S., Koziol, K. K. K., Butler, S.A., Elliott, J.A., Shaffer, M.S.P., Mackley, M.R. and Windle, A.H. (2006) "Optical microstructure and viscosity enhancement for an epoxy resin matrix containing multiwall carbon nanotubes." Journal of Rheology **50**(5): 599-610.

Schartel, B., Potschke, P., Knoll, U. and Abdel-Goad, M. (2005) "Fire behaviour of polyamide 6/multiwall carbon nanotube nanocomposites." European Polymer Journal **41**(5): 1061-1070.

Shih, W.-H., Shih, W.Y., Kim, S.I., Liu, J. and Aksay, I.A. (1990) "Scaling behavior of the elastic properties of colloidal gels." Physical Review A **42**(8): 4772-4779.

Song, Y.S. and Youn, J.R. (2005) "Influence of dispersion states of carbon nanotubes on physical properties of epoxy nanocomposites." Carbon **43**(7): 1378-1385.

Song, Y.S. (2006) "Effect of surface treatment for carbon nanotubes on morphological and rheological properties of poly(ethylene oxide) nanocomposites." Polymer Engineering and Science **46**(10): 1350-1357.

Sonntag, R.C. and Russel, W.B. (1986) "Structure and breakup of flocs subjected to fluid stresses : I. Shear experiments." Journal of Colloid and Interface Science **113**(2): 399-413.

Sonntag, R.C. and Russel, W.B. (1987) "Structure and breakup of flocs subjected to fluid stresses: II. Theory." Journal of Colloid and Interface Science **115**(2): 378-389.

Switzer, L.H. and Klingenberg, D.J. (2003) "Rheology of sheared flexible fiber suspensions via fiber-level simulations." Journal of Rheology **47**(3): 759-778.

Thostenson, E.T., Li, C. and Chou, T.-W. (2005) "Nanocomposites in context." Composites Science and Technology **65**(3-4): 491-516.

Wu, H. and Morbidelli, M. (2001) "A model relating structure of colloidal gels to their elastic properties." Langmuir **17**(4): 1030-1036.

Wu, D., Zhou, C., Hong, Z., Mao, D. and Bian, Z. (2005) Study on rheological behaviour of poly(butylene terephthalate)/montmorillonite nano-composites, Eur. Polym. J., **41** (9) 2199-2207.

Wu, D., Wu, L., Zhou, W., Sun, Y. and Zhang, M. (2010) "Relations between the aspect ratio of carbon nanotubes and the formation of percolation networks in biodegradable polylactide/carbon nanotube composites." Journal of Polymer Science, Part B: Polymer Physics **48**(4): 479-489.

Wypych, G. (2000) *Handbook of Fillers - A Definitive User's Guide and Databook.* ChemTec Publishing.

Xu, D.-H., Wang, Z.-G. and Douglas, J.F. (2008) "Influence of carbon nanotube aspect ratio on normal stress differences in isotactic polypropylene nanocomposite melts." Macromolecules **41**(3): 815-825.

Yziquel, F., Carreau, P.J., Moan, M. and Tanguy, P.A. (1999) "Rheological modeling of concentrated colloidal suspensions." Journal of Non-Newtonian Fluid Mechanics **86**(1-2): 133-155.

Zhang, Q., Rastogi, S., Chen, D., Lippits, D. and Lemstra, P.J. (2006) "Low percolation threshold in single-walled carbon nanotube/high density polyethylene composites prepared by melt processing technique." Carbon **44**(4): 778-785.

# APPENDIX A – COMPARISON OF DIFFERENT MIXING TECHNIQUES

In this appendix, the dispersion quality of a 1 wt% MWCNT in an epoxy prepared by different mixing techniques was compared by optical microscopy. An epoxy Epon 828 (HEXION™ Specialty Chemicals Inc.) with a density of 1.16 g/mL and viscosity of 12.33 Pa.s (at 25 °C) was used as the dispersing medium. MWCNTs from Cheap Tubes Inc.© with no surface treatment were dispersed in epoxy. Three different mixing techniques were employed including mixing by ultrasonic mixer (which is called sonication hereafter) with and without solvent and mixing in a three-roll mill. The mixing procedure is summarized as follows:

- sonication without solvent at the mixing amplitude of 114 W for 1 h at 45 $^{o}$C.
- solution mixing (sonication with solvent) in aceton at the mixing amplitude of 114 W for 1 h at 45 $^{o}$C followed by solvent removal under vacuum at 60 $^{o}$C for 4 weeks.
- mixing in three-roll-mill at 150 rpm at different gap sizes from 100 to 5 μm at room temperature.

The resulting micrographs of the suspensions microstructure were compared by optical microscopy for different mixing techniques in Figure A-1 to Figure A-3 at 400 μm and 200 μm scales. Large aggregates were observed when the suspensions were prepared by sonication without (Figure A-1) and with the solvent (Figure A-2), respectively. It was also difficult to perform rheological measurements when the suspensions contained such large aggregates where wall slip and sedimentation were major obstacles. On the contrary, mixing by three-roll-mill was more efficient as shown in Figure A-3. The resulting structure of the suspensions was homogenous up to 200 μm scale and the rheological properties of the suspensions were reproducible within small experimental errors. Moreover, the suspensions were stable over a

couple of months. This mixing technique was used for preparing the suspensions of various concentrations in this thesis.

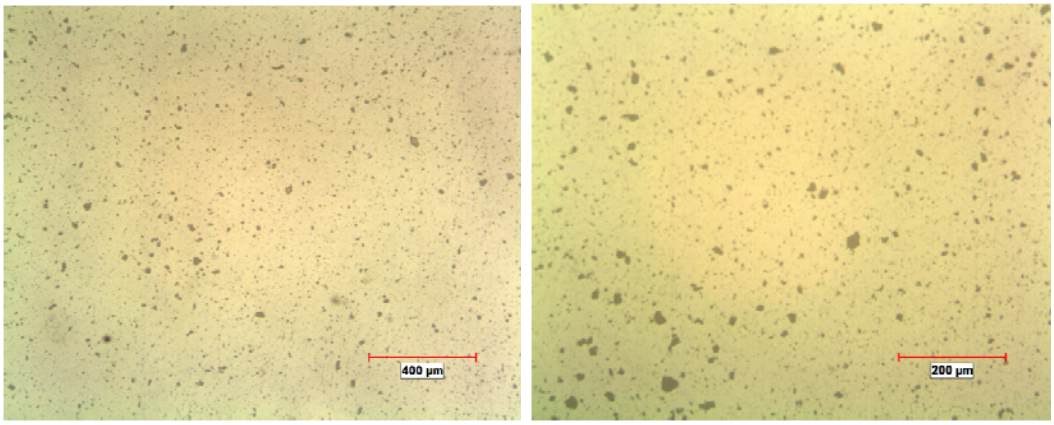


Figure A-1: Optical micrographs of 1 wt% CNT-epoxy suspension prepared by direct mixing with ultrasound.

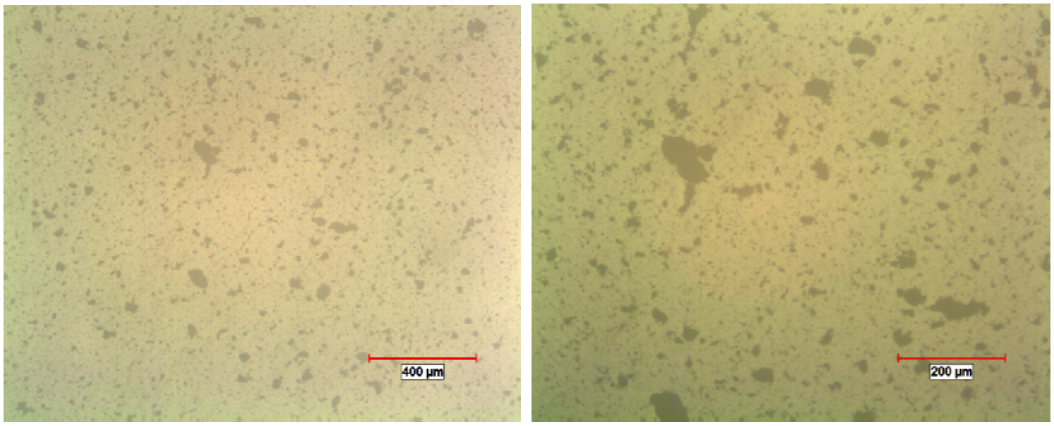


Figure A-2: Optical micrographs of 1 wt% CNT-epoxy suspension prepared by solution mixing.

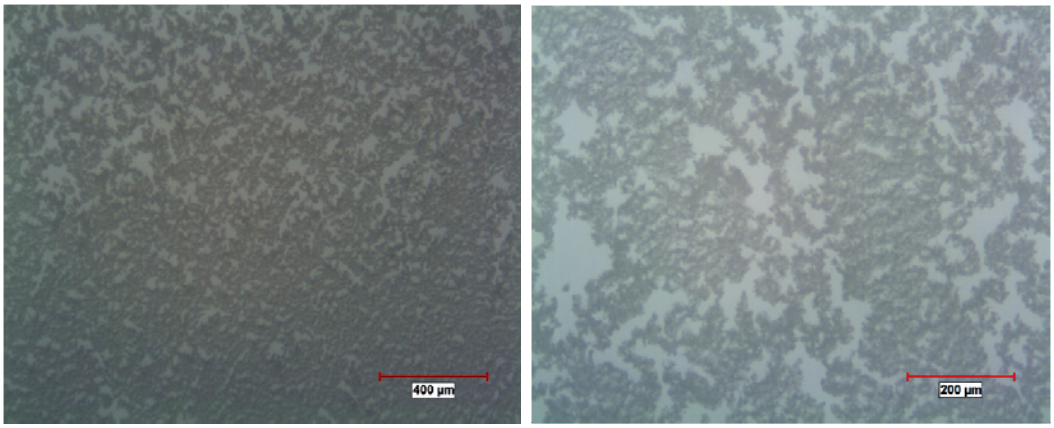


Figure A-3: Optical micrographs of 1 wt% CNT-epoxy suspension prepared by three-roll mill.